MULTIFOCAL SPHERICAL FISH LENSES

Gagnon, Yakir

2010

MULTIFOCAL SPHERICAL FISH LENSES

by

Yakir Luc Gagnon

Doctoral Thesis
Lund, October 2010

LUND UNIVERSITY
Faculty of Science

An academic thesis in the fulfillment of the degree of Doctor of Philosophy at the Faculty of Natural Science at Lund University. Time of thesis defense is 14:00, October 15th 2010 at the Ecology Building, Sölvegatan 37, Lund, Sweden. Faculty opponent is Prof. Dr. rer. nat. Frank Schaeffel, Institute for Ophthalmic Research Tübingen, Department of Pathophysiology of Vision and Neuroophthalmology, Tübingen, Germany.

∗All figures by author, unless otherwise stated

DOKUMENTDATABLAD enl SIS 61 41 21

Organization
LUND UNIVERSITY

Department of Biology
Sölvegatan 35
223 62 Lund
Sweden

Author(s)
Yakir Luc Gagnon

Document name
DOCTORAL DISSERTATION

Date of issue
15/10/2010

Sponsoring organization

Title and subtitle

Multifocal spherical fish lenses

Abstract

Vision is an important source of information for many animals. The lens plays a central role in the visual pathway and hence the ecology of these animals. Fish have spherically shaped crystalline lenses that contain a gradient of refractive index. Like all refracting elements, lens performance depends on the wavelength of the refracted light. This wavelength dependent focusing leads to chromatic aberration where only one wavelength interval is being focused correctly. Fish lenses compensate for this by dividing the lens into multiple concentric zones each responsible for focusing a particular wavelength interval. In this thesis I explore the optical and visual benefits these multifocal lenses offer. In order to minimize light scattering by the lens, all cells except the lens periphery are devoid of nuclei and cell organelles. Interestingly, the refractive index of this outer most zone is constant, maintaining a physiologically stable environment for these cells to function (Paper I). It has been shown that light or dark-adapting fish change their lenses' properties within hours while fish reared under differently colored artificial light regimes do so after several months. I explored the effects of the light regimes found in the Mediterranean and the Red Sea on lenses of the rivulated rabbitfish, *Siganus rivulatus*. Such natural spectral differences affected the mean focal length of the lenses making the Mediterranean fish eyes more light sensitive than those found in the Red Sea population (Paper II). This coincides well with the darker and tinted waters found in the Mediterranean. Dispersion describes the wavelength dependency refractive media have. I therefore described a dispersion model that fitted measured refractive indices of various ocular media as well as the longitudinal chromatic aberration determined by laser scanning of fish lenses (Paper III). Relying on the results of the previous papers (Paper I & III), I compared multifocal fish lenses to a simplified monofocal lens. The multifocal lenses showed to be superior to monofocal ones. While monofocal lenses perfectly focus one wavelength, the short focal length in combination with the chromatic aberration these fish lenses have degrades the image at all other wavelengths. This results in an image relatively rich in spatial information (i.e. high contrast and sharp edges) but no spectral integrity (wrong hues and bland colors). Multifocal lenses offer an optimal trade off between spatial and spectral information (Paper IV).

Key words: Vision, Optics, Lens, Dispersion, Spherical, Model, Fish, Ray-trace, Chromatic, Aberration, Multifocal, Refractive, Index, Gradient.

Classification system and/or index termes (if any):

Supplementary bibliographical information:

Language
English

ISSN and key title:

ISBN
978-91-7473-010-4

Recipient's notes

Number of pages
87

Price

Security classification

"The best material model of a cat is another, or preferably the **same**, cat"

Arturo Rosenblueth, Philosophy of Science, 1945

For *Francois-Marc Gagnon*

Contents

Glossary

Notation	Description	Page
α	The angle between the tangent of the ray and the center of the lens	17–19
b	The distance between the entrance beam and the optical axis, normalized to the medium refractive index (n_m)	17–19, 21, 22
BCD	The distance between the center of the lens and the point where the exit beam intercepts the optical axis, Back Center Distance	18–20, 23
BEP	The distance between the entrance beam and the optical axis, Beam Entrance Position	17, 18, 21
C	The center of the lens	17
CZ	A zone in the lens that has a constant refractive index, ranging from ~ 0.94 lens radius to the inner border of the lens capsule	15, 20, 22
γ	The cumulative deflection angle achieved from the ray's refraction at the lens's periphery	19, 20
LCA	Longitudinal Chromatic Aberration	16, 17, 23

Notation	Description	Page
LSA	Longitudinal Spherical Aberration	14, 16, 17, 22, 23
MTF	Modulation Transfer Function	7
n_m	The refractive index of the medium surrounding the lens	17, 18
$n(r)$	The refractive index of the lens as a function of the distance from the center of the lens	17, 19, 21
OA	Optical axis	11, 16, 17, 19, 20, 22
P	A point on the light-ray trajectory	17
ϕ	The polar angle between the optical axis and a line pointing at a point on the light-ray trajectory from the center of the lens	17, 19
PSF	Point Spread Function	7, 24
ψ	Deflection angle	17–19, 21, 22
R	The lens radius	14, 16, 19–22
r	The distance from the center of the lens	17–19
RI	Refractive index	3–6, 9, 10, 14–18, 20–23
RIG	Refractive index gradient	6, 13, 15, 16, 18–23
ξ	The product of the refractive index function and the distance from the center of the lens, $r \cdot n(r)$	19, 21, 22

Original papers and manuscripts

Paper I Y. L. Gagnon, B. Söderberg, and R. H. H. Kröger (2008) Effects of the peripheral layers on the optical properties of spherical fish lenses. Journal of the Optical Society of America A, **25**: 2468–2475

Paper II Y. L. Gagnon, N. Shashar, and R. H. H. Kröger (2010) Spectral influence on the refractive properties of the crystalline lens in *Siganus rivulatus* (Forsskål, 1775). Submitted to the Journal of Experimental Biology.

Paper III Y. L. Gagnon, R. H. H. Kröger, and B. Söderberg (2010) Adjusting a light dispersion model to fit measurements from vertebrate ocular media as well as ray-tracing in fish lenses. Vision Research, **50**: 850–853

Paper IV Y. L. Gagnon, B. Söderberg, and R. H. H. Kröger (2010) Superior optics through multifocal spherical fish lenses. Manuscript

Contribution

Paper I RK conceived the experiments and designed them together with YG. YG executed the experiments and had the initial observation. Ray-tracing calculations were supervised by BS. Data analysis was done by YG. YG wrote the paper. BS and RK commented on earlier versions of the manuscript.

Paper II YG conceived the experiments and designed them together with RK and NS. YG executed the experiments. Data analysis was done by YG. YG wrote the paper. RK and NS commented on earlier versions of the manuscript.

Paper III YG conceived the idea and wrote the algorithms. Ray-tracing calculations were supervised by BS. Data analysis was done by YG. YG wrote the paper. RK and BS commented on earlier versions of the manuscript.

Paper IV YG and RK conceived the idea. YG designed and executed the data analysis. Ray-tracing and retina emulations were supervised by BS. YG wrote the paper. RK and BS commented on earlier versions of the manuscript.

Populärvetenskaplig sammanfattning

Syn är avgörande för många djurs överlevnad. En väldigt viktig del av ögat är linsen då ljuset fokuseras genom den. I denna studie har jag undersökt hur fisklinser fokuserar ljus. Valet av fiskar som försöksdjur berodde på att de är lätta att skaffa och deras linser är klotformade, vilket underlättar beräkningen av strålgången och linsens optiska egenskaper.

Hos fiskar innehåller linserna genomskinliga proteiner, *krystalliner*. Proteinhalten bestämmer brytningsindexen som i sin tur påverkar hur ljuset bryts. En lins med hög proteinhalt har en hög brytningsindex och bryter ljuset mer än vad en lins med låg brytningsindex gör. De klotformade fisklinser kräver en brytningsindex gradient för att fungera bra. Det innebär att proteinhalten ökar från linsens periferi till dess centrum.

Ett materials brytningsindex beror inte bara på dess proteinhalt utan också på ljusets våglängd som passerar genom matrialet (de olika ljusvåglängder uppfattas av människor som färger). Detta beroendeförhållande kallas för *dispersion*. Det innebär att olika våglängder bryts annorlunda genom en och samma lins; medan vissa våglängder fokuseras rätt kommer andra att bli ofokuserade.

I vissa fisklinser är detta problem löst genom att linsen har ett antal delar där varje del ansvarar för att fokusera en våglängdsintervall (motsvarar färg). En sådan lins kallas för *multifokal* på grund av att varje del av linsen fokuserar ljus av samma våglängd vid olika avstånd från linsen.

Proteinhaltsgradienten justeras av cellerna i linsen. Linsen består av så kallade fiberceller. Dessa smala celler är avlånga och sträcker sig från en linspol till den andra. Cellerna vid linsens periferi innehåller cellorganeller (till exempel cellkärnan) som sköter ämnesomsättningen och funktionaliteten i cellerna. För att förminska ljusspridning, som annars skulle försämra linsoptiken, saknar resten av linscellerna inre organeller (detta sker vid $\sim 95\%$ av linsens radius och inåt). Det visar sig att proteinhaltsgradienten börjar bara där cellorganellerna slutar. Proteinhaltsgradienten avsaknas alltså i linsens periferi. Detta sammanträffande indikerar att proteinhalten måste hållas vid en viss nivå där cellerna fortfarande har fungerande organeller (Papper I).

Fiskar som har vant sig vid mörker visar sig kunna anpassa linsens brytningsindex gradient till den låga ljusnivån på ett par timmar. Fiskar som uppföds under olika artificiella ljusmiljöer ändrar sina linser inom några månader. Jag ville se om de naturliga ljusskillnaderna som finns mellan Röda havet och Medelhavet också påverkar linsernas anpassning. Jag hittade att hos kaninfisken, *Siganus rivulatus*, som förekommer i båda haven, har linserna från Medelhavets fiskar en kortare *fokallängd* än Röda havets population (avståndet mellan linsen och där ljuset

fokuseras är kortare i dessa linser). Detta visar sig vara en anpassning till det relativt mörkare och färgade vattnet som finns i Medelhavet då sådana linser hjälper fisken se bättre i denna miljö (Papper II).

För att bättre förstå dispersion hos fisklinser utforskade jag brytningsindexens beroendeförhållande av våglängd. Jag anpassade en matematisk modell som beskrev fisklinsers dispersion. Denna modell beskrev den experimentella datan noggrant när den testades mot två helt olika datasatser. Den ena datasats var brytningsindexvärden från ögon som tillhörde ett stort antal olika ryggradsdjur. Den andra datasatsen beskrev hur fisklinser fokuserar laserstrålar av olika våglängder (Papper III).

Genom att använda kunskapen om linsernas brytningsindexgradient och dispersionmodellen (Papper I & III), beskrev jag hur pass bra fiskarnas lösning på dispersion fungerade. Fiskarnas multifokala linser skapade skarpa färgbilder som var välanpassade till fiskarnas levnadssätt (Papper IV).

Chapter 1

Light, optics and imaging

Understanding vision requires basic knowledge of the physics of light. In this chapter, the basic concepts and principal properties of light in air and water are explained. Some of the various ways in which light interacts with matter are also presented. Finally, some central ideas concerning image formation are explained.

1.1 Light

The human world is a visual one. Vision occupies a large portion of our daily lives, thoughts, and culture. But without light sight is impossible. To understand any subject related to vision one must start with light's basic properties. Visible light is electromagnetic radiation. The three primary properties of light are its intensity, frequency and polarization. Light intensity describes the amount of radiant energy, the frequency relates to the wavelength of the light, and the polarization defines the orientation of the electromagnetic oscillations of the light waves. Due to it's dual nature, light simultaneously behaves as both a wave and a particle.

Light intensities vary greatly in nature. This holds true when comparing the difference in light intensities between a bright day on land and a dark night in the deep sea (as high as 20 orders of magnitude: Warrant and McIntyre (1992)). The frequency range of electromagnetic radiation found in natural environments is limited by the earth's atmosphere. The most prevalent visible wavelengths found in terrestrial habitats range between about 300 nm and 750 nm. In terrestrial environments the percentage of light that is polarized is generally low except when reflected from water bodies (such as lakes) or emitted by the sky at dawn and dusk (Cronin and Shashar, 2001; Shashar et al., 1998). While sunlight is not initially polarized,

it becomes polarized when scattered from various particles (such as the atmospheric molecules - the angle between the observer and the sun is closest to 90° at dawn and dusk, resulting in higher polarization in zenith).

Because polarization is dependent on the amount of scattered light, underwater light is highly polarized in silty waters (water with high organic material contents, dissolved minerals, and/or suspended materials such as in coastal waters). At depths greater than a few hundred meters the light field becomes cylindrically symmetrical around the vertical axis, regardless of the position of the sun (Jerlov, 1976; Johnsen and Widder, 1998), mainly due to the scattering of downwelling light. In contrast, at shallower depths, the light field is generally asymmetric, especially during sunset and sunrise (Jerlov, 1976; Johnsen, 2002), being brighter at azimuth angles pointing towards the sun and darker in the opposite direction.

A wave of light has an amplitude, phase, and frequency. The square of the amplitude is equivalent to the amount of energy the light wave's oscillations have at a particular point in time. The phase is the distinct time period in the wave cycle, while the frequency is the number of cycles per unit time that the light wave oscillates in. For simplicity, one could represent a wave as a sine function for an interval of 0° to 360°. Phase would be the X value in that function while amplitude would be the Y value. All natural light environments are not coherent; the phases of light waves are not all equal, not all light waves "start" at the same temporal point of the wave cycle.

1.2 The interaction of light with matter

Apart from of the intrinsic properties of light presented in the previous section, the way light interacts with matter is essential for understanding visually related phenomena occurring in nature. Following are some of the more relevant light-matter interactions that affect all visual input.

1.2.1 Absorption

In the oceans, the decline in the downwelling light intensity is exponential and reaches near zero values at a depth of about one kilometer when the water is clear (such nutrient deprived water is referred to as Jerlov water type I). This phenomenon is caused by the water molecules' light absorbance properties (Figure 1.1).

The water's absorbance coefficient is wavelength-dependent, and only a narrow band of light (in the blue) penetrates to greater depths. The spectral content of the downwelling light narrows quickly to 490 nm making the marine light environment bluer. The color of the water and the depth at which this color becomes dominant depends on the water quality. The absorption due to organic materials suspended

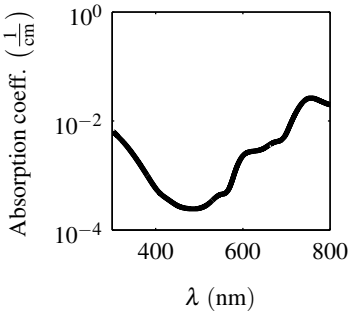

Figure 1.1: The absorption of pure water for wavelengths 300-800 nm. Taken from Hale and Querry (1973).

in the water is different from absorption due to water. In eutrophic lakes (i.e. lakes with high nutrient content), this affects the downwelling light's spectral content with longer wavelengths being relatively less absorbed making the light more yellow than blue.

1.2.2 Refraction

A light beam's trajectory is affected by the medium it travels through. The density of a non opaque material affects the speed with which a light beam penetrates through it. This phenomenon is called refraction and depends on the speed difference with which light travels through one medium compared to another. Snell's law describes that the ratio of the sines of the incident angle and the refracted angle (θ_1 & θ_2, respectively, in Equation (1.1) and Figure 1.2) is equal to the reciprocal ratio of the refractive indices (RIs) of the two materials (n_2 & n_1 in Equation (1.1) and Figure 1.2) through which the light travels:

$$n_1 \sin(\theta_1) = n_2 \sin(\theta_2). \tag{1.1}$$

The higher the refractive index of the material that the light enters, the slower the light travels through it, which results in a smaller refracted angle (θ_2).

When the incident angle is large enough so that $\frac{n_1 \sin(\theta_1)}{n_2}$ exceeds one, total

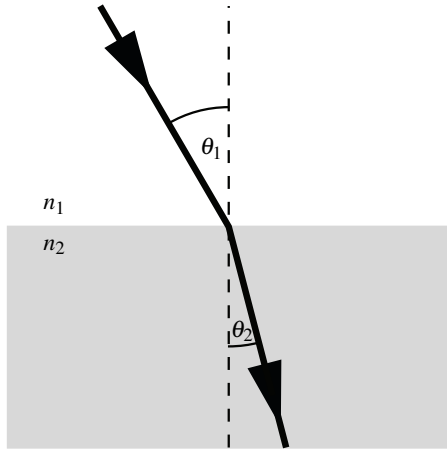

Figure 1.2: A refracted ray, traveling from one medium with refractive index n_1 to another medium with refractive index n_2. The ray's incident angle is θ_1 while the resulting refracted angle is θ_2. The relation between the two angles follows Snell's law (Equation 1.1).

reflection occurs. The light does not enter the second medium (with $RI = n_2$), and is totally reflected with an angle equal to the incident angle θ_1.

1.2.3 Diffraction

Another optical phenomenon is diffraction. Linked to the wave property of light, it refers to the way in which electromagnetic waves behave after passing a small opening (e.g. an iris). One of the most visible effects of diffraction is the so-called Airy disk, an image that results from shining light through a hole (where the size of this opening is on the order of the wavelength of that light) (Figure 1.3). This pattern can be explained by the Huygens-Fresnel principle. Consider the wavefront of the incoming light to be made of many (endless) wavefronts each of which having own amplitude and phase. These wavefronts propagate through the small opening and hit some arbitrary plane at a given distance from the hole. The resulting diffraction pattern can be explained by summing the amplitudes of all of these wavefronts. The amplitude is related to the phase the wavefronts had when passing the opening and the distance of the plane from the hole. The bright areas in the pattern are caused by the reinforcement of wavefronts; wavefronts having the same phase when hitting the plane will have the same amplitude. The dark areas can be explained by the anni-

hilation of wavefronts; wavefronts of phases such that the wave amplitudes oppose each other will cancel out one another. The phenomenon of wave reinforcement and annihilation is called interference.

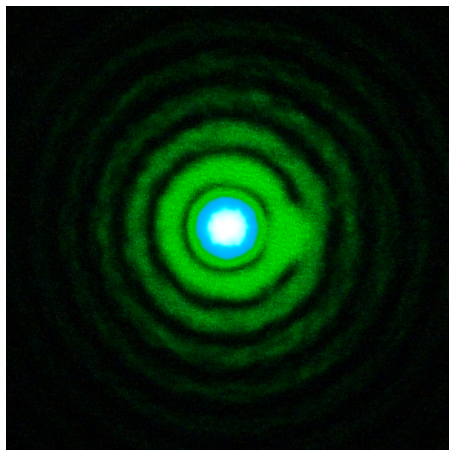

Figure 1.3: The diffraction pattern of a laser beam. Notice the concentrically arranged rings of light.

1.2.4 Dispersion

Dispersion describes the phenomenon that light rays of different wavelengths have different speeds while traveling through the same medium. Light passing through a medium can be described as the absorption and release of photons by the medium's atoms. When the resonance frequency of the material is close to that of the frequency of the light, absorption is large, and the light will not pass through that medium. However, in all other cases the medium will only slow down the photon's passage through the medium. Since the decrease in photon speed depends on the energy of the photon, and the latter is equivalent to the frequency of the light, two light rays with different frequencies (i.e. wavelengths) will pass through the same material at different speeds. The result being that a given material's RI is wavelength dependent. This affects the refraction of each wavelength separately causing a beam of white light to separate into its spectral colors when directed through a prism. Due to this wavelength-refraction dependency, optical systems that aim at focusing all wavelengths suffer from chromatic aberration, or chromatic blur (Figure 1.4): rays of different wavelengths are focused at different distances behind the optical system.

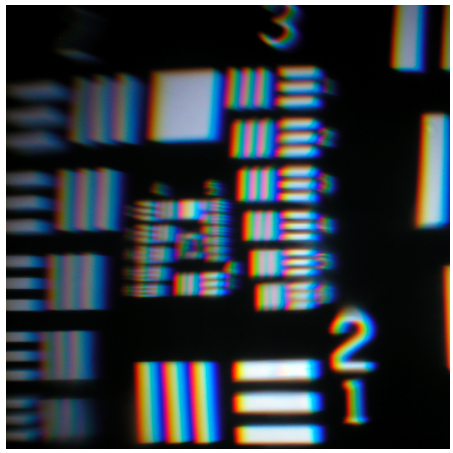

Figure 1.4: White light off-axis shown through a lens from an eye of the Humboldt squid, *Dosidicus gigas*. Notice the chromatic aberration visible at the colored borders of the white bars and numbers (picture taken by Alison Sweeney).

1.3 Imaging

A lens, an optical device which transmits and refracts light, is affected by the previously mentioned optical phenomena. Simple glass lenses have a homogeneous RI that differs greatly from that of air (air RI ≈ 1, glass ≈ 1.5). Their specific shapes (e.g. concave, convex, spherical, etc.) is responsible for their optical function (e.g. parallel light beams that strike a convex lens refract to a well defined focal point dependent of the beams' incidence angles). Some lenses, commonly known as gradient index (GRIN) lenses, are not homogeneous and have a refractive index gradient (RIG), describing the distribution of the different RI values in the lens. It is however important to notice that all lenses suffer from optical defects. Even a perfectly corrected lens is "diffraction limited"; such a lens still suffers from the diffraction pattern produced by its own aperture (Figure 1.3). Furthermore, this nearly perfect "diffraction limited" lens performs optimally for one wavelength only, and suffers from chromatic aberration caused by the lens material's dispersive properties (Figure 1.4).

The goal of an optical system is to deliver a relevant representation of the surroundings in the form of light signals. This is done by focusing the incident light onto an image plane. Light-sensitive components can be placed in the imaging plane. These convert light into electrical signals that can be further processed. In a digital

camera these components are the pixels on the camera chip. In most animal eyes, the image plane is the retina. This layer of cells contains the photoreceptors, light-sensitive cells that transform light energy into a change in cell membrane potential.

The vertebrate retina is a light-sensitive multi-layered structure at the back of the eye. A scene is imaged through the optics onto the retina. The distribution of the different light intensities and wavelengths present within the image is registered by the photoreceptors. The vertebrate retina generally has two types of photoreceptors, the rods and cones. These are tightly packed in the retina and form the mosaic of pixels that sample the animal's visual field. Rods and cones differ morphologically in most species. However, while rods are sensitive to one wavelength interval and low light levels, the cones come in different classes that are sensitive to different ranges of wavelength and require high light levels. The cones allow for color vision, based on opponent processing of signals from different classes of cones (short-, middle-, and long wavelength). The cone classes are used as opposing pairs of colors, where one class inhibits the resulting signal and the other excites it. This mechanism has a more cost effective information rate and is based on the fact that one cone's wavelength sensitivity overlaps another's (Hurvich and Jameson, 1957).

A formal way to assess the quality of an optical system is the point spread function (PSF) (Figure 1.5(a)). The PSF is a description of the extent to which a point light source is modulated through an optical system, and is a means by which one can measure image degradation. The ideal PSF has exactly the same shape and form as the point light source (the distribution of light intensities for the ideal point light source is a single point). The PSF reveals the sum of all the optical aberrations present in the system.

Using the PSF it is possible to calculate the modulation transfer function (MTF), which is simply the Fourier transform of the PSF (Figure 1.5(b)). The MTF describes how a spatial pattern is modulated by an optical system at increasing spatial frequency. By calculating signal degradation in terms of contrast (typically from 0 to 1), the optical system's performance can be evaluated across all relevant spatial frequencies. Since the sampling frequency of the retina is limited by the density of its individual light-sensitive units, frequencies that are higher than that of the light-sensitive-units can not be registered by the retina. This upper limit is called the *cutoff sampling frequency*.

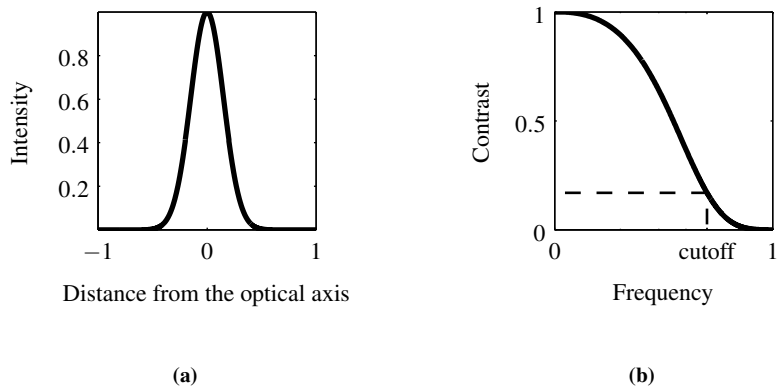

Figure 1.5: (a) An arbitrary point spread function. The X-axis is the distance between the optical axis and where a beam of light that passed through the optical system intersects the image plane. The Y-axis is the light intensity at that point. (b) The modulation transfer function of the point spread function in (a). The X-axis is the spatial frequency of the image being viewed through the optical system at hand, the Y-axis is the contrast at that frequency. The dashed line denotes an arbitrary cutoff frequency that limits the optical system due to the sampling frequency of the retina and its respective contrast.

Chapter 2

Biological imaging systems in air and water

Evolution gave rise to a myriad of different eyes, all of which being solutions to visual tasks characterized by the animals' ecological niches. Two such different habitats are the terrestrial and aquatic environments. Light's intensity, spectrum, and polarization differ markedly between these two habitats (see Section 1.1). In this chapter, an introduction to nature's diversified solutions to vision in air, water, and both are discussed with more emphasis on vision in fishes.

2.1 Eyes in air and water

There are many different eye designs in nature (e.g. compound, mirror, lens). However, one of the eye types that convergently evolved in both vertebrates and mollusks is the camera type eye (lens eye or simple eye). In fact, all vertebrates with eyes have camera type eyes. Mollusks can posses other types of eyes in addition to camera type eyes (e.g. mirror eyes in scallops, Pectinidae).

Aquatic camera eyes are not differently structured than terrestrial ones. Both types of camera eyes have a cornea as the external interface between the eye and its surroundings, a crystalline lens that further focuses the incoming light, and a retina that captures the light signal. The main differences is the RI of the media the eyes need to cope with, namely 1 and 1.34 for air and (sea) water, respectively. Due to this difference, light entering the terrestrial eye is refracted mostly by the cornea (where the difference between the air and cornea RI is ~ 0.4), while in the aquatic

eye it is the lens that does most (if not all) of the focusing. In aquatic vertebrates, the cornea is surrounded by water on the outside and the watery aqueous humor on the inside. Both media have relatively high refractive index and if the cornea is thin, which is the case in most species, then its refractive power is negligible (Matthiessen, 1886; Mandelman and Sivak, 1983).

Some animals are visually active in both media. These are amongst others many sea birds such as the cormorants (Phalacrocoracidae), the four-eyed fish (*Anableps anableps*), the Archer fish (*Toxotes chatareus*), many sea mammals such as harbor seals (*Phoca vitulina*), and even some tribes of sea nomads in Southeast Asia. These animals and humans use a variety of mechanisms to cope with the optical challenges of seeing in both water and air. Due to both the curvature and RI of the cornea, an emmetropic animal (i.e. an animal with a well focused visual system) in air becomes hyperopic (far sighted) underwater, while an animal that is emmetropic underwater becomes myopic (near sighted) when above water. This is due to the fact that the RI of the cornea is very close to that of the water, leaving the cornea with virtually no refractive power when immersed in water. In cormorants, corneal refractive power is approximately 55 Diopters. All this refractive power is lost when the bird submerges while pursuing fish. To accommodate for this optical change, the hypertrophied iris sphincter muscle presses the lens against the iris, increasing the curvature of the lens and thus its refractive power as well (Katzir and Howland, 2003; Glasser and Howland, 1996). Since *A. anableps* lives mostly at the water surface, its divided eyes are both exposed to air and water, where one part looks into the air and the other one into the water. These fish have a lens that is structured so that light coming ventrally from the water scene refracts more while light coming from the air scene above is refracted less by the lens and more by the cornea. Two separate retinas capture the focused images for further processing (Sivak, 1976). The archer fish has specialized areas in its retina with markedly different spectral sensitivities and spatial resolutions. These allow the fish to tackle the different visual tasks of predator avoidance from below (fish) or above (birds) as well as to sharpshoot its own prey (insects) (Temple et al., 2010). Seals are known to have flattened corneas. This allows an aquatically corrected optical system to operate above water. The flatness has no or very little effect on the eye underwater while minimizing the refractive power of the cornea in air. In combination with the powerful lens, images are well focused in both media (Sivak et al., 1989). The sea nomads compensate for their hyperopic eyes underwater by maximally constricting their pupils. This leads to larger depth of focus, compensating for hyperopia (Gislén et al., 2003).

2.2 Vision in fishes

The open sea is devoid of shelter, making vision an important sense for both predation and predator avoidance (Hamner, 1996; McFall-Ngai, 1990). In this environment, the visibility (or invisibility) of an animal is critical for its survival. Many complex adaptations have developed in response to these conditions. Among these are transparency (Chapman, 1976; Johnsen and Widder, 1998, 1999, 2001), cryptic coloration (Endler, 1978, 1990, 1991; Fuiman and Magurran, 1994; Herring and Roe, 1988; Muntz, 1990), mirrored body surfaces (Denton, 1970), counter shading and counter illumination (Cott, 1940; Denton et al., 1972; Ferguson and Messenger, 1991; Kiltie, 1988; McAllister, 1967), as well as morphological and behavioral adaptations that minimize apparent body or organ size (Seapy and Young, 1986). Further adaptations involve behavior: at least one function of diurnal vertical migration is to minimize visual predation. It has been suggested that animals that have mirrored sides would benefit from orienting their bodies to or away from the sun to minimize intense light reflections (Johnsen and Sosik, 2003), and cephalopods and heteropods orient their thin intestines into a vertical position regardless of their bodies' orientation (Seapy and Young, 1986). Counter adaptations for breaking these camouflage strategies include polarization vision, ultraviolet vision, colored ocular filters and offset visual pigments (Bowmaker and Kunz, 1987; Browman et al., 1994; Loew et al., 1993; Lythgoe, 1984; Muntz, 1990; Waterman, 1981).

Eye designs vary from simple folded regions of pigmented cells with an array of sensory cells to more complex designs, such as superposition eyes or eyes with multifocal lenses. In all cases, the evolutionary progress from the simplest to more complex systems was shown to depend on optical improvements in image quality (Nilsson and Pelger, 1994). A folded indentation of the area containing the light-sensitive cells allows directionality, where the simplified retina reacts only to stimuli coming from the non-shaded direction. The camera obscura like eyes of Nautilidae allow for some spatial resolution, limited by the surrounding light intensity. Lower light intensity requires a larger pupil, while for more acute vision a smaller pupil is advantageous. A larger pupil results in lower spatial resolution in darker light environments. The existence of a lens allows for good spatial resolution while still keeping a large pupil. The presence of a lens extended the range of light intensities in which animals can be active. The ability to move the lens along the optical axis (OA), or change its shape, allows for accommodation, changing the optical power of the optical system while maintaining good focus. Multifocal lenses allow for correct focusing of multicolored images while keeping the optical system small (Kröger et al., 1999). These lenses have several focal lengths in monochromatic light. The distances between the focal points along the OA are equivalent to the chromatic aber-

rations present in the lenses, and this compensates for chromatic blur (this will be explained in greater detail in 3.3.1 on page 17). Many other modifications exist in nature, allowing for optical finesses that are relevant for the different ecological requirements of the animals. Among the aquatic vertebrates, the lenses of bony fishes (teleosts) have received most attention, mainly because of easy access to fresh material and the simple geometry of the lenses, which typically are spherical (Pumphrey, 1961; Walls, 1964; Sivak and Luer, 1991).

Chapter 3

The optics of the fish lens

The visual scene of many fishes is colored. Many fish relay on color-rich signals for various tasks. The flickering light in shallow underwater environments complicates these tasks. Flickering augments the variation in light intensities present in the fish environment, making a system that is sensitive only to light intensity variations susceptible. However, color vision in combination with opponent processing simplifies visual processing in such an environment. Since the light flicker is not wavelength dependent (i.e. it occurs at all wavelengths), a visual system that can detect color differences, as opposed to only brightness differences, is advantageous (Maximov, 2000). However, such important color-rich signals are degraded by chromatic aberration. It is thus interesting to know to what extent this aberration affects image quality and with what optical mechanisms the animals cope with these effects. In order to learn more about the visual world of fishes, a more detailed understanding of their lens optics is required.

It is my aim to solve some of the unanswered questions regarding the form, function, and role of the periphery of the spherical fish lens (Paper I), light dispersion in the lens (Paper III), and compensation for chromatic aberration by the multifocal principle (Paper IV). In this chapter the functional morphology of the fish lens is explained. The formal methodology of ray-tracing is detailed by first presenting some experimental results and later theoretical ray-tracing. Last, the calculations related to inferring the RIG of the fish lens are shown.

3.1 Morphology

Spherical lenses made of homogeneous materials (e.g. glass) suffer from longitudinal spherical aberration (LSA). James C. Maxwell was the first to notice that fish lenses are almost free of LSA, and he postulated that they are gradient-index lenses (Maxwell, 1854). This was the first indication that the optical system of a fish eye is not as simple as it appears at first sight. In fish lenses, the outermost optical layer is the lens capsule, a thin acellular sheet of extracellular fibers that keeps the lens together and withstands its internal pressure. Thereafter follows the lens epithelium, a monolayer of metabolically active cells. The epithelium is absent from the posterior pole of the lens. Further inward there are many layers of lens fiber cells; thin cells that within each layer stretch from pole to pole, all concentrically arranged (Figure 3.1). In many vertebrates, including bony fishes, fiber cell geometry is somewhat more complicated, originating and ending in suture conformations that are line, 'Y', or star shaped (Kuszak et al., 2004). In the outer fiber layers of the lens, the cells contain all typical eukaryote organelles (Bassnett and Beebe, 1992; Bantseev et al., 1999, 2004). Further inwards, the cells lack organelles, including the nucleus with the genetic information, and appear at first sight to be little more than membrane bags filled with protein solutions of different concentrations, depending on the radial position in the lens. The RI distribution in the lens is a result of the crystallin protein concentration gradient. In fish lenses these are mainly α, β, and γ crystallin proteins (De Jong et al., 1988; Lindquist and Craig, 1988; Lubsen et al., 1988; Wistow et al., 1983, 1985). The highest concentration of crystallins is in the center of the lens, while the lowest is at its periphery. The RI distribution in the periphery of the lens (i.e. the capsule, epithelium, and outer fiber cell layers) has been speculated to follow the shape of a simplified polynomial function. While this interpretation would allow for good correction for LSA, I have shown that the RI distribution is different. A zone with a constant refractive index is present from about 0.94 lens radius (R) to the inner border of the capsule (Figure 3 in Paper I on page 41).

3.2 Physiology

Many fishes relay on visual input for locomotion control, mate finding, sustenance, and survival. Although these ecological needs are met by different modalities of the visual system in the animal (i.e. directionality, intensity, color, spatial and temporal resolution, edge detection, etc.), all gain from well-adapted optics throughout the lifespan of the animal. Regarding the fact that fish lenses can grow up to a thousandfold in volume throughout their lives (Fernald, 1991), maintaining high lens functionality requires a very precise regulative process.

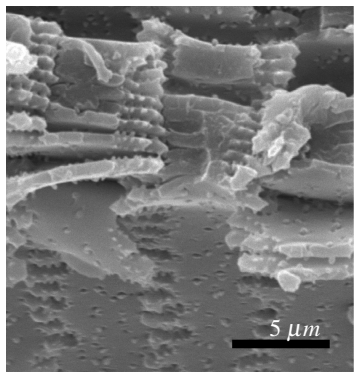

Figure 3.1: Scanning electron micrograph of *Astatotilapia burtoni* lens fiber cells. Lens radius was approximately 1 mm (picture taken by Ola Gustafsson).

The distribution of the RIG is rotationally symmetric. This allows the refraction of more peripheral rays of light to be mainly caused by the curvature of the lens (the incident angle) resulting in a relatively large deflection angle. The opposite occurs with more central rays, resulting in a smaller deflection angle. The shape of the RIG in the periphery of the lens is of crucial importance because all light enters the lens through its periphery and a large amount of this light bypasses the more central parts of the lens. Thus, even slight changes in the peripheral RIG result in significant differences in the optical quality of the lens (Campbell, 1984; Campbell et al., 1990; Jagger, 1992; Kröger et al., 2001). It has also been unclear how the metabolic activities and demands of epithelial and differentiating lens fiber cells affect the gradient in the peripheral region. In Paper I, I found that the nuclei containing zone has a constant refractive index (constant index zone, CZ). The correlation between the zone in which cell organelles are still present and where the refractive index is constant (the CZ) is probably due to physiological constraints on the metabolically active cells (Paper I). The part of the lens that is metabolically active (maintaining a metabolic level that requires the presence of cell organelles) requires a relatively constant concentration of ions, nutrients, and proteins, resulting in the constant RI. Additionally, the CZ seems to be a more parsimonious solution to the definition of the lens' RIG. This functionality requires some theoretical background which is explained in both Section 3.3.3 and Paper I.

3.3 Ray-tracing

3.3.1 Experimental background

Considerable efforts have been spent on finding rotationally symmetric refractive index gradients that minimize LSA in spherical lenses. The refractive index distribution has been studied since Matthiessen first proposed a parabolic form of this distribution (Matthiessen, 1882). Later he found that an elliptical index profile gives even better compensation for LSA (Matthiessen, 1893). Luneburg found an analytical solution to a spherical lens that is entirely free of LSA and has its focal point at its posterior pole (Luneburg, 1944). Attempts to understand animal lenses included measuring the refractive index in sections of the lens (Huggart, 1948; Nakao et al., 1968), or the protein concentrations in those sections (Philipson, 1969; Bando et al., 1976; Fagerholm et al., 1981). Scanning the lens with a thin laser beam and measuring the way the beam was deflected by the lens became the first non-destructive method for estimating the refractive index profiles in vertebrate lenses (Campbell and Hughes, 1981; Campbell, 1982). Fletcher et al. used the inverse Abel transform to infer what the RIG of a spherical lens must be for a given focal length (Fletcher et al., 1954). An LSA curve describes the distance between the center of the lens and the point where the refracted beam intercepts the OA as a function of the distance between the OA and the entering beam. The same idea was used by Chu to determine the RIs in cylindrical optical fiber preforms (Chu, 1977) and later extended to elliptical preforms (Barrell and Pask, 1978). Based on these studies Campbell used laser scanning and the inverse Abel transform to study the RIG of the rat lens (Campbell, 1984). This method demands that the examined lens is immersed in a medium of an RI that matches that of the lens surface (Campbell, 1984; Kröger et al., 1994) or is higher. Laser scanning methods have been used to investigate the optical properties of a variety of animal lenses (Sivak, 1982b,a; Fernald and Wright, 1983; Mandelman and Sivak, 1983; Sivak and Kreuzer, 1983) as well as to deduct the lenses' RIGs using the inverse Abel transform (Campbell, 1984; Axelrod et al., 1988; Pierscionek, 1988; Kröger et al., 1994; Pierscionek, 1995). Magnetic Resonance Imaging and Optical Coherence Tomography are two methods recently introduced for determining the RIGs of animal and human lenses (Garner et al., 2001; Acosta et al., 2005; Vazquez et al., 2006; Verma et al., 2007). However, none of these methods can produce results that are sufficiently detailed and exact to study the solution to another complication for animal vision: longitudinal chromatic aberration (LCA).

Fish lenses are powerful, and focal lengths shorter than 2.5 R have been frequently reported (Matthiessen, 1882, 1893; Campbell and Gubish, 1967; Sroczyński, 1975a,b, 1977, 1978, 1979; Fernald and Wright, 1983; Campbell, 1984; Sivak and Luer, 1991; Kröger and Campbell, 1996). Powerful lenses have a short depth of fo-

cus, such that chromatic defocus is a serious problem. In fishes, the problem of LCA is particularly severe, since a number of species are sensitive to wavelengths from the near ultraviolet to the near infrared (Bowmaker and Kunz, 1987; Bowmaker et al., 1991). In the blue to ultraviolet range, color dispersion - and thus LCA - increases rapidly with decreasing wavelength. It was therefore unclear how well-focused color images could be created by a single lens.

The enigma was solved when it was discovered that fish lenses are multifocal (Kröger et al., 1999). The lenses have LSA curves of complex shapes that lead to several focal lengths in each lens for monochromatic light. The distances between the focal points along the OA are equal to the focal length differences due to LCA between the wavelengths that are of highest importance to the animals. This means that for each of these wavelengths there is a focal point on the retina. A sharp color image is created on the background of defocused light that has passed through the 'wrong' zones in the lens. The multifocal principle is a successful solution, being present not only in fishes (Karpestam et al., 2007; Kröger et al., 1999, 2009; Malkki et al., 2003; Schartau et al., 2009) but also in tetrapods (Hanke et al., 2008; Lind et al., 2008; Malmström and Kröger, 2006). The optical systems of animal eyes have turned out to be much more sophisticated than previously realized, which motivates more detailed investigations of crystalline lenses and their optical properties. This is the aim of the present thesis.

3.3.2 Theoretical background

The procedure used to simulate the functions of a gradient index lens is based on the approximation that fish lenses are spherically symmetrical. In these lenses, the trajectory of a ray can be described using three angles (Figure 3.2). The angle between the tangent of the ray at a given point P and the radius is α, the polar angle between the OA and a line pointing at point P from the lens center C is ϕ and ψ is the deflection angle of the ray from its original course at point P. These angles relate to each other as follows:

$$\psi = \phi + \alpha. \tag{3.1}$$

The following conservation law is true for all spherically symmetrical systems:

$$rn(r)\sin\alpha = n_m \mathrm{BEP} = b, \tag{3.2}$$

where r is the distance between point P and the system's center, C, $n(r)$ is the RI at that point, α is the angle between the tangent of the ray and the line between point P and C, and n_m is the medium's RI (Figure 3.2).

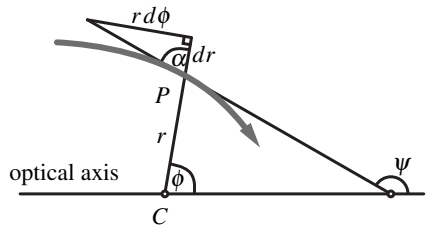

Figure 3.2: A light ray's trajectory through a rotationally symmetrical spherical lens. C denotes the lens' center, r is the distance from point P to the center, ϕ is the angle between the optical axis and point P, α is the angle between the tangent of point P and the radius and ψ is the deflection angle of the ray at point P.

The right hand side of Equation (3.2) is a constant depending only on the distance between the entrance beam and the optical axis, beam entrance position (BEP) and will hereafter be referred to as b. By normalizing all RIs to n_m, b is equal to the ray's BEP value. Notice that when α equals 90°, r reaches its smallest value. In rotationally symmetrical lenses, all rays have a symmetry point. This is the point where the ray is the closest to the lens' center. After the ray has reached this point, it starts exiting the lens on a path that is symmetrical to the ray's entering path. Snell's conservation law (Equation 1.1) states that for any given distance r from the lens center,

$$n_{in} \cdot \sin \alpha_{in} = n_{out} \cdot \sin \alpha_{out}, \tag{3.3}$$

where n_{in} and n_{out} stand for the RIs inside and outside any layer, respectively. Multiplying Equation (3.3) by r and taking into account the relationship in (3.2) the contribution of one layer to the deflection angle ψ equals:

$$\Delta\psi = 2 \cdot \left[\arcsin \frac{b}{r \cdot n_{out}} - \arcsin \frac{b}{r \cdot n_{in}} \right]. \tag{3.4}$$

Regarding the RIG as a step function, where each fiber cell layer contains a homogeneous RIG, the contribution of all the layers each given ray passed through is summed up to calculate the ray's deflection angle (Equation 3.4). Using each beam's deflection angle and BEP value, the Back Center Distance (BCD) can be calculated. If the RIG is regarded as a continuous function, the deflection angle ψ can be calculated as follows. Continuing from Equation (3.1), the trajectory of the

ray can now be described by,

$$\frac{dr}{r} = \frac{d\phi}{\tan\alpha}, \tag{3.5}$$

where ϕ is the polar angle between the OA and a line pointing at a point on the light-ray trajectory from the center of the lens. Logarithmic derivation of Equation (3.2) gives:

$$\frac{d\xi}{\xi} = \frac{d\alpha}{\tan\alpha}, \tag{3.6}$$

where ξ is $r \cdot n(r)$, implying:

$$\frac{d\xi}{\xi} = \frac{dr}{r} + \frac{dn}{n}. \tag{3.7}$$

By subtracting Equation (3.5) from Equation (3.6) and using the equalities in equations (3.7) and (3.1), the relationship between the total deflection of the ray (the cumulative deflection), and the RIG function is expressed as:

$$\frac{dn}{n} = -\frac{d\psi}{\tan\alpha}. \tag{3.8}$$

From Equation (3.4), tan α can be calculated to be:

$$\tan\alpha = \pm\frac{b}{\sqrt{\xi^2 - b^2}}. \tag{3.9}$$

The sign of the right hand side of Equation (3.9) depends on whether the ray is on its way in (i.e. before reaching the symmetry point) or out. For simplicity we can also normalize all the length units to the lens' radius, R. We can now write Equation (3.5) and (3.8) using Equation (3.9) as:

$$\Delta\phi(b) = 2b\int_{r_{min}}^{1} \frac{1}{r\sqrt{(rn(r))^2 - b^2}}dr \tag{3.10}$$

$$\Delta\psi(b) = -2b\int_{n(r_{min})}^{n_R} \frac{1}{n\sqrt{n^2r^2 - b^2}}dn. \tag{3.11}$$

The deflection angle can be used to calculate the resulting BCD (and thus the angular spread):

$$BCD = \frac{b}{\sin(\Delta\psi(b) + 2\gamma)}. \tag{3.12}$$

BCD denotes the distance from the lens' center to where the ray intersects with the OA (Figure 1 in Paper I on page 39). γ is the cumulative deflection angle achieved from the ray's refraction at the lens' periphery, where the capsule, epithelium, and CZ are. This was calculated in the same way as described for the finite model since these layers have a homogeneous RI.

3.3.3 Inferring the refractive index gradient

The model lens was based on a spherical lens consisting of a number of layers with varying thicknesses and RIs. Scanning and transmission electron microscopy (Figure 3.1) revealed approximately 1500 cell layers with an average thickness of $0.67 \cdot 10^{-3}$ R (all values normalized to lens radius, 1 mm). Each layer was homogeneous in RI. To find the RIG, an optimization algorithm was used (Figure 3.3).

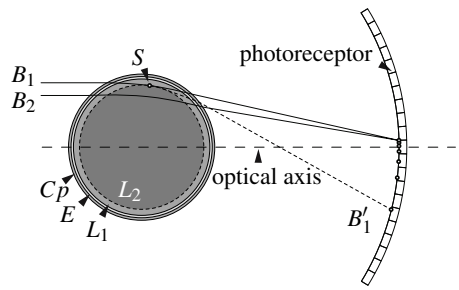

Figure 3.3: Illustration of the finite algorithm. The lens was initially constructed of the capsule, epithelium, and a single inner layer, Cp, E, and L_1, respectively, where the inner layer was the rest of the lens to its center. A ray of light, B_1, was sent through the lens. The symmetry point of the ray trajectory through the lens, S, denoted the location for the border to the next layer. A second ray, B_2, with a smaller beam entrance position value was then used to calculate the refractive index of the new inner layer, L_2, so that the ray would hit the retina at the edge of the centered photoreceptor. The initial ray, B_1, will now overshoot the focal point, B'_1. More inner layers and their respective refractive indices were iteratively found in the same way (i.e. B_2's symmetry point denoted the border of the next layer etc.). This process was stopped when the resulting, inner refractive index was smaller than the previous, outer refractive index. The dots show the typical skewed distribution of light on the retina. This pattern is true only for rays that have their symmetry points within the same layer.

The basic algorithm of the optimization process of the RIG is described as follows. The lens was initially constructed of the capsule, epithelium and inner layer

alone, where the inner layer was the rest of the lens to the center (i.e. 0 to 0.98 R). A ray of light was sent through the lens from BEP equal to 1 R. Its symmetry point denoted the location for the border of the next layer. A second ray with a smaller BEP value (a decrease of 0.0007 R was used) was then used to calculate the RI of the new inner layer so that the ray would hit the retina at the edge of the centered photoreceptor (Figure 3.3). More inner layers and their respective refractive indices were iteratively found in the same way. This process was stopped when the resulting RI was smaller than the previous RI.

The advantages of this algorithm lie in the manner with which rays distribute on the retina. Because of the curvature of the lens, the incident angle and the constant RI in each layer, the rays' distribution on the retina is skewed. Given two BEP values, $B_2 < B_1$, such that all rays between these two values have symmetry points that lie within the same layer, rays with smaller BEP (i.e. larger than but closer to B_2) will be aggregated together. Rays with larger BEP (i.e. smaller than but closer to B_1) will be more dispersed (Figure 3.3). Thus a layer's RI should be adjusted so that the ray with the innermost symmetry point (i.e. the ray with the symmetry point closest to the border of the next inner layer) will hit the edge of the center photoreceptor. In this way the skewed distribution of light on the retina contributes to minimizing point source dispersion.

If we regard the lens RIG as a smooth function (i.e. not as a step function), the number of layers in the lens is infinite. It is possible to use Equation (3.11) to calculate what $n(r)$ needs to be for a given $\Delta\psi(b)$. This is done with the inverse Abel transform. The forward Abel transform for a function $f(q)$ is defined as:

$$g(p) = 2p \int_p^\infty \frac{f'(q)dq}{\sqrt{q^2 - p^2}}. \tag{3.13}$$

The function $f(q)$ is retrieved by the inverse Abel transform:

$$f(q) = -\frac{1}{\pi} \int_q^\infty \frac{g(p)dp}{\sqrt{p^2 - q^2}} + c, \tag{3.14}$$

with c as the integration constant.

Since the RIG does not stretch beyond the surface of the lens, the upper bound of the integral in Equation (3.14) can be set to the (normalized) radius of the lens, and Equation (3.11) can be written as:

$$\Delta\psi(b) = -2b \int_b^1 \frac{\frac{1}{n}\frac{dn}{d\xi}}{\sqrt{\xi^2 - b^2}} d\xi = -2b \int_b^1 \frac{\ln(n(\xi))'}{\sqrt{\xi^2 - b^2}} d\xi. \tag{3.15}$$

We then implement the inverse Abel transform and get the implicit RIG as a function of ξ:

$$n(\xi) = n_R \exp\left(\frac{1}{\pi}\int_{\xi}^{1} \frac{\Delta\psi(b)}{\sqrt{b^2-\xi^2}}db\right), \tag{3.16}$$

where n_R is the RI on the surface of the lens. The inverse Abel transform implicitly requires the function $\xi(r)$ to be non-decreasing, and hence in particular to have a maximum value not exceeding the lens radius times the immersion medium's RI or $\xi \leq 1$ in the normalized case. Without the requirement of an increasing $\xi(r)$, there is an infinite number of possible RIGs all leading to lenses with identical LSA curves. This lack of uniqueness prohibits inferring the true RIG from the LSA curve. With the extra condition of an increasing ξ function throughout the lens and into the surrounding medium, uniqueness is secured and the inverse Abel transform can be used to determine the RIG from the LSA curve.

The monotonicity condition is not met at the surface of the lens because of a downward jump in refractive index (and hence in ξ) from the lens surface into the surrounding medium (Campbell, 1984; Kröger et al., 1994). Because of this, one has to experimentally determine the RIGs of fish lenses from the surface inwards to the point where the normalized ξ has decreased to the value of 1 or below. From this point and further inwards, Equation (3.16) (slightly modified: since the RIG starts from the CZ inwards, the upper bound of the integral is set to equal the radial distance of the CZ's inner border) can be used to determine the exact shape of the RIG if the focusing properties of the lens are known. Since a rotationally symmetric lens is also rotationally symmetric around the OA, it is sufficient to know the ray paths in a meridional plane of the lens. Interestingly, a constant RI will result in the shortest distance from the lens surface needed to diminish the normalized ξ to 1. The CZ of the cichlid *H. burtoni* lens stretches well beyond the point at which $\xi = 1$, uniquely defining the lens RIG. Since the width of the CZ is larger than what is needed for a unique RIG, it is most probably affected by physiological constraints as well (Paper I).

3.4 Lens adaptations

Fishes' optical systems are adapted to the specific visual needs of each species. These adaptations include spectral adaptive tuning of the photoreceptors' absorptions in the fish retina, matching the photoreceptor's peak sensitivity to the light environment's spectrum (Bowmaker et al., 1994; Lythgoe et al., 1994; McDonald and Hawryshyn, 1995; Cummings and Partridge, 2001). Equivalent adaptations are present in fish

lenses as well. It was found that the LSA shape of a number of teleosts is species-specific, implying that the fishes' different visual ecologies required unique optical solutions (Karpestam et al., 2007; Malkki et al., 2003). Kröger et al. (2001) demonstrated this connection by rearing fish under different light regimes for long periods of time and showing that the change in light environment affected their lenses. Schartau et al. (2009) have shown in the South American cichlid *Aequidens pulcher* changes in the optical properties of the lens between day and night. These changes occur in parallel to retinomotor movements in the retina: from a functionally all-cone retina (color vision) at day to an all-rod retina (grayscale vision) at night. The refractive changes lead to a switch from a multifocal lens at day to a monofocal lens at night.

The Suez Canal (opened 1869) has enabled the comparison between populations of the same species living in two markedly different light environments, the Red Sea and the Mediterranean Sea, with clearer waters in the Red Sea than in the Mediterranean (see Section 1.1 for factors affecting the water's inherent optical properties). I showed that the rivulated rabbitfish, *Siganus rivulatus*, Forsskål 1775, lenses are adapted to the darker and tinted waters of the Mediterranean (Paper II). Lenses from the Mediterranean increased the fish's visual sensitivity and compensated for the monochromatic light with lenses that had a shorter mean BCD value than those found in the Red Sea population (Figure 3 in Paper II on page 50). These examples indicate that the optical properties of the fish lens are plastic and can change to better suit a specific visual task.

3.5 Multifocal lenses

While theoretical dispersion equations rely on physical constants and hold true for relatively homogeneous materials, the complexity of the material found in living vertebrate lenses (e.g. water, different proteins and lipids, ions, ion complexes, etc.) discourages their use. The multitude of different dispersive factors (electrons at various energetic levels and electric dipole molecules) results in the same number of parameters to be included in the dispersion Equation. The established shape of the RIG (Paper I) was therefore used to investigate dispersion in the fish lens (see Section 1.2.4 for a more detailed explanation of dispersion). A dispersion model was successfully fitted to two separate datasets: 1) measured RIs of various ocular media from a multitude of different vertebrates and 2) the LCA determined by laser-scanning in the crystalline lens of the African cichlid fish, *Astatotilapia burtoni* (see Figure 3 in Paper III on page 60). This dispersion model was essential for determining the specific functionality of the multifocal principle in fishes.

Although the multifocal principle has been discovered in many vertebrate species (see Section 3.3.1), its actual visual benefit and function has not yet been

demonstrated. In Paper IV the advantages of multifocal lenses are therefore explored by comparing a variety of optical properties between natural, monofocal, and multifocal lenses. While monofocal lenses perfectly focus one wavelength, the short focal length in combination with the chromatic aberration these fish lenses have degrades the image at all other wavelengths. This results in an image relatively rich in spatial information (i.e. high contrast and sharp edges) but no spectral integrity (wrong hues and bland colors). Multifocal lenses offer an optimal trade-off between spatial and spectral information. A somewhat blurry image at all wavelengths is superior to one with one very sharp wavelength and many very blurry wavelengths (see Figure 3 in Paper IV on page 67).

A wavelength mismatch between the light being focused by the multifocal lens and the light that is maximally absorbed by the photoreceptors resulted in defocused images. Only matching combinations of retina - lens resulted in good performance. Considering the large variation of visual pigments in fish retinas (Lythgoe et al., 1994; Bowmaker et al., 1994), the adaptive variation of the optical properties of fish lenses should follow the spectral tuning of fish retinas (see Section 3.4), accompanied by physiological mechanisms that regulate the lens properties to match those of the retina.

3.6 Future work

A necessary and interesting step in the investigation of multifocal lenses will be testing them in the laboratory. Real fish lenses' PSFs should be measured *in vitro* and compared to model results as well as used to simulate the modulation of hyperspectral images as done in Paper IV. This step will bolster the methodology and insights gained in Paper IV.

The adaptation of these lenses should be further explored by comparing more animals from divergent light regimes. Fish living at different depths and/or in various habitats with deviating life styles and ecologies (e.g. fish with different visual tasks) should display differences in multifocality equivalent to the expected (or recorded) variations in their spectral sensitivities. This kind of studies may shed more light on the adaptation and tuning of the lens' multifocality.

Bibliography

Acosta, E., D. Vazquez, L. Garner, and G. Smith (2005). Tomographic method for measurement of the gradient refractive index of the crystalline lens. i. the spherical fish lens. *Journal of the Optical Society of America A 22*(3), 424 – 433.

Axelrod, D., D. Lerner, and P. J. Sands (1988). Refractive index within the lens of a goldfish eye determined from the paths of thin laser beams. *Vision Research 28*(1), 57–66.

Bando, M., A. Nakajima, M. Nakagawa, and T. Hiraoka (1976). Measurement of protein distribution in human lens by micro spectrophotometry. *Experimental Eye Research 22*(4), 389–392.

Bantseev, V., K. L. Herbert, J. R. Trevithick, and J. G. Sivak (1999). Mitochondria of rat lenses: distribution near and at the sutures. *Investigative Ophthalmology and Visual Science 40*(4), 881.

Bantseev, V., K. L. Moran, D. G. Dixon, J. R. Trevithick, and J. G. Sivak (2004). Optical properties, mitochondria, and sutures of lenses of fishes: a comparative study of nine species. *Canadian Journal of Zoology 82*(1), 86–93.

Barrell, K. F. and C. Pask (1978). Nondestructive index profile measurement of noncircular optical fibre preforms. *Optics Communications 27*(2), 230–234.

Bassnett, S. and D. C. Beebe (1992). Coincident loss of mitochondria and nuclei during lens fiber cell differentiation. *Developmental Dynamics 194*(2), 85–93.

Bowmaker, J., V. Govardovskii, S. Shukolyukov, J. L. Zueva, D. Hunt, V. Sideleva, and O. Smirnova (1994). Visual pigments and the photic environment: The cottoid fish of lake baikal. *Vision Research 34*(5), 591–605.

Bowmaker, J. K. and Y. W. Kunz (1987). UV receptors tetrachromatic color vision and retinal mosaics in the brown trout *Salmo trutta* age-dependent changes. *Vision Research 27*(12), 2101–2108.

Bowmaker, J. K., A. Thorpe, and R. H. Douglas (1991). UV-sensitive cones in the goldfish. *Vision Research 31*(3), 349–352.

Browman, H., I. Novales-Flamarique, and C. Hawryshyn (1994). Ultraviolet photoreception contributes to prey search behaviour in two species of zooplanktivorous fishes. *Journal of Experimental Biology 186*(0), 187–198.

Campbell, F. W. and R. W. Gubish (1967). The effect of chromatic aberration on visual acuity. *Journal of Physiology 186*, 558–578.

Campbell, M. C., E. M. Harrison, and P. Simonet (1990). Psychophysical measurement of the blur on the retina due to optical aberrations of the eye. *Vision Research 30*(11), 1587–1602.

Campbell, M. C. W. (1982). *Gradient refractive index optics and image quality in the rat eye*. Ph. D. thesis, Australian National University.

Campbell, M. C. W. (1984). Measurement of refractive index in an intact crystalline lens. *Vision Research 24*(5), 409–416.

Campbell, M. C. W. and A. Hughes (1981). An analytic, gradient index schematic lens and eye for the rat which predicts aberrations for finite pupils. *Vision Research 21*(7), 1129–1148.

Chapman, G. (1976). Transparency in organisms. *Experientia (Basel) 32*(1), 123–125.

Chu, P. L. (1977). Nondestructive measurement of index profile of an optical-fibre preform. *Electronics Letters 13*(24), 736–738.

Cott, H. B. (1940). *Adaptive colouration in animals*. Meuthen and Co. Ltd Press.

Cronin, T. W. and N. Shashar (2001). The linearly polarized light field in clear, tropical marine waters: Spatial and temporal variation of light intensity, degree of polarization and e-vector angle. *The Journal of experimental biology 204*, 2461–2467.

Cummings, M. and J. Partridge (2001). Visual pigments and optical habitats of surfperch (embiotocidae) in the california kelp forest. *Journal of Comparative Physiology A: Neuroethology, Sensory, Neural, and Behavioral Physiology 187*, 875–889.

De Jong, W. W., J. A. M. Leunissen, P. J. M. Leenen, A. Zweers, and M. Versteeg (1988). Dogfish alpha crystallin sequences comparison with small heat shock proteins and schistosoma egg antigen. *Journal of Biological Chemistry 263*, 5141–5149.

Denton, E. (1970). On the organization of reflecting surfaces in some marine animals. *Philosophical Transactions of the Royal Society of London B Biological Sciences 258*(824), 286–313.

Denton, E., J. Gilpin-Brown, and P. Wright (1972). The angular distribution of the light produced by some meso pelagic fish in relation to their camouflage. *Proceedings of the Royal Society of London Series B Biological Sciences 182*(1067), 145–158.

Endler, J. (1978). A predator's view of animal color patterns. *Evolutionary Biology 11*, 319–364.

Endler, J. (1990). On the measurement and classification of color in studies of animal color patterns. *Biological Journal of the Linnean Society 41*(4), 315–352.

Endler, J. (1991). Variation in the appearance of guppy color patterns to guppies and their predators under different visual conditions. *Vision Research 31*(3), 587–608.

Fagerholm, P. P., B. Philipson, and B. Lindström (1981). Normal human lens - the distribution of protein. *Experimental Eye Research 33*(6), 615–620.

Ferguson, G. and J. Messenger (1991). A countershading reflex in cephalopods. *Proceedings of the Royal Society of London Series B Biological Sciences 243*(1306), 63–68.

Fernald, R. D. (1991). Teleost vision: seeing while growing. *The journal of experimental zoology supplement 5*, 167–180.

Fernald, R. D. and S. E. Wright (1983). Maintenance of optical quality during crystalline lens growth. *Nature 301*(5901), 618–620.

Fletcher, A., T. Murphy, and A. Young (1954). Solutions of two optical problems. *Proceedings of the Royal Society of London A 223*, 216–225.

Fuiman, L. and A. Magurran (1994). Development of predator defences in fishes. *Reviews in Fish Biology and Fisheries 4*(2), 145–183.

Garner, L. F., G. Smith, S. Yao, and R. C. Augusteyn (2001). Gradient refractive index of the crystalline lens of the black oreo dory (*Allocyttus niger*): comparison of magnetic resonance imaging (MRI) and laser ray-trace methods. *Vision Research 41*(8), 973–979.

Gislén, A., M. Dacke, R. H. H. Kröger, M. Abrahamsson, D.-E. Nilsson, and E. J. Warrant (2003). Superior underwater vision in a human population of sea gypsies. *Current Biology 13*, 833–836.

Glasser, A. and H. C. Howland (1996). A history of studies of visual accommodation in birds. *Quarterly review of biology 71*, 475–509.

Hale, G. M. and M. R. Querry (1973). Optical constants of water in the 200 nm to 200 μm wavelength region. *Appl. Opt. 12*, 555–563.

Hamner, W. (1996). *Predation, cover, and convergent evolution in epipelagic oceans*, pp. 17–37. Gordon and Breach Publishers.

Hanke, F. D., R. H. H. Kröger, U. Siebert, and G. Dehnhardt (2008). Multifocal lenses in a monochromat: the harbour seal. *Journal of Experimental Biology 211*, 3315–3322.

Herring, P. and H. Roe (1988). The photoecology of pelagic oceanic decapods. *Symposia of the Zoological Society of London 59*, 263–290.

Huggart, A. (1948). On the form of the iso-indicial surfaces of the human crystalline lens. *Acta Ophthalmologica Scandinavica 64*, 1–126.

Hurvich, L. M. and D. Jameson (1957). An opponent-process theory of color vision. *Psychological Review 64*, 384–404.

Jagger, W. S. (1992). The optics of the spherical fish lens. *Vision Research 32*(7), 1271–1284.

Jerlov, N. G. (1976). *Marine Optics*. Elsevier.

Johnsen, S. (2002). Cryptic and conspicuous coloration in the pelagic environment. *Proceedings of the Royal Society Biological Sciences Series B 269*(1488), 243–256.

Johnsen, S. and H. Sosik (2003). Cryptic coloration and mirrored sides as camouflage strategies in near-surface pelagic habitats: Implications for foraging and predator avoidance. *Limnology and Oceanography 48*(3), 1277–1288.

Johnsen, S. and E. Widder (1998). Transparency and visibility of gelatinous zooplankton from the northwestern atlantic and gulf of mexico. *Biological Bulletin (Woods Hole) 195*(3), 337–348.

Johnsen, S. and E. Widder (1999). The physical basis of transparency in biological tissue: Ultrastructure and the minimization of light scattering. *Journal of Theoretical Biology 199*(2), 181–198.

Johnsen, S. and E. Widder (2001). Ultraviolet absorption in transparent zooplankton and its implications for depth distribution and visual predation. *Marine Biology (Berlin) 138*(4), 717–730.

Karpestam, B., J. Gustafsson, N. Shashar, G. Katzir, and R. H. H. Kröger (2007). Multifocal lenses in coral reef fishes. *Journal of experimental biology 210*, 2923–2931.

Katzir, G. and H. C. Howland (2003). Corneal power and underwater accommodation in great cormorants (*Phalacrocorax carbo sinensis*). *The Journal of experimental biology 206*(5), 833–841.

Kiltie, R. (1988). Countershading universally deceptive or deceptively universal? *Trends in Ecology and Evolution 3*(1), 21–23.

Kröger, R. H. H., S. C. Braun, and H.-J. Wagner (2001). Rearing in different photic and chromatic environments modifies spectral responses of cone horizontal cells in adult fish retina. *Visual Neuroscience 18*(6), 857–64.

Kröger, R. H. H. and M. C. W. Campbell (1996). Dispersion and longitudinal chromatic aberration of the crystalline lens of the african cichlid fish *Haplochromis burtoni*. *Journal of the Optical Society of America A 13*(12), 2341 – 2347.

Kröger, R. H. H., M. C. W. Campbell, and R. D. Fernald (2001). The development of the crystalline lens is sensitive to visual input in the african cichlid fish, *Haplochromis burtoni*. *Vision Research 41*, 549–559.

Kröger, R. H. H., M. C. W. Campbell, R. D. Fernald, and H. J. Wagner (1999). Multifocal lenses compensate for chromatic defocus in vertebrate eyes. *Journal of Comparative Physiology A Sensory Neural and Behavioral Physiology 184*(4), 361–9.

Kröger, R. H. H., M. C. W. Campbell, R. Munger, and R. D. Fernald (1994). Refractive index distribution and spherical aberration in the crystalline lens of the african cichlid fish *Haplochromis burtoni*. *Vision Research 34*, 1815–1822.

Kröger, R. H. H., K. A. Fritsches, and E. J. Warrant (2009). Lens optical properties in the eyes of large marine predatory teleosts. *Journal of comparative physiology a-neuroethology sensory neural and behavioral physiology 195*, 175–182.

Kuszak, J. R., R. K. Zoltoski, and C. Sivertson (2004). Fibre cell organization in crystalline lenses. *Experimental Eye Research 78*(3), 673–687.

Lind, O. E., A. Kelber, and R. H. H. Kröger (2008). Multifocal optical systems and pupil dynamics in birds. *Journal of Experimental Biology 211*, 2752–2758.

Lindquist, S. and E. A. Craig (1988). *The heat-shock proteins*, pp. 631–678. Annual Reviews, Inc.: Palo Alto.

Loew, E., W. McFarland, E. Mills, and D. Hunter (1993). A chromatic action spectrum for planktonic predation by juvenile yellow perch, *Perca flavescens*. *Canadian Journal of Zoology 71*(2), 384–386.

Lubsen, N. H., H. J. M. Aarts, and J. G. G. Schoenmakers (1988). The evolution of lenticular proteins: the beta- and gamma-crystallin super gene family. *Progress in Biophysics and Molecular Biology 51*, 47–76.

Luneburg, R. K. (1944). *Mathematical theory of optics*. Providence, R.I.: Brown U. Press.

Lythgoe, J. (1984). Visual pigments and environmental light. *Vision Research 24*, 1539–1550.

Lythgoe, J. N., W. R. A. Muntz, J. C. Partridge, J. Shand, and D. M. B. Williams (1994). The ecology of the visual pigments of snappers (Lutjanidae) on the great barrier reef. *Journal of Comparative Physiology A: Neuroethology, Sensory, Neural, and Behavioral Physiology 174*, 461–467.

Malkki, P. E., E. Löfblad, and R. H. H. Kröger (2003). Species - specific differences in the optical properties of crystalline lenses of fishes. *ARVO Annual Meeting Abstract Search and Program Planner 2003*, 3483.

Malmström, T. and R. H. H. Kröger (2006). Pupil shapes and lens optics in the eyes of terrestrial vertebrates. *Journal of Experimental Biology 209*(1), 18–25.

Mandelman, T. and J. G. Sivak (1983). Longitudinal chromatic aberration of the vertebrate eye. *Vision Research 23*(2), 1555–1560.

Matthiessen, L. (1882). Ueber die beziehungen, welche zwischen dem brechungsindex des kerncentrums der krystalllinse und den dimensionen des auges bestehen. *Pflüger's Archiv 27*, 510–523.

Matthiessen, L. (1886). Ueber den physikalisch-optischen bau des auges der cetaceen und der fische. *Pflüger's Archiv 38*, 521–528.

Matthiessen, L. (1893). Beiträge zur dioptrik der kristalllinse. *X. Zeitschrift für vergleichende Augenheilkunde 7*, 102–146.

Maximov, V. V. (2000). Environmental factors which may have led to the appearance of colour vision. *Philosophical Transactions of the Royal Society B 355*, 1239–1242.

Maxwell, J. (1854). Some solutions of problems 2. *Cambridge and Dublin Mathematical Journal 8*, 188–195.

McAllister, D. (1967). The significance of ventral bio luminescence in fishes. *Science Report of the Yokosuka City Museum 13*(13), 5–6.

McDonald, C. G. and C. W. Hawryshyn (1995). Intraspecific variation of spectral sensitivity in threespine stickleback (*Gasterosteus aculeatus*) from different photic regimes. *Journal of Comparative Physiology A: Neuroethology, Sensory, Neural, and Behavioral Physiology 176*, 255–260.

McFall-Ngai, M. (1990). Crypsis in the pelagic environment. *American Zoologist 30*(1), 175–188.

Muntz, W. (1990). *Stimulus, environment and vision in fishes*, pp. 491–511. New York: Chapman & Hall.

Nakao, S., S. Fujimoto, R. Nagata, and K. Iwata (1968). Model of refractive index distribution in the rabbit crystalline lens. *Journal of the Optical Society of America A 58*(8), 1125–1130.

Nilsson, D.-E. and S. Pelger (1994). A pessimistic estimate of the time required for an eye to evolve. *Proceedings of the Royal Society of London Series B Biological Sciences 256*, 53–58.

Philipson, B. (1969). Distribution of protein within the normal rat lens. *Investigative Ophthalmology and Visual Science 8*(3), 258–270.

Pierscionek, B. K. (1988). Nondestructive method of constructing 3-dimensional gradient index models for crystalline lenses .1. theory and experiment. *American Journal of Optometry and Physiological Optics 65*(6), 481–491.

Pierscionek, B. K. (1995). The refractive index along the optic axis of the bovine lens. *Eye (London, England) 9*, 776–782.

Pumphrey, R. J. (1961). *Concerning vision*. London: Cambridge University Press.

Schartau, J. M., B. Sjögreen, Y. L. Gagnon, and R. H. H. Kröger (2009). Optical plasticity in the crystalline lenses of the cichlid fish *Aequidens pulcher*. *Current Biology 19*, 122–126.

Seapy, R. and R. Young (1986). Concealment in epipelagic pterotracheid heteropods gastropoda and cranchiid squids cephalopoda. *Journal of Zoology Series A 210*(1), 137–148.

Shashar, N., T. W. Cronin, L. B. Wolff, and M. A. Condon (1998). The polarization of light in a tropical rain forest. *Biotropica 30*, 275–285.

Sivak, J. G. (1976). Optics of eye of 4-eyed fish (*Anableps-anableps*). *Vision Research 16*, 531.

Sivak, J. G. (1982a). Optical characteristics of the eye of the flounder. *Journal of Comparative Physiology A Sensory Neural and Behavioral Physiology 146*(3), 345–350.

Sivak, J. G. (1982b). Optical properties of a cephalopod eye (the short finned squid *Illex illecebrosus*). *Journal of Comparative Physiology A Sensory Neural and Behavioral Physiology 147*(3), 323–328.

Sivak, J. G., H. C. Howland, J. West, and J. Weerheim (1989). The eye of the hooded seal *Cystophora cristata* in air and water. *Journal of Comparative Physiology A Sensory Neural and Behavioral Physiology 165*(6), 771–778.

Sivak, J. G. and R. O. Kreuzer (1983). Spherical aberration of the crystalline lens. *Vision Research 23*(1), 59–70.

Sivak, J. G. and C. A. Luer (1991). Optical development of the ocular lens of an elasmobranch *Raja eglanteria*. *Vision Research 31*(3), 373–382.

Sroczyński, S. (1975a). Die sphärische aberration der augenlinse der regenbogenforelle (*Salmo gairdneri, Rich.*). *Zoologische Jahrbücher, Physiologie 79*, 204–212.

Sroczyński, S. (1975b). Die sphärische aberration der augenlinse des hechts (*Esox lucius L.*). *Zoologische Jahrbücher, Physiologie 79*, 547–558.

Sroczyński, S. (1977). Spherical aberration of crystalline lens in the roach *Rutilus rutilus*. *Journal of Comparative Physiology A Sensory Neural and Behavioral Physiology 121*(1), 135–144.

Sroczyński, S. (1978). Die chromatische aberration der augenlinse der bachforelle (*Salmo trutta fario, L.*). *Zoologische Jahrbücher, Physiologie 82*, 113–133.

Sroczyński, S. (1979). Das optische system des auges des flussbarsches (*Perca fluviatilis, L.*). *Zoologische Jahrbücher, Physiologie 83*, 224–252.

Temple, S., N. S. Hart, N. J. Marshall, and S. P. Collin (2010). A spitting image: specializations in archerfish eyes for vision at the interface between air and water. *Proceedings of the Royal Society B: Biological Sciences 277*(1694), 2607–2615.

Vazquez, D., E. Acosta, G. Smith, and L. Garner (2006). Tomographic method for measurement of the gradient refractive index of the crystalline lens. ii. the rotationally symmetrical lens. *Journal of the Optical Society of America A 23*(10), 2551–2565.

Verma, Y., K. D. Rao, M. K. Suresh, H. S. Patel, and P. K. Gupta (2007). Measurement of gradient refractive index profile of crystalline lens of fisheye in vivo using optical coherence tomography. *Applied Physics B: Lasers and Optics 87*, 607–610.

Walls, G. L. (1964). *The vertebrate eye and its adaptive radiation*. New York: The Cranbrook Press.

Warrant, E. J. and P. D. McIntyre (1992). *The trade off between resolution and sensitivity in compound eyes*, pp. 391–421. CRC Press.

Waterman, T. (1981). *Polarization sensitivity*, pp. 281–469. New York: Springer.

Wistow, G., L. Summers, and T. Blundell (1985). *Myxococcus xanthus* spore coat protein S may have a similar structure to vertebrate lens $\beta\,\gamma$-crystallins. *Nature 315*, 771–773.

Wistow, G., B. Turnell, L. Summers, C. Slingsby, D. Moss, L. Miller, P. Lindley, and T. Blundell (1983). X-ray analysis of the eye lens protein gamma-2 crystallin at 1-9 angstrom resolution. *Journal of Molecular Biology 170*, 175–202.

Acknowledgments

I thank *Ronald K.* for the endless support and priceless guidance. You have sparked my curiosity to start, encouraged me to continue, and helped me to finish this Ph.D. I enjoyed and probably will continue enjoying our discussions about the bigger and much smaller details of fish optics.

I also thank *Bosse* for the tireless and meticulous explanations about everything mathematic. I would have never been able to accomplish this without your iron patience.

Thank you *Ola* for reminding me to stop and smell the stones, and thank you *Marcus* for laughing (on the inside) at my jokes. Being utterly insane and obnoctious is entirely remedied by having good friends like You. Thank you for the fruitful discussions and support. We did this together. *Olle*, thank you for your music, brain, and sympathetic outcries.

Thank you *Henrik* for jumping off bridges with me, and thank you *Magnus* for understanding everything I mean to say. You have helped me countless of times (and will continue doing so in the future no doubt) in everything concerning the set of non-negative integers between 0 and 255. But moreover I cherish your friendship and support.

I thank our two Danish representatives, *Thomas* for saving me from becoming all fishy and *Anders* for being kind of fishy. Thank you *Rikard* for all the help and the absence of any red line. Thank you *Wilma* for playing with me and introducing me to *Eva*. Thanks *Joaquin* for teaching me to stop and smell the flowers, and *Jochen* for teaching me to stop and smell the beer.

I thank *Almut* for all the laughs and helpful advice. Thank you *Eric W.* for encouraging me to do my MSc, reading my texts, and 4$^{\text{th}}$ last word in Section 1.2.4 at page 5. Thank you *Dan* for being an encyclopedia of visual facts (even better than WIKIPEDIA). I cannot believe you did not move your office *Marie*, thank you for your support, stamina, and advice.

Thank you *Malin* for your "hummer". Thank you *Emily*, *Femke*, *Lina*, *Linda*, *Megan*, *Miriam*, *Therese*, *Torill*, *Björn*, *David*, *Ekatarina*, *Eric H.*, *Josef*, *Lars E.*, *Ronald P.*, *Birgit*, *Tim*, *Hema*, *Jamie*, *Johan*, and *Tony* for tons of fun and keeping this place a joy to work at.

Thanks to the technical help of *Lennart*, *Carina*, *Eva*, *Rita*, *Ylwa*, *Margaret*, *Stefan*, *Camilla*, and *Peter* I survived these 4 years without burning the lab, destroying a computer, or ruining a microscope (to either my knowledge or anyone else's).

I thank all my wonderful friends and family. My mother *Pnina*, for giving me the curiosity, imagination, and courage needed to be a researcher. My father *Francois*, for the logics, methodology, and humor. My sister *Iris*, for the music we

hear. My brother *Yarden*, for setting the standard. My *Cohen* part of the family, for believing in me. *Bob*, for being my best friend and introducing me to *Ron*. *Guy* for making me laugh so hard. *Jonathan*, for being a real person. *Flavius*, for making me look polite. *Martin*, for teaching me the true value of details.

Thank you *Ninna* ♡ for being the best thing that ever happened to me. For supporting me in every way, without you I would have never been able to finish this thesis.

Paper I

Effects of the peripheral layers on the optical properties of spherical fish lenses

Yakir L. Gagnon,[1,*] Bo Söderberg,[2] and Ronald H. H. Kröger[1]

[1]*Department of Cell and Organism Biology, Lund University, Helgonavägen 3, 22 362 Lund, Sweden*
[2]*Department of Theoretical Physics, Lund University, Sölvegatan 14, 22 362 Lund, Sweden*
[*]*Corresponding author: 12.yakir@gmail.com*

Received January 28, 2008; revised July 17, 2008; accepted August 8, 2008;
posted August 12, 2008 (Doc. ID 92100); published September 17, 2008

We created a computational optical model of spherical fish lenses that takes into account the effects of the peripheral layers, which differ in cellular composition from the bulk of the lens. A constant refractive index, except for the lens capsule, in the outer about 6% of lens radius made it possible to uniquely infer the refractive index gradient in more central layers from a known or desired longitudinal spherical aberration curve using the inverse Abel transform. Since the zone of constant refractive index is wider than necessary to make the solution unique and for optimal optical performance of the lens, we propose that its width be set by the metabolic needs of the lens.
OCIS codes: 330.7326, 000.1430, 080.6755, 110.2760, 170.1420.

1. INTRODUCTION

Vision is an important source of information for many animals, and a variety of different eye types have evolved [1]. In this paper we concentrate on the camera-type eyes of vertebrates. Although generally similar in design to a camera, the optical systems of these eyes are apparently much simpler than that of a good camera objective, which consists of a number of lenses to correct for various kinds of optical aberrations. In the vertebrate eye, there are at maximum only two refractive elements: the cornea and the crystalline lens.

In aquatic vertebrates, the cornea is surrounded by water on the outside and the watery aqueous humor on the inside. Both media have relatively high refractive index, and if the cornea is thin, which is the case in most species, then its refractive power is negligible [2,3]. The task of focusing light on the retina is thus left to the lens alone. Among the aquatic vertebrates, the lenses of bony fishes (teleosts) have received the most attention, mainly because of easy access to fresh material and the simple geometry of the lenses, which typically are spherical [4–6].

Spherical lenses made of homogenous materials (e.g., glass) suffer from longitudinal spherical aberration (LSA). James C. Maxwell was the first to notice that fish lenses are almost free of LSA, and he postulated that they are gradient-index lenses [7]. This was the first indication that the optical system of a fish eye is not as simple as it appears at first sight.

Considerable efforts have been spent on finding radially symmetric refractive index gradients (RIGs) that minimize LSA in spherical lenses. The refractive index distribution has been studied since Matthiessen first proposed a parabolic form of this distribution [8]. Later he found that an elliptical index profile gives even better compensation of LSA [9]. Luneburg found an analytical solution to a spherical lens that is entirely free of LSA and has its focal point at its posterior pole [10]. Attempts to understand animal lenses included measuring the refractive index in sections of the lens [11,12] and the protein concentrations in those sections [13–15]. Scanning the lens with a thin laser beam and measuring the way the beam was deflected by the lens became the first nondestructive method for estimating the refractive index profiles in vertebrate lenses [16,17]. Fletcher *et al.* used the inverse Abel transform to infer what the RIG of a spherical lens must be for a given LSA curve [18]. Such an LSA curve describes the distance between the center of the lens and the point where the refracted beam intercepts the optical axis (OA) as a function of the distance between the OA and the entering beam. The same idea was used by Chu to determine the refractive indices in cylindrical optical fiber preforms [19] and later extended to elliptical preforms [20]. Based on these studies Campbell used laser scanning and the inverse Abel transform to study the RIG of the rat lens [21]. This method reqires that the examined lens be immersed in a medium of a refractive index (RI) that at least matches that of the lens surface [21,22] or is higher.

Laser scanning methods have been used to investigate the optical properties of a variety of animal lenses [2,23–26] as well as to deduct the lenses' RIGs using the inverse Abel transform [21,22,27–29]. Magnetic resonance imaging and optical coherence tomography are two methods recently introduced for determining the RIGs of animal and human lenses [30–33]. However, none of these methods can produce results that are sufficiently exact and detailed to study the solution to another complication for animal vision: longitudinal chromatic aberration (LCA).

Fish lenses are powerful, and focal lengths shorter than 2.5 lens radii (R) have been reported frequently [5,8,9,21,23,34–40]. Powerful lenses have short depth of focus, such that chromatic defocus is a serious problem. In fishes, the problem of LCA is particularly severe, since a

number of species are sensitive to wavelength from the near ultraviolet (UV) to the near infrared (IR) [41,42]. In the blue to UV range, color dispersion—and thus LCA—increases rapidly with decreasing wavelength. It was therefore unclear how well-focused color images could be created by a single lens.

The enigma was solved when it was discovered that fish lenses are multifocal [43]. The lenses have LSA curves of complex shapes that lead to several focal lengths in each lens for monochromatic light. The distances between the focal points along the optical axis are equal to the focal length differences due to LCA between the wavelengths that are of highest importance to the animals. This means that for each of these wavelengths there is a focal point on the retina. A sharp color image is created on the background of defocused light that has passed through the "wrong" zones in the lens. The multifocal principle is a successful solution, being present not only in fishes [43–45] but also in a wide variety of terrestrial vertebrates [46]. The optical systems of animal eyes have turned out to be much more sophisticated than previously realized, which motivates more detailed investigations of crystalline lenses and their optical properties. We studied the simplest case, i.e., the spherical fish lens with radial internal symmetry.

Most of the above-mentioned studies ignored the optical importance of the outer region of the lens and assumed a continuous RIG from the center of the lens to its surface. This is, however, not compatible with lens morphology. In fish lenses, the outmost optical layer is the lens capsule, a thin acellular sheet of collagen fibers that keeps the lens together and withstands its internal pressure. Thereafter follows the lens epithelium, a monolayer of metabolically active cells. Further inward there are many layers of lens fiber cells; thin cells that within each layer stretch from pole to pole, all concentrically arranged. In many vertebrates, including bony fishes, fiber cell geometry is somewhat more complicated [47], but this is not of relevance to our considerations. We also neglect that the epithelium is absent from the posterior pole of the lens. In the outer fiber layers of the lenses the cells contain all typical eukaryote organelles [48–50]. Further inward, the cells have broken down their organelles, including the nucleus with the genetic information, and appear at first sight to be little more than membrane bags filled with protein solutions of different concentrations, depending on the radial position in the lens.

The peripheral layers of fish lenses pose a vexing problem. The shape of the RIG in the periphery of the lens is of crucial importance because all light enters the lens through its periphery and a large amount of this light bypasses the more central parts of the lens. Thus, even slight changes in the peripheral RIG result in significant differences in the optical quality of the lens [21,51–53]. It is also unclear how the metabolic activities and demands of epithelial and differentiating lens fiber cells affect the gradient in the peripheral region.

The aims of this study were to (i) measure the thickness and RI of the lens capsule, (ii) determine the shape of the RIG in the peripheral cell layers of the lens, (iii) develop an optical model of a monofocal fish lens, and (iv) use this model to investigate the functional importance of the RIG's shape in fish lenses. Extending the studies to multifocal lenses was beyond the scope of the work presented here.

2. MATERIAL AND METHODS

The experimental investigations were performed in accordance with Swedish animal welfare legislation and approved by governmental bodies. We used lenses from the African cichlid fish *Astatotilapia* (formerly *Haplochromis*) *burtoni*. The animals were obtained from Simontorp Säteri (Blentarp, Sweden) and sacrificed by rapid decapitation and pithing.

A. Lens Capsule

Whole lens capsules were peeled off freshly excised lenses and cut into pieces with a razor blade (5–10 pieces per lens capsule) with the preparation immersed in phosphate buffered saline (PBS, pH 7.4, 290 mosmol). The pieces of lens capsule were stained for 1 min with 1% acid fuchsin in PBS and washed once with PBS for a few seconds. The specimens were mounted on microscope slides and cover-slipped with spacers in PBS. The preparation was sealed with nail polish.

Stacks of optical sections, starting at the surface of the capsule and ending at the surface of the microscope slide, were obtained with an LSM 510 Meta confocal microscope (Zeiss, Oberkochen, Germany) using a green He–Ne laser (567 nm). The thickness of each optical section was 0.42 μm. The thickness of the capsule was determined from 3D representations of the stack of optical sections and converted to units of lens radius (R).

The RI of the capsule was measured with a Zeiss interference microscope equipped with an Ehringhaus tilting compensator. The phase shift of monochromatic light of 650 nm was determined at the position at which capsule thickness had been measured. The RI of PBS was measured with a DR 5000 automatic digital refractometer (Krüss, Hamburg, Germany) at 589 nm. Correction for the difference in RI between 589 and 650 nm was not performed because the RI of water changes only at the fourth decimal between these wavelengths [54]. Refractive index of the lens capsule was calculated following earlier work by Nilsson and co-workers [55,56]. Control measurements were performed on unstained pieces of lens capsule and at increasing times after the dissection.

B. Outer Cell Layers

Transmission electron microscopy was used to qualitatively determine differences in protein concentrations in the peripheral cell layers of the lens. Freshly excised lenses were fixated over night in 2.5% glutaraldehyde, 1% paraformaldehyde in 0.07 M phosphate buffer, pH 7.4, washed 6 times 10 min in PBS, stained with 1% osmium tetroxide in 0.07 M phosphate buffer, washed 6 times 10 min in demineralized water, dehydrated in an ethanol series to acetone, and embedded in Epon.

Sections 50 nm in thickness were made of the periphery of the lens in a meridional plane with an Ultracut UCT ultramicrotome (Leica Microsystems, Wetzlar, Germany) using a diamond knife. The sections were poststained with 2% uranyl acetate in demineralized water

and lead citrate according to [57] and examined with a JEM-1230 transmission electron microscope (JEOL, Tokyo, Japan). The intensity of the electron beam was adjusted so that the embedding medium (the brightest area in the section) did not become so bright as to flare. Images were taken with a digital camera (MultiScan 791, Gatan, Pleasanton, California, USA) with an exposure time that was equal for all images. All slices came from the same area of the lens, which was not controlled in any manner in relation to the OA of the lens.

Image densitometry was performed on 15 micrographs each (1024×1024 pixels) from three lenses of three different animals. The analysis was performed with MATLAB (R2007a) and without any image improvement measures. Similar procedures have been used in earlier studies [13,15]. Within a 20-pixel-wide strip that had its long axis perpendicular to the lens surface and ran across the micrograph, pixel intensity values were read out. The strips were placed so that abnormalities such as dirt, scratches, folds of the section, and gaps in the cell layers were avoided as much as possible. For smoothing of the data, 20 (short axis of strip) times 15 (long axis of strip) pixel values were averaged (windowed-average) after the highest and lowest 5% of the values had been excluded. The resulted value was assigned to the center of the window along the long axis of the strip.

C. The Model

The modeled lens used in this study is partly based on the inverse Abel transform, in a way similar to that in earlier studies [18–22,28,29,35,58–60]. The reader is advised to consult the mentioned reports (e.g. [19,21]) for more detailed descriptions of the mathematical procedures involved in calculating ray trajectories. Generally, these procedures require the lens to have a RI distribution that is radially symmetric. The correctness of this assumption has been bolstered specifically for the lenses of *A. burtoni* by the results of Fernald and Wright [23]. Thus the deflection angle, $\Delta\psi(b)$, of any given paraxial ray is evaluated with

$$\Delta\psi(b) = -2b\int_{r_{\min}}^{1}\frac{\mathrm{d}n/\mathrm{d}r}{n\sqrt{\xi^2-b^2}}\mathrm{d}r, \qquad (1)$$

where b is the entrance position of the ray (i.e., the distance from the ray to the OA), n is the RI of the lens at each r distance from the lens center, $r_{\min}$ is the minimum distance of each given ray from the lens center, and ξ is equal to $r\,\mathrm{n}(r)$. All units are normalized to the lens radius and the surrounding medium's RI (see Fig. 1).

As has been done in the earlier studies, the RIG can be inferred from the LSA curve of a given lens by using an inverse Abel transform on Eq. (1), which yields the index n as a function of $\xi=rn$:

$$n(\xi) = 1\exp\left[\frac{1}{\pi}\int_{\xi}^{1}\frac{\Delta\psi(b)}{\sqrt{b^2-\xi^2}}\mathrm{d}b\right]. \qquad (2)$$

The inverse Abel transform implicitly requires the function $\xi(r)$ to be nondecreasing and hence in particular to have a maximum value not exceeding the lens radius times the immersion medium's RI or $\xi\leqslant 1$ in the normalized case. Without the requirement of an increasing $\xi(r)$, there are an infinite number of possible RIGs all leading to lenses with identical LSA curves. This lack of uniqueness prohibits inferring the true RIG from the LSA curve. With the extra condition of an increasing ξ function throughout the lens and into the surrounding medium, uniqueness is secured, and the inverse Abel transform can be used to determine the RIG from the LSA curve.

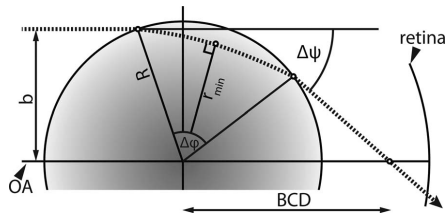

Fig. 1. Trajectory of a ray (dotted line) passing through the lens. R denotes the radius of the lens, while $r_{\min}$ is the distance from the lens center to the point where the ray comes closest to the center. This point is called the symmetry point because the ray's trajectory outward from this point is symmetrically identical to its way inward. $\Delta\psi$ is the total deflection angle, $\Delta\varphi$ is the angular extent of the ray's trajectory in the lens, b is the ray's entrance position, which is the lateral distance between the incoming ray and the optical axis, OA, and BCD is the back center distance, i.e., the distance from the lens center to where the beam intercepts the OA.

The monotonicity condition is not met at the surface of the lens because of a downward jump in refractive index (and hence in ξ) from the lens surface into the surrounding medium [21,22]. Because of this, we experimentally determined the RIGs of fish lenses from the surface inward to the point where the normalized ξ has decreased to the value of 1 or below. From this point and further inward, Eq. (2) (slightly modified as explained below) can be used to determine the exact shape of the RIG if the focusing properties of the lens are known. Since a radially symmetric lens also is rotationally symmetric around the OA, it is sufficient to know the ray paths in a meridional plane of the lens.

To create the lens model, we incorporated the measured RI and thickness of the lens capsule as well as the measured thickness of the lens epithelium. With the dimensions and RIs of the peripheral layers being determined by experimental results, we used the method of the inverse Abel transform to determine the RIG for a hypothetical monofocal fish lens with an assumed focal length of 2.322 R, which is the mean focal length of *A. burtoni* lenses at a wavelength of 633 nm. The RIs of the aqueous and vitreous humors, i.e., the media in which the lens is immersed in the intact eye, were set to 1.336 [22].

3. RESULTS

A. Lens Capsule

The results of control measurements indicated that the RI of the lens capsule was unaffected by the staining with acid fuchsin and that the time needed to do the preparation and take measurements was well below the lifetime of the preparation. A typical interference micrograph is shown in Fig. 2. On these micrographs, large similarly

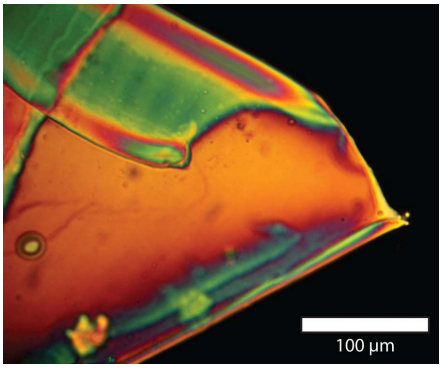

Fig. 2. (Color online) Interference micrograph of a piece of a lens capsule. Note the large orange area that indicates constant phase shift. Other colors occur because of folds and edge disturbances.

colored zones were visible, indicating a constant phase shift equivalent to a constant optical path length.

Overall mean capsule thickness was 11.6±1.7 μm standard deviation (SD), and the capsule RI was 1.394±0.012 SD (N=4). The RI of the capsule, normalized to the RI of the medium (1.336), was equal to 1.043 (Table 1).

B. Outer Cell Layers

The average radius of the lenses used for the densitometry was 1.01±0.02 mm SD (N=3). The capsule and epithelium thicknesses were pooled among the lenses because all slices were taken from the same vicinity in the lens and were not expected to show any of the possible variation in the lens as a whole (as opposed to the interference microscope experiment). The mean capsule and epithelium thicknesses were 13.0±2.8 μm SD and 9.6±1.9 μm SD, respectively (N=47).

The transmission electron micrograph in Fig. 3(a) shows that the capsule and epithelium are clearly defined and that the subsequent layers of lens fiber cells are concentrically arranged, parallel to the lens surface. Each layer has about the same density throughout the micrograph.

It was evident that pixel brightness did not drop rapidly directly after the epithelium, but dropped first at some distance from the lens surface. This zone of constant density will be referred to as the constant-index zone (CZ). The inward-following zone where pixel brightness gradually decreased will be called the gradient zone (GZ).

Table 1. Mean Lens Radius, Capsule Thickness, and Refractive Index with Their Corresponding Standard Deviations for Multiple Measurements from Four Individual *A. burtoni* Fish

Fish #	N[a]	Radius (mm)	Thickness (μm)	RI (λ=633 nm)
1	10	1.50	10.7±1.3	1.410±0.022
2	5	1.28	9.9±0.6	1.392±0.017
3	7	1.19	12.2±0.6	1.385±0.012
4	7	1.46	13.7±0.4	1.387±0.019
Mean		1.36±0.15	11.6±1.7	1.394±0.012

[a]Number of individual capsule pieces measured (not the number of radius measurements, which was measured only once per lens).

The numerical results are plotted in Fig. 3(b) as a function of the distance from the lens center. Between 952 μm and the interior border of the epithelium at about 991 μm there was little change in pixel brightness, which confirmed the existence of a CZ, as can be seen in Fig. 3(a). Further inward, pixel brightness gradually decreases, first slowly, then more rapidly. At 880 μm, pixel brightness approached zero, i.e., the lower end of the dynamic range of the camera. The full complement of cell organelles is present only in fiber cells more peripheral than 92% R [61]. For the examined lenses this border was at approximately 932 μm from the lens center. The border was thus located 20 μm interior to where the GZ began and just exterior to the steepest decrease in pixel brightness [see Fig. 3(b)]. The absence of an increase in density at the capsule may have been due to differences in how osmium tetroxide, lead citrate, and uranyl acetate bound to the collagen fibers in the capsule and the crystallin proteins in the fiber cells.

C. The Model

The epithelium and lens fiber cells in the CZ differed little in electron density, such that we assume them to have the same concentration of proteins and thus also the same RI. This enables the restriction of the RIG reconstruction based on the inverse Abel transform to the part of the lens inside the CZ. To adjust the calculation of the RIG to account for these observations, we change the upper bound of the integral in Eq. (2) (normalized) from 1 to $\xi(r_{CZ})$, as well as the multiplicative constant from 1 to $n(r_{CZ})$. Since the integral can be used to infer the RIG only for the interval of $0 \leq r \leq r_{CZ}$, the deflection angle function, $\Delta\psi(b)$, used in the Abel transform must describe the contribution of the GZ alone. We therefore adjust $\Delta\psi(b)$ to read [for $0 \leq b \leq \xi(r_{CZ})$]

$$\Delta\psi(b) = \sin^{-1}\left(\frac{b}{BCD}\right) - 2\sum_{i=1}^{m}\left[\sin^{-1}\left(\frac{b}{n_i r_i}\right) - \sin^{-1}\left(\frac{b}{n_{i+1} r_i}\right)\right], \quad (3)$$

where m=2 is the number of distinct borders between different RIs. These are the capsule's outer surface and the epithelium's outer surface, with i equal to 1 and 2, respectively. The calculated RIG presented in Fig. 4(a) was obtained for a capsule thickness of 0.009 R, an epithelium and CZ thickness together of 0.051 R (with the CZ bordering at 0.94 R), and an epithelium CZ RI of 1.361. This is the lowest RI value measured for metabolically active living cells (1.361–1.364) [62] and was used as the peripheral index by Kröger and co-workers [22]. This RIG produces a completely constant-index LSA curve for all beams hitting the lens between the OA and out to a b value, given by the product of the CZ RI and the radial position of the CZ's inner border, which will hereafter be referred to as the largest corrected b (LCB). More peripheral beams pass only through the capsule, epithelium, and CZ. Figure 4(b) shows that constant RI of the

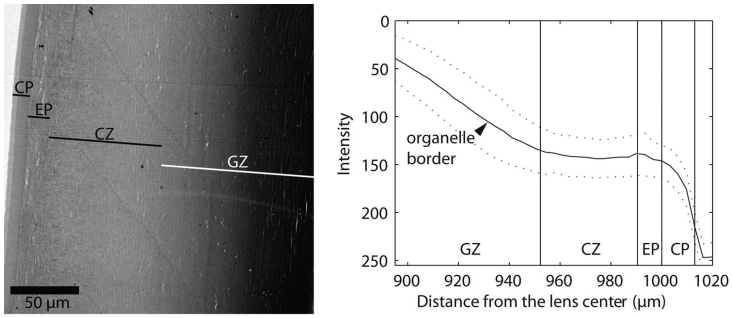

(a) (b)

Fig. 3. (a) Transmission electron micrograph of the peripheral region of a meridional section of an *A. burtoni* lens. CP, capsule; EP, epithelium. The concentric layers of lens fiber cells are divided into two zones: CZ, the constant-index zone, and GZ, the gradient zone. (b) Pixel brightness is plotted as a function of radial distance from the lens center in micrometers. Note that the y axis is reversed. The thick black curve is a windowed average of all the slices, while the dotted curves indicate the standard deviations (N=47). The vertical lines separate the different lens zones shown in (a). The 92% R border more central to which cell organelles are absent is also marked in the figure.

epithelium/CZ leads to considerable positive LSA for high b values. This aberration persists until b is equal to or smaller than the LCB. For the constant-index zone RI, we also used the capsule's RI (1.394, Fig. 4(c)), which is close to values for peripheral fiber cell layers measured by Matthiessen in fishes [63] and Pierscionek in bovine lenses [64]. In that case, LCB increases but is still smaller than R (Fig. 4(d)). However, the grazing incidence of light on the lens capsule for high b values leads to a severe loss of intensity by reflection (Fig. 4(e)), which together with a strong positive LSA in the peripheral part causes spreading and thus loss of light incident at high b values (Fig. 4(f)).

We used the model to further investigate the effects of different CZ widths and RIs and found that the central RI is positively correlated with the CZ RI and negatively correlated with the CZ width. The width and RI of the constant-index zone have effects on the LSA curve and thus influence the optical quality of the lens. In was beyond the scope of this study to investigate these effects in full detail.

4. DISCUSSION

A. Strengths and Weaknesses of the Model

The lens model presented here is the first one that takes into account the structure of the outermost layers of vertebrate lenses. The main weakness of the model is the abrupt start of the GZ (Figs. 4(a) and 4(c)), which is incompatible with the densitometry results (Fig. 3), which indicate a smooth transition between the CZ and GZ. Such a gradual start of the RIG most likely has a dampening effect on the strong positive LSA in the periphery of the lens (Figs. 4(b) and 4(d)). However, in the absence of reliable experimental results and/or well-founded assumptions, we refrained from incorporating in the model such a smooth start of the RIG.

Another problem is the RI of the epithelium/CZ, because experimental results are difficult to obtain. Matthiessen [63] found 1.386 to 1.388 as the cortical index in fish lenses. Pierscionek [64] measured the surface index of decapsulated bovine lenses with a fiber sensor and found values of about 1.4. If bovine lenses have CZs similar similar to those of fish lenses, this would reflect the RI of the CZ, although some peripheral cell layers were lost in the decapsulation procedure. Kröger *et al.* [22] measured the RI of fish lens cortical material with an Abbe refractometer and argued that such measurements can be biased only toward higher values by more central cell layers being included. They therefore assumed the lowest of their readings, 1.361, to be correct. The wide span of values in the available experimental results indicates a strong need for further work to obtain more exact data.

The evidence for CZ zone is indirect for the time being. The densitometry results may be misleading if the peripheral fiber cell layers have complements of proteins with varying affinity to the contrasting agents used for electron microscopy. However, we consider such a scenario as unlikely, since the differentiating fiber cells should have similar metabolic needs. The results from the laser scanning experiment are affected by the lens capsule, which at the near-grazing incidence of the laser beam has a significant effect because of its high refractive index and possible small surface irregularities. The experiment to ultimately test whether or not there is a CZ in the periphery of fish lenses has yet to be designed.

B. Functional Significance of the Outer Lens Layers

Typical spherical fish lenses are rigid structures because of high intralenticular pressure [22]. The capsule has to withstand this pressure, and in order to fill this structural role, the capsule's content of collagen fibers has to be high, which results in the relatively high RI we have observed (1.394). This agrees well with values found by Campbell [21] for rat lens capsules.

With the RIs of the immersion medium and the epithelium/CZ RI being 1.336 and 1.361, the horizon, from which on inward the RI of any layer within the lens

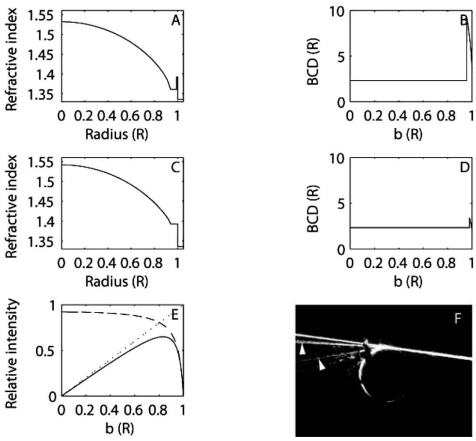

Fig. 4. A, Refractive index gradient of a hypothetical monofocal fish lens with a zone of constant RI in the periphery of the lens (epithelium and CZ) equal to 1.361 and a capsule of higher RI (1.394). B, LSA curve, i.e., back center distance, BCD, as a function of beam entrance position, b, for a spherical lens with the RIG shown in A. Note the strong longitudinal spherical aberration for peripheral b values. C, Same as in A with an epithelium/CZ refractive index of 1.394. D, Same as in B with the gradient shown in C. E, The relative intensity transmitted through the lens as a function of b (solid curve). The transmission as a function of b is represented by the dashed curve. The relative amount of light incident on the lens's entire aperture at different b values is represented by the dotted line. F, An image taken from a laser scanning experiment on a fish lens [44]. The original image was manipulated to clearly show the laser beam (Gaussian blur, enhanced contrast, and gray scaling). Note how the peripheral longitudinal spherical aberration splits up the exiting laser beam, resulting in long back center distances for some of the visible portions of the beam (white arrowheads).

can be calculated with (the modified) Eq. (2) (normalized $\xi=1$), is 98.16% R. Allowing the epithelium/CZ RI to equal 1.394 results in the horizon equaling 95.84% R. Using the total mean capsule thickness and lens radius from the interference microscope experiment, and assuming a similar thickness for the epithelium, the inner border of the epithelium (i.e., where the RI may begin rising) equaled 98.29% R. Combining the capsule thickness and the epithelium thickness from the Epon embedded material used for densitometry resulted in 97.78% R as the inner border of the epithelium, with shrinkage effects because of fixation and dehydration neglected. Even when using the relatively high epithelium/CZ RI of 1.394, the point where normalized ξ becomes smaller than 1 is more peripheral than 94% R, i.e., the CZ's inner border. This means that the CZ was about 3% R wider than the minimum CZ width that would fulfill the requirements for uniqueness. If RI in the CZ is close to 1.361, it is more likely that the metabolic needs of developing lens fiber cells determine the width of the CZ. If the RIG were to start directly interior to the epithelium, protein concentrations in the organelle-containing, differentiating fiber cells would rapidly increase toward the center of the lens and might reach values that would hamper diffusion and thus efficient metabolism.

In lenses with thinner capsules and/or epithelia, however, there is an optical need for an CZ even if the epithelium/CZ index is low. A lack of uniqueness would make the regulation of the RIG more complex. Regulating a nonunique RIG with a set of parameters would result in the same LSA for an infinite number of parameter sets. With a single-valued regulation function, on the other hand, each distinct set of parameters results in a distinct LSA. It is thus more parsimonious for a system to have one set of parameters that can result in only one RIG. In such cases and if the epithelium/CZ index is relatively high ($\approx$1.4), the CZ is a means of reducing normalized $\xi(r)$ down to a value of 1 as quickly as possible. A reduction of $\xi(r)$ can be brought about by a reduction of r, n(r), or both. Barring a reduction of RI (toward the lens center) as improbable, $\xi(r)$ will at most be reduced linearly with decreasing r. Any rise in n(r) toward the lens center would require a smaller r before the requirement of $\xi \leqslant 1$ is met and thus increase the peripheral undefined interval where $\xi > 1$. Therefore, a constant RI in the CZ decreases $\xi(r)$ in the fastest possible way.

Another effect of the rather wide CZ is that the central RI in the lens is reduced. The limit for the highest possible central RI is set by the maximally achievable concentration of crystallins and the central RI in spherical fish lenses is believed to be close to this limit. Sroczyński measured an extremely short mean focal length in roach (*Rutilus rutilus*) lenses, 2.19 R, and noted that the inferred central RI is problematically high [36]. Excluding both the capsule and the epithelium and using an unlikely lens surface RI of 1.336 (matched to that of the surrounding medium) resulted in a central RI of 1.546. Recalculating the roach lens's central RI with a capsule and a peripheral RI of 1.361 and 1.394 resulted in 1.552 and 1.560, respectively) The existence of the CZ, however, may explain the existence of a lens with such a short mean focal length while maintaining a relatively low central RI. Sroczyński's observation of a short "effective entrance area" (i.e., LCB) of 91% R indicates the existence of a prominent CZ with a maximal position of the inner border at 91% R. Recalculation of the central RI for the same lens with an inner border of the CZ at 91% R and an epithelium/CZ index of 1.361 and 1.394 yielded central RIs of 1.539 and 1.550, respectively.

The LCB can be increased by reducing the width of the CZ, increasing its RI, and increasing the focal length of the lens. The latter is not desirable for fishes that need high light-gathering ability and thus short focal length of the lens. Increasing the RI of the CZ would lead to an increase in the central RI. In the case where the central RI is as high as physiologically possible, a CZ RI elevation will result in a longer focal length for a well-corrected lens. The correlation between the inner borders of cells containing nuclei and the CZ suggests that the CZ exists because of physiological requirements. Lens growth and maintenance may require a minimum number of metabolically active cells, and it is likely that protein concentration in these cells cannot exceed a certain value for them to maintain efficient metabolic activity. The negative effects of the CZ are reduced by reflection of light for high b values (Fig. 4(e)). Such reflection could only be avoided if the lens capsule also had a RIG or by some an-

tireflection measure. So far, there is no evidence for either one of these possible solutions.

5. CONCLUSIONS

The results of a histological analysis strongly suggest that there is a zone of constant refractive index in the periphery of fish lenses. This finding simplifies the task of uniquely inferring the refractive index gradient in the central region of the lens using the inverse Abel transform. Results from optical modeling suggest that the width of the constant-index zone is determined by the metabolic needs of the lens because it is wider than the optically optimal solution. The negative effects of strong longitudinal spherical aberration in the periphery of the lens because of the constant-index zone are reduced by partial reflection of light that passes only through this part of the lens. The maximum necessary central refractive index is reduced by the existence of the constant-index zone. Further experimental work is needed to determine the refractive index in the constant-index zone and to investigate its effects on the optical performance of animal lenses.

ACKNOWLEDGMENTS

We thank Rita Wallén for technical assistance and guidance in the transmission electron microscope analysis. The interference microscopy was performed with support by Dan-Eric Nilsson and the confocal microscopy with Peter Ekström's help.

REFERENCES

1. M. F. Land and D.-E. Nilsson, *Animal Eyes*, Animal Biology Series (Oxford 2002).
2. T. Mandelman and J. G. Sivak, "Longitudinal chromatic aberration of the vertebrate eye," Vision Res. **23**, 1555–1560 (1983).
3. L. Matthiessen, "Ueber den physikalisch-optischen Bau des Auges der Cetaceen und der Fische," Pfluegers Arch. **38**, 521–528 (1886).
4. R. J. Pumphrey, "Concerning vision," in *The Cell and the Organism*, J. A. Ramsay and V. B. Wigglesworth, eds. (Cambridge U. Press, 1961), pp. 193–208.
5. J. G. Sivak and C. A. Luer, "Optical development of the ocular lens of an elasmobranch *Raja eglanteria*," Vision Res. **31**, 373–382 (1991).
6. G. L. Walls, *The Vertebrate Eye and Its Adaptive Radiation* (Hafner, 1964).
7. J. C. Maxwell, "Some solutions of problems 2," Cambridge Dublin Math. J. **8**, 188–195 (1854).
8. L. Matthiessen, "Ueber die Beziehungen, welche zwischen dem Brechungsindex des Kerncentrums der Krystalllinse und den Dimensionen des Auges bestehen," Pfluegers Arch. **27**, 510–523 (1882).
9. L. Matthiessen, "X. Beiträge zur Dioptrik der Kristalllinse," Z. vergleich. Augen. **7**, 102–146 (1893).
10. R. K. Luneburg, *Mathematical Theory of Optics* (Brown U. Press, 1944).
11. A. Huggart, "On the form of the iso-indicial surfaces of the human crystalline lens," Acta Ophthalmol. Scand. **64**, 1–126 (1948).
12. S. Nakao, S. Fujimoto, R. Nagata, and K. Iwata, "Model of refractive index distribution in the rabbit crystalline lens," J. Opt. Soc. Am. **58**, 1125–1130 (1968).
13. B. Philipson, "Distribution of protein within the normal rat lens," Invest. Ophthalmol. Visual Sci. **8**, 258–270 (1969).
14. M. Bando, A. Nakajima, M. Nakagawa, and T. Hiraoka, "Measurement of protein distribution in human lens by micro spectrophotometry," Exp. Eye Res. **22**, 389–392 (1976).
15. P. P. Fagerholm, B. Philipson, and B. Lindström, "Normal human lens—the distribution of protein," Exp. Eye Res. **33**, 615–620 (1981).
16. M. C. W. Campbell and A. Hughes, "An analytic, gradient index schematic lens and eye for the rat which predicts aberrations for finite pupils," Vision Res. **21**, 1129–1148 (1981).
17. M. C. W. Campbell, "Gradient refractive index optics and image quality in the rat eye," Ph.D thesis (Australian National University, Canberra, 1982).
18. A. Fletcher, T. Murphy, and A. Young, "Solutions of two optical problems," Proc. R. Soc. London, Ser. A **223**, 216–225 (1954).
19. P. L. Chu, "Nondestructive measurement of index profile of an optical-fibre preform," Electron. Lett. **13**, 736–738 (1977).
20. K. F. Barrell and C. Pask, "Nondestructive index profile measurement of noncircular optical fibre preforms," Opt. Commun. **27**, 230–234 (1978).
21. M. C. W. Campbell, "Measurement of refractive index in an intact crystalline lens," Vision Res. **24**, 409–416 (1984).
22. R. H. H. Kröger, M. C. W. Campbell, R. Munger, and R. D. Fernald, "Refractive index distribution and spherical aberration in the crystalline lens of the African cichlid fish Haplochromis burtoni," Vision Res. **34**, 1815–1822 (1994).
23. R. D. Fernald and S. E. Wright, "Maintenance of optical quality during crystalline lens growth," Nature **301**, 618–620 (1983).
24. J. G. Sivak, "Optical properties of a cephalopod eye the short finned squid Illex illecebrosus," J. Comp. Physiol., A **147**, 323–328 (1982).
25. J. G. Sivak, "Optical characteristics of the eye of the flounder," J. Comp. Physiol., A **146**, 345–350 (1982).
26. J. G. Sivak and R. O. Kreuzer, "Spherical aberration of the crystalline lens," Vision Res. **23**, 59–70 (1983).
27. D. Axelrod, D. Lerner, and P. J. Sands, "Refractive index within the lens of a goldfish eye determined from the paths of thin laser beams," Vision Res. **28**, 57–66 (1988).
28. B. K. Pierscionek, "Nondestructive method of constructing 3-dimensional gradient index models for crystalline lenses. 1. Theory and experiment," Am. J. Optom. Physiol. Opt. **65**, 481–491 (1988).
29. B. K. Pierscionek, "The refractive index along the optic axis of the bovine lens," Eye **9**, 776–782 (1995).
30. E. Acosta, D. Vazquez, L. Garner, and G. Smith, "Tomographic method for measurement of the gradient refractive index of the crystalline lens. I. the spherical fish lens," J. Opt. Soc. Am. A **22**, 424–433 (2005).
31. L. F. Garner, G. Smith, S. Yao, and R. C. Augusteyn, "Gradient refractive index of the crystalline lens of the Black Oreo Dory (*Allocyttus niger*): comparison of magnetic resonance imaging (MRI) and laser ray-trace methods," Vision Res. **41**, 973–979 (2001).
32. D. Vazquez, E. Acosta, G. Smith, and L. Garner, "Tomographic method for measurement of the gradient refractive index of the crystalline lens. II. The rotationally symmetrical lens," J. Opt. Soc. Am. A **23**, 2551–2565 (2006).
33. Y. Verma, K. D. Rao, M. K. Suresh, H. S. Patel, and P. K. Gupta, "Measurement of gradient refractive index profile of crystalline lens of fisheye in vivo using optical coherence tomography," Appl. Phys. B: Photophys. Laser Chem. **87**, 607–610 (2007).
34. F. W. Campbell and R. W. Gubish, "The effect of chromatic aberration on visual acuity," J. Physiol. (London) **186**, 558–578 (1967).
35. R. H. H. Kröger and M. C. W. Campbell, "Dispersion and longitudinal chromatic aberration of the crystalline lens of the African cichlid fish *Haplochromis burtoni*," J. Opt. Soc. Am. A **13**, 2341—2347 (1996).
36. S. Sroczyński, "Spherical aberration of crystalline lens in the roach *Rutilus rutilus*," J. Comp. Physiol., A **121**, 135–144 (1977).

37. S. Sroczyński, "Die sphärische Aberration der Augenlinse der Regenbogenforelle (*Salmo gairdneri*, Rich.)," Zool. Jahrb. Physiol. **79**, 204–212 (1975).
38. S. Sroczyński, "Die sphärische Aberration der Augenlinse des Hechts (*Esox lucius* L.)," Zool. Jahrb. Physiol. **79**, 547–558 (1975).
39. S. Sroczyński, "Die chromatische Aberration der Augenlinse der Bachforelle (*Salmo trutta* fario, L.)," Zool. Jahrb. Physiol. **82**, 113–133 (1978).
40. S. Sroczyński, "Das optische System des Auges des Flussbarsches (*Perca fluviatilis*, L.)," Zool. Jahrb. Physiol. **83**, 224–252 (1979).
41. J. K. Bowmaker and Y. W. Kunz, "UV receptors tetrachromatic color vision and retinal mosaics in the brown trout *Salmo trutta* age-dependent changes," Vision Res. **27**, 2101–2108 (1987).
42. J. K. Bowmaker, A. Thorpe, and R. H. Douglas, "UV-sensitive cones in the goldfish," Vision Res. **31**, 349–352 (1991).
43. R. H. H. Kröger, M. C. W. Campbell, R. D. Fernald, and H.-J. Wagner, "Multifocal lenses compensate for chromatic defocus in vertebrate eyes," J. Comp. Physiol., A **184**, 361–369 (1999).
44. P. E. Malkki and R. H. H. Kröger, "Visualization of chromatic correction of fish lenses by multiple focal lengths," J. Opt. A, Pure Appl. Opt. **7**, 691–700 (2005).
45. B. Karpestam, J. Gustafsson, N. Shashar, G. Katzir, and R. H. H. Kröger, "Multifocal lenses in coral reef fishes," J. Exp. Biol. **210**, 2923–2931 (2007).
46. T. Malmström and R. H. H. Kröger, "Pupil shapes and lens optics in the eyes of terrestrial vertebrates," J. Exp. Biol. **209**, 18–25 (2006).
47. J. R. Kuszak, R. K. Zoltoski, and C. Sivertson, "Fibre cell organization in crystalline lenses," Exp. Eye Res. **78**, 673–687 (2004).
48. V. Bantseev, K. L. Herbert, J. R. Trevithick, and J. G. Sivak, "Mitochondria of rat lenses: distribution near and at the sutures," Invest. Ophthalmol. Visual Sci. **40**, S881 (1999).
49. S. Bassnett and D. C. Beebe, "Coincident loss of mitochondria and nuclei during lens fiber cell differentiation," Dev. Dyn. **194**, 85–93 (1992).
50. V. Bantseev, K. L. Moran, D. G. Dixon, J. R. Trevithick, and J. G. Sivak, "Optical properties, mitochondria, and sutures of lenses of fishes: a comparative study of nine species," Can. J. Zool. **82**, 86–93 (2004).
51. M. C. Campbell, E. M. Harrison, and P. Simonet, "Psychophysical measurement of the blur on the retina due to optical aberrations of the eye," Vision Res. **30**, 1587–1602 (1990).
52. W. S. Jagger, "The optics of the spherical fish lens," Vision Res. **32**, 1271–1284 (1992).
53. R. H. H. Kröger, M. C. W. Campbell, and R. D. Fernald, "The development of the crystalline lens is sensitive to visual input in the African cichlid fish, *Haplochromis burtoni*," Vision Res. **41**, 549–559 (2001).
54. P. Schiebener, J. Straub, L. S. J. M. H., and J. S. Gallagher, "Refractive index of water and steam as function of wavelength, temperature and density," J. Phys. Chem. **19**, 677 (1990).
55. D.-E. Nilsson, M. Andersson, E. Hallberg, and P. McIntyre, "A micro interferometric method for analysis of rotation symmetric refractive index gradients in intact objects," J. Microsc. **132**, 21–30 (1983).
56. D.-E. Nilsson, L. Gislen, M. M. Coates, C. Skogh, and A. Garm, "Advanced optics in a jellyfish eye," Nature **435**, 201–205 (2005).
57. E. S. Reynolds, "The use of lead citrate at high pH as an electron-opaque stain in electron microscopy," J. Cell Biol. **17**, 208–212 (1963).
58. M. C. W. Campbell and P. J. Sands, "Optical quality during crystalline lens growth," Nature **312**, 291–292 (1984).
59. B. K. Pierscionek, "Refractive index of the human lens surface measured with an optic fibre sensor," Ophthalmic Res. **26**, 32–35 (1994).
60. B. K. Pierscionek and R. C. Augusteyn, "The refractive index and protein distribution in the blue eye trevally lens," J. Am. Optom. Assoc. **66**, 739–743 (1995).
61. J. M. Schartau, B. Sjögreen, Y. L. Gagnon, and R. H. H. Kröger, "Optical plasticity in fish crystalline lenses," submitted to Curr. Biol. (posted July 25, 2008).
62. R. Barer, "Refractometry and interferometry of living cells," J. Opt. Soc. Am. **47**, 54–556 (1957).
63. L. Matthiessen, "Untersuchungen über Aplanatismus und die Periskopie der Kristalllinsen in den Augen der Fische," Pfluegers Arch. **21**, 287–307 (1880).
64. B. K. Pierscionek, "Refractive index of decapsulated bovine lens surfaces measured with a reflectometric sensor," Vision Res. **34**, 1927–1933 (1994).

Paper II

Spectral influence on the refractive properties of the crystalline lens in *Siganus rivulatus* (Forsskål, 1775)

Yakir L. Gagnon [a], Nadav Shashar [b], Ronald H. H. Kröger [a]
[a] Department of Biology, Lund University, Helgonavägen 3, Lund, Sweden
[b] Department of Life Sciences, Eilat Campus, Ben Gurion University of the Negev, P.O. Box 84105, Beer Sheva, Israel

Running head: Lens changes in a migrating fish

Key words: Lessepsian migration, multifocal lens, adaptation, fish.

Abstract

Vision is an important source of information for many animals. The lens plays a central role in the visual pathway and hence the ecology of fishes. It has been shown that light- or dark-adapting fish change their lenses' properties within hours while fish reared under differently colored light regimes do so after several months. In this study, effects of the light regimes found in the Mediterranean and the Red Sea were tested on lenses of the rivulated rabbitfish, *Siganus rivulatus* which populates both seas. Longitudinal spherical aberration curves and focal lengths of the fish lenses were measured with laser scans and compared between the two populations. To test these effects in situ, rivulated rabbitfish from the Mediterranean Sea were additionally exposed to colored light (yellow, green, blue, and control) for periods of one or 13 days. While the shape of the longitudinal spherical aberration curve was similar among the two seas and filtered light regimes, the focal length was significantly different between the groups (Kruskal Wallis; $P = 0.008$). The Rea Sea population had a 3% longer focal length of 2.38 lens radius units vs the 2.32 lens radius of the Mediterranean population. This difference can be explained by either a) an adaptation to the dimmer light environment as this difference makes the Mediterranean eyes 5% more sensitive than the eyes of the Red Sea population; or b) a compensation for the red shifted waters of the Mediterranean into which the fish have migrated; or c) a combination of both.

List of abbreviations

ANOSIM	analysis of similarities
BCD	back center distance
BEP	beam entrance position
LCA	longitudinal chromatic aberration
LSA	longitudinal spherical aberration
R	lens radius
RI	refractive index
RIG	refractive index gradient

Introduction

A variety of different eye types has evolved and vision provides vital information on the external world to many animals (Land and Nilsson, 2002). Vertebrate eyes are camera-type eyes and are generally similar in design to a photographic camera. However, the optical systems of these eyes are apparently much simpler than a good camera objective that consists of a number of lenses to correct for various kinds of optical aberrations. There are at maximum only two lenses in a vertebrate eye: the cornea and the crystalline lens.

In aquatic vertebrates, the cornea is surrounded by water on the outside and the watery aqueous humor on the inside. Both media have relatively high refractive indices and if the cornea is thin, which is the case in most species, its refractive power is negligible (Mandelman and Sivak, 1983; Matthiessen, 1893). The task of focusing light on the retina is thus left to the lens alone. Among the aquatic vertebrates, the lenses of bony fishes (teleosts) have received the most attention, mainly because of easy access to fresh material and the simple geometry of the lenses, which are typically spherical (Pumphrey, 1961; Sivak and Luer, 1991; Walls, 1964).

Vertebrate lenses are modified inverted epithelia and the outmost layer, the lens capsule, is a modified basement membrane. This thin acellular sheet of mainly collagen fibers keeps the lens together and withstands its internal pressure. Thereafter follows a monolayer of metabolically active cells, usually called the lens epithelium that in fishes covers most of the interior surface of the lens capsule. Further inward there are many layers of lens fiber cells; thin cells that stretch from pole to pole in concentrically arranged layers. In many vertebrates, including bony fishes, fiber cell geometry can be somewhat more complicated with the fiber tips ending in a line, Y, or star-shaped junction rather than a point (Kuszak et al., 2004).

Spherical lenses made of homogenous materials (e.g. glass) suffer from longitudinal spherical aberration (LSA). Maxwell (Maxwell, 1854) was the first to note that fish lenses are almost free of LSA. He suggested that LSA is greatly reduced in fish lenses by a gradient of refractive index (RIG) with the highest refractive index (RI) in the center and lowest RI at the surface of the lens.

Another optical problem arises from dispersion: the RI of any transparent medium, except for vacuum, is wavelength dependent. In consequence, optical systems focusing a wide range of wavelengths (polychromatic light) suffer from longitudinal chromatic aberration (LCA): light of different wavelengths is focused at different distances from the optical system, which leads to chromatic blur on the retina. The blurring effect is most pronounced in optical systems of high refractive powers, i.e. systems with

small f-numbers (i.e. the system's focal length divided by its aperture diameter). Fish have powerful lenses with normalized focal lengths of 2.2-3.3 lens radii (Kröger et al., 2009; Matthiessen, 1882).

As a mechanism that compensates for LCA, many fish lenses have several focal lengths when examined with monochromatic light, i.e. they are multifocal. The distances between the focal points along the optical axis are equal to the focal length differences due to LCA between the wavelengths that are of highest importance to the animals. This means that these wavelengths are correctly focused on the retina. A sharp color image is created on the background of defocused light that has passed through "wrong" zones in the lens (Kröger et al., 1999). The multifocal principle compensating for the defocusing effect of LCA is present in a variety of fishes(Karpestam et al., 2007; Kröger et al., 1999; Kröger et al., 2009; Malkki et al., 2003; Schartau et al., 2009) and tetrapods (Hanke et al., 2008; Lind et al., 2008; Malmström and Kröger, 2006).

The multifocal properties of fish lenses show species-specific adaptations that suit different visual needs (Karpestam et al., 2007; Kröger et al., 2009; Malkki et al., 2003). Furthermore, the optical properties of fish lenses are actively fine-tuned. Rearing fish under different light regimes for long periods of time (10 months) induced optical changes in the lenses of the South American cichlid *Aequidens pulcher* (Kröger et al., 2001). Optical changes in the lens between day and night have been detected in the African cichid *Astatotilapia burtoni* (Schartau et al., 2009). These changes occur in parallel to retinomotor movements in the retina: from a functionally all-cone retina (color vision) at day to an all-rod retina (grayscale vision) at night (Kröger and Wagner, 1998). The refractive changes lead to a switch from a multifocal lens at day to a monofocal lens at night. The shapes of the LSA curves of the day and night adapted lenses are therefore significantly different. The neuro-modulatory substance dopamine that is produced in the retina and diffuses freely within the eye (Witkovsky et al., 1993) appears to play an important role in this regulation (Schartau et al., 2010a; Schartau et al., 2009). These examples indicate that the optical properties of fish lenses are plastic and can change to better suit specific visual tasks.

We investigated whether regulatory mechanisms may optimize the optical properties of fish lenses under natural and experimental conditions. The Suez Canal (opened 1869) has enabled the migration of animals from the Red Sea to the Mediterranean (Lessepsian migration), allowing some species to live in both areas (Bilecenoglu et al., 2002; Golani, 1993; Streftaris et al., 2005). The rivulated rabbitfish, *Siganus rivulatus* Forsskål, 1775, has migrated from the Red Sea to the Mediterranean (Ben-Tuvia, 1964) and is well established from the eastern Mediterranean to the Tunisian coast (George, 1972).

The light environments differ markedly between both seas, with clearer and less tinted waters in the Red Sea than in the Mediterranean. The type and amount of dissolved and suspended material in the water column affects the water's inherent optical properties, leading to differences in the spectral composition and intensity of the ambient light. We compared the optical properties of *S. rivulatus* lenses between populations from both seas.

We investigated also whether regulatory mechanisms may induce optical changes in fish lenses with time courses intermediate between the short-term and long-term changes described previously. Rabbitfish from the Mediterranean Sea were exposed to different light regimes for periods of one and thirteen days and tested for adaptations in the lens.

Material and Methods

Rivulated rabbitfish were caught at the east coast of the Mediterranean Sea off-shore the Maritime College of Michmoret, Israel, in August 2007. The fish were placed either in an aquarium for no longer than 20 minutes or kept in an underwater basket for as long as one hour, at which point the fish were moved to the indoor treatment aquaria with oxygenated filtered sea water. Lighting was through multiple windows located close to the aquaria and supplemented with fluorescent lamps. *S. rivulatus* is a diurnal herbivorous species and the animals were fed algae from the local coast. The Red Sea population had been sampled similarly in an earlier study by our group (Karpestam et al., 2007). The main differences between both studies were the laser wavelengths used in the scans (547 nm vs. 534 nm in the current experiments) and the camera model used to record the scans (Sony DCR TRV140E vs. Sony HDR-HC7E in the current experiments). The current results are more precise because the newer camera had higher resolution. The use of different wavelengths led to a systematic bias in focal length because of LCA. The magnitude of this effect was estimated from measured LCA in fish lenses (Kröger and Campbell, 1996). Both main differences are more formally inspected below.

Experimental transfer of fish between the Mediterranean and the Red Sea is prohibited by the Israeli Nature Protection Authority, to avoid ecological and biological contamination. Forty-nine fish from the Mediterranean were divided into six groups, each containing between 5 and 9 individuals. The groups were placed in aquaria with/without a covering colored filter for different amounts of time. We used a midrange band-pass filter (green; Lee Filters) and no filter for one day and two more groups for thirteen days. In addition, we exposed two groups to short-pass (blue, cellophane) and long-pass (red, cellophane) filtered light for one day. See fig. 1 for the transmittance curves of the filters used.

All measurements were performed during daytime (before noon). The fish were individually sacrificed by rapid decapitation and pithing. The eyes were excised and each lens was extracted from the eye through a large section in the cornea and immersed in phosphate buffered saline (PBS, pH 7.4, 290 mosmol). The optical properties of the fish lenses were determined by laser scans (Malkki and Kröger, 2005). Each lens was scanned in a meridional plane parallel to the optical axis with a thin 534 nm laser beam. Beam paths were recorded with a digital video camera. The video sequences were processed using a custom-written program that detects the laser beams in the video footage [this program was tested in previous studies (Gagnon et al., 2008; Schartau et al., 2010a; Schartau et al., 2010b)].

The analysis resulted in an LSA curve for each lens that describes the deflection of laser beams as a function of where those beams entered the lens. The dependent variable of this function is the distance between the center of the lens and the point where the exiting – now deflected – beam intercepts the optical axis (back center distance, BCD), while the independent variable is the lateral

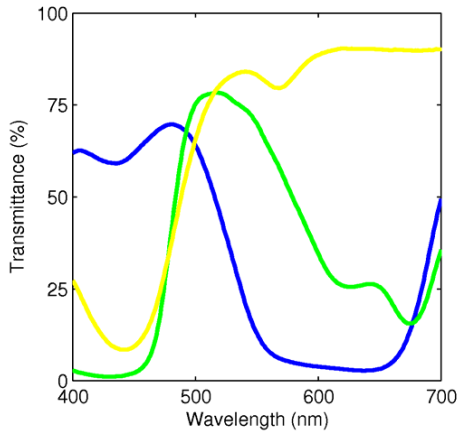

Figure 1. The relative transmittance of the 3 colored filters used in the light regimes of the aquariums. The x-axis is the wavelength in nm and the y-axis is the relative transmittance in percent. The filters are color coded: yellow, green, and blue.

distance between the optical axis of the lens and the entering beam (beam entrance position, BEP). BEP values range between 0 R (R = lens radius), i.e. the center of the lens, and 1 R, i.e. the surface of the lens, while typical BCD values range between 2-3 R (resulting in a lens with an f-number of 1-1.5). BCD values for BEP smaller than 0.3 R or larger than 0.95 R were excluded from the analysis because the laser scanning method has relatively low resolution close to the optical axis and in the outer periphery of the lens (Malkki and Kröger, 2005). Furthermore, most of the incident energy is lost by reflection for BEPs larger than 0.95 R (Sroczyński, 1977), and the central region of the lens contributes little to retinal illumination because of its small area.

There were seven groups in this study: the Red Sea population and the six treated aquaria from the Mediterranean population. These include three colored filter one day exposure groups, and two 13 days exposure groups with the green filter and the no filter aquaria. The optical properties of the lenses were quantified as the LSA curve shapes and the focal lengths of the lenses.

The lens focuses a cone of light on the retina if the entire aperture is illuminated. The results from scanning a lens in a meridional plane with a thin laser beam are equivalent to an axial section through such a cone of light. To determine the mean focal length of a lens, we interpolated between measured beam paths and let the number of beams used increase by a square root function towards the periphery of the lens. The focal lengths of the lenses were normalized to lens radius and compared between groups using the Kruskal Wallis test (Matlab2008a)

Left and right eye LSA curves were averaged for each fish. To maintain a balanced test, 5 (the number of samples in the smallest group) randomly chosen replicates from each group were included in the analysis. The shapes of the LSA curves were compared using Analysis of Similarities (ANOSIM) on the resemblance matrix of the 2nd stage analysis of the curves with Primer-E 6 software (see Clarke et al. (Clarke et al., 2006) for a detailed explanation of the statistical reasoning behind 2nd stage analysis of transect curves). Each BCD value was associated with two factors: the group the fish came from and its BEP value. A resemblance matrix (Bray Curtis similarity) was calculated from the (square root transformed) BCD values. A 2nd stage analysis (2STAGE in Primer-E 6) was performed on this resemblance matrix with the filter period as the outer factor (the factor of interest) and BEP as the inner factor (Somerfield and Clarke, 1995). This was done to calculate the statistical difference between statistical distance estimations (from the resemblance matrix) for all possible combinations of distance pairs across BEP (i.e. per unique BEP value). This results in a resemblance matrix whose columns and rows represented the individual levels of the outer factor. This matrix was analyzed with a one-way ANOSIM to test for significant differences between the groups (Clarke and Green, 1988).

Results

The different light environments in the Mediterranean and Red Sea had no effect on the shape of the LSA curves of the crystalline lenses in *S. rivulatus*. Differences in LSA curve shape were also absent between the groups experimentally exposed to different light environments (Fig. 2). For all groups, ANOSIM returned a global R of -0.21, P = 1.

There was, however, a statistically significant difference in the focal lengths of the lenses between the groups (Kruskal Wallis; P = 0.008). A post-hoc test (Tukey's honestly significant difference criterion) showed that the focal lengths of the lenses were significantly longer in the Red Sea population than in the Mediterranean population, while keeping fish from the Mediterranean in spectrally unfiltered or filtered light for one to thirteen days had no effect on the focal length of the lens. Average focal length of the lenses was 2.38 R in the Red Sea population, while the lenses from the Mediterranean fish had a 3% shorter mean focal length of 2.32 R (pooled across the Mediterranean groups) (Fig. 3).

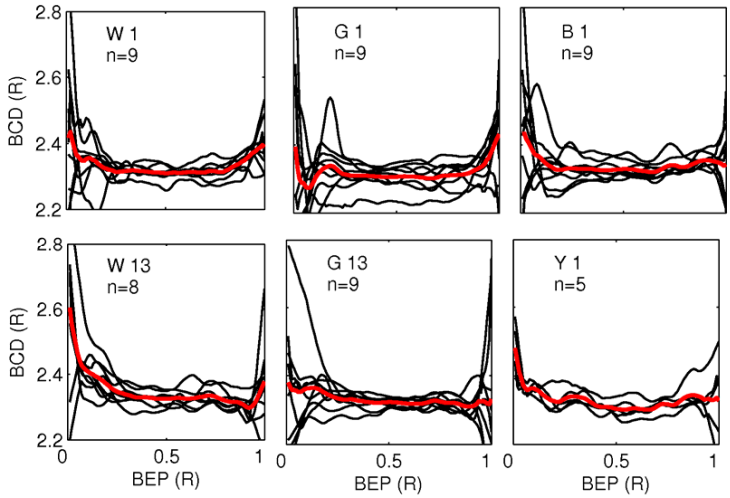

Figure 2. Longitudinal spherical aberration (LSA) curves of *S. rivulatus* lenses from the Mediterranean. The x-axis denotes the beam entrance position (BEP) while the y-axis is the back center distance (BCD) of the laser beam, both in units of lens radius (R). The black lines are the individual scans of each fish while the red lines are the mean LSA curves of those scans. The capital letters stand for the filter color used in each group (W – no filter, G – green, Y – yellow, and B – blue). The number following those letters stands for the number of days that group was exposed to the respective light regime (1 or 13 days). The number of replicates (fish) is denoted as *n*.

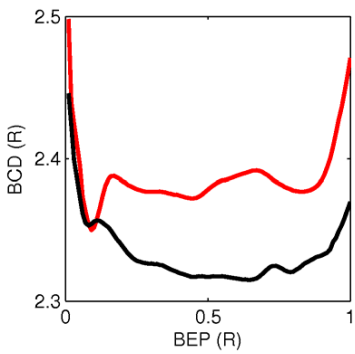

Figure 3. The mean longitudinal spherical aberration (LSA) curves of lenses from the Mediterranean Sea (pooled across the Mediterranean groups seen in Fig. 2) (black line) and the Red Sea populations (red line). The x-axis denotes the beam entrance position (BEP) while the y-axis is the back center distance (BCD) of the laser beam, both are in lens radius (R) units.

Discussion

Lenses from the Mediterranean had shorter focal length than the Red Sea population while all groups had similarly shaped LSA curves. The lack of any significant differences between the LSA curve shapes in the groups indicates that the multifocal properties of the lenses were independent of light regime. In the study by Karpestam and co-workers the herbivorous rivulated rabbitfish was considered to have a more monofocal lens than the zooplanktivores. The absence of ultraviolet (u.v.) -sensitive cones in diurnal herbivores and the high cutoff transmittance of ocular media in three other (Australian) rabbitfishes (> 400 nm) indicates that u.v. light is not used by these species. This explains the relatively flat LSA curves these fish have. Although the rivulated rabbitfish has trichromatic vision in the respect that it has three different photopigments (with absorbance maxima at 440, 450, and 512 nm; A. Chaouat and N. Shashar, unpublished measurements; cited also by Karpestam et al., 2007), it is possible that the visual system of the rivulated rabbitfish does not suffer from the introduced changes in the light environment so that a change in the lens' multifocality

would be necessary for the animal to flourish. The lenses did not have sufficiently different multiple focal lengths for the LSA curve to significantly change under the different light regimes.

Kröger et al. (Kröger et al., 2001) showed that the optical properties of a cichlid lens change after rearing the fish in monochromatic light for a period of 10 months, demonstrating the existence of a mechanism that regulates the refractive index gradient of the lens according to the light environment. While it is unlikely that the spectral changes between the treated aquariums were too small to affect the animals' visual scene, it is possible that the time period of exposure (13 days) was not sufficient for inducing a detectable change in LSA shape. Additionally, while fish from the Mediterranean were exposed to the sea's light regime for a long period, the spectral differences between the two seas might be too mild for a significant change in the lens's multifocality.

The use of a longer laser wavelength by Karpestam et al. was expected to result in a longer focal length due to longitudinal chromatic aberration. Model calculations indicated that the longer laser wavelength amounted to a 0.3% longer focal length (Gagnon et al., 2010; Kröger and Campbell, 1996). Although a differently colored laser could have introduced a systematic disparity which would result in a statistically significant difference between the two measurements, such a difference could not amount to a 3% longer focal length as seen in this comparison. Differences in light sensitivity between the two cameras could have resulted in a consistent difference in lens diameter. If one camera is more sensitive than the other, lens diameter might seem larger than what it really is due to light scattering at the lens surface (tissue residue adhering to the lens capsule increased light scattering). Over estimating lens diameter results in smaller BCD values which leads to shorter focal lengths. Brighter laser beam intensity may result in the same bias. In Fig. 4 a shift in lens radius equivalent to the difference between the two seas is portrayed. It is visible that such a change would constitute a deviation which is too large to be explained by glare.

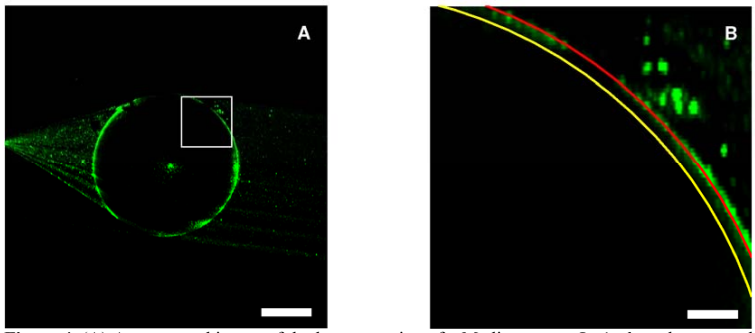

Figure 4. (A) A compound image of the laser scanning of a Mediterranean *S. rivulatus* lens assembled of the video frames taken from the scan footage. Notice the distinct circular shape of the lens caused by light scattering at the outer surface of the lens capsule. The scale bar is 1 mm long. (B) A magnified part of the image in A, (indicated by the white square in A). The green pixels are the interface between the lens and the medium, pointed out by the dashed red line. The yellow line depicts a lens of a size equivalent to that of the Red Sea population. Notice the absence of any green pixels under the yellow line. The scale bar is 150 µm long.

Genetic differences between the populations are a highly unlikely explanation for the difference in focal length. The *S. rivulatus* populations of the Mediterranean and Red Sea do not differ in mitochondrial DNA, which indicates that the migration of fish is either a continuous process or that the initial number of migrating fish was sufficiently high (Bonhomme et al., 2003). Furthermore, the parasitofaunas of both populations do not differ (Diamant, 1998).

The focal length difference between the two populations can lead to a difference in the fish eye sensitivity. Sensitivity is equivalent to the square of the ratio of the lens diameter divided by its focal length $(D/f)^2$, therefore, one possible way to increase photon catch in an eye is to minimize its f number. An animal can be active at low light levels as long as the sensitivity of its eye allows it. Contrast detection and acuity are compromised under dim light conditions, while higher eye sensitivity counteracts these negative effects, allowing the animal to be active in those light levels (Land and Nilsson, 2002). Since the BCD values are normalized to the lens radius and the iris does not cover any significant area of the lens, the f number of the eye is equal to half the focal length of the lens. Assuming that the distance between the retina and the nodal point of the lens matches the lens focal length in both populations (i.e. the populations have different distances between the retina and the lens nodal point), the shorter focal length of the Mediterranean group allows those eyes to be 5% more sensitive than those of the Red Sea population. This agrees well with the generally higher absorption coefficient the Mediterranean Sea has, making those waters slightly darker than those of the Red Sea. Another possible explanation can be related to LCA. Assuming the opposite, that the location of the retina did not match the lens focal length in the two different populations (i.e. the two populations have the same distance between the retina and the lens nodal point), the lower focal length the Mediterranean group has allows longer wavelengths to be better focused. Since the coastal East Mediterranean tends to be generally greener than the Red Sea (i.e. the intensities of light are relatively higher for midrange wavelengths than for the short and long wavelengths), such an adaptation is beneficial to a migrant from one environment to the other.

In conclusion, the small changes mediated in the lens could be caused by intensity differences, spectral content, or a combination of both and seem to be adaptations allowing for better vision by this migrating fish. Such adaptations may require a considerable amount of time and certainly more than 13 days.

Acknowledgments

We thank the friendly staff of the Maritime College of Michmoret, Israel and the helpful local fishermen. This study was made possible thanks to financial support from the Müllerska travel fund.

References

Ben-Tuvia, A. (1964). Two siganid fishes of the Red Sea origin in the eastern Mediterranean. *Bull. Sea Fish. Res. Sta. Haifa* **37**, 3-9.

Bilecenoglu, M., Taskavak, E. and Kunt, K. B. (2002). Range extension of three lessepsian migrant fish (*Fistularia commersoni*, *Sphyraena flavicauda*, *Lagocephalus suezensis*) in the mediterranean sea. *Journal of the Marine Biological Association of the United Kingdom* **82**, 525-526.

Bonhomme, F., Baranes, A., Golani, D. and Harmelin-Vivien, M. (2003). Lack of mitochondrial differentiation between Red Sea and Mediterranean populations of the Lessepsian rabbitfish, *Siganus rivulatus* (Perciformes: Siganidae). *Scientia Marina* **67**, 215-217.

Clarke, K. R. and Green, R. H. (1988). Statistical design and analysis for a 'biological effects' study. *Marine Ecology Progress Series* **46**, 213-226.

Clarke, K. R., Somerfield, P. J., Airoldi, L. and Warwick, R. M. (2006). Exploring interactions by second-stage community analyses. *Journal of Experimental Marine Biology and Ecology* **338**, 179-192.

Diamant, A. (1998). Parasitological aspects of Red-Med fish migration. In *Actes du Colloque Scientifique*, (ed. P. I. S. Colloq), pp. 175-178: OCEANOS, Montpellier, France.

Gagnon, Y. L., Kröger, R. H. H. and Söderberg, B. (2010). Adjusting a light dispersion model to fit measurements from vertebrate ocular media as well as ray-tracing in fish lenses. *Vision Research* **50**, 850-853.

Gagnon, Y. L., Söderberg, B. and Kröger, R. H. H. (2008). Effects of the peripheral layers on the optical properties of spherical fish lenses. *Journal of the Optical Society of America A* **25**, 2468-2475.

George, C. J. (1972). Notes on the breeding and movements of the rabbitfishes *Siganus rivulatus* (Forsskal) and *S. luridus* Rüppell, in the coastal waters of Lebanon. *Ann. Mus. Storia Nat. Genova* **79**, 32-44.

Golani, D. (1993). The biology of the Red Sea migrant, *Saurida undosquamis* in the Mediterranean and comparison with the indigenous confamilial *Synodus saurus* (Teleostei: Synodontidae). *Hydrobiologia* **271**, 109-117.

Hanke, F. D., Kröger, R. H. H., Siebert, U. and Dehnhardt, G. (2008). Multifocal lenses in a monochromat: the harbour seal. *Journal of Experimental Biology* **211**, 3315-3322.

Karpestam, B., Gustafsson, J., Shashar, N., Katzir, G. and Kröger, R. H. H. (2007). Multifocal lenses in coral reef fishes. *Journal of Experimental Biology* **210**, 2923-2931.

Kröger, R. H. H. and Campbell, M. C. W. (1996). Dispersion and longitudinal chromatic aberration of the crystalline lens of the African cichlid fish *Haplochromis burtoni*. *Journal of the Optical Society of America A* **13**, 2341-2347.

Kröger, R. H. H., Campbell, M. C. W. and Fernald, R. D. (2001). The development of the crystalline lens is sensitive to visual input in the African cichlid fish, *Haplochromis burtoni*. *Vision Research* **41**, 549-559.

Kröger, R. H. H., Campbell, M. C. W., Fernald, R. D. and Wagner, H. J. (1999). Multifocal lenses compensate for chromatic defocus in vertebrate eyes. *Journal of Comparative Physiology A Sensory Neural and Behavioral Physiology* **184**, 361-9.

Kröger, R. H. H., Fritsches, K. A. and Warrant, E. J. (2009). Lens optical properties in the eyes of large marine predatory teleosts. *Journal of comparative physiology a-neuroethology sensory neural and behavioral physiology* **195**, 175-182.

Kröger, R. H. H. and Wagner, H. J. (1998). A fluorescent double stain for visualization of neural tissue by confocal laser scanning microscopy. *Journal of Neuroscience Methods* **84**, 87-92.

Kuszak, J. R., Zoltoski, R. K. and Sivertson, C. (2004). Fibre cell organization in crystalline lenses. *Experimental Eye Research* **78**, 673-687.

Land, M. F. and Nilsson, D.-E. (2002). Animal eyes. Oxford: Animal Biology Series.

Lind, O. E., Kelber, A. and Kröger, R. H. H. (2008). Multifocal optical systems and pupil dynamics in birds. *Journal of Experimental Biology* **211**, 2752-2758.

Malkki, P. E. and Kröger, R. H. H. (2005). Visualization of chromatic correction of fish lenses by multiple focal lengths. *Journal of Optics A: Pure and Applied Optics* **7**, 691-700.

Malkki, P. E., Löfblad, E. and Kröger, R. H. H. (2003). Species - specific differences in the optical properties of crystalline lenses of fishes. *ARVO Annual Meeting Abstract Search and Program Planner* **2003**, 3483.

Malmström, T. and Kröger, R. H. H. (2006). Pupil shapes and lens optics in the eyes of terrestrial vertebrates. *Journal of Experimental Biology* **209**, 18-25.

Mandelman, T. and Sivak, J. G. (1983). Longitudinal chromatic aberration of the vertebrate eye. *Vision Research* **23**, 1555-1560.

Matthiessen, L. (1882). Ueber die Beziehungen, welche zwischen dem Brechungsindex des Kerncentrums der Krystalllinse und den Dimensionen des Auges bestehen. *Pflüger's Archiv* **27**, 510-523.

Matthiessen, L. (1893). Beiträge zur Dioptrik der Kristalllinse. *X. Zeitschrift für vergleichende Augenheilkunde* **7**, 102-146.

Maxwell, J. C. (1854). Some solutions of problems 2. *Cambridge and Dublin Mathematical Journal* **8**, 188-195.

Pumphrey, R. J. (1961). Concerning vision. London: Cambridge University Press.

Schartau, J. M., Kröger, R. H. H. and Sjögreen, B. (2010a). Dopamine induces optical changes in the cichlid fish lens. *PLoS ONE* **5**, e10402.

Schartau, J. M., Kröger, R. H. H. and Sjögreen, B. (2010b). Short-term culturing of teleost crystalline lenses combined with high-resultotion optical measurements. *Cytotechnology* **62**, 167-1743.

Schartau, J. M., Sjögreen, B., Gagnon, Y. L. and Kröger, R. H. H. (2009). Optical Plasticity in the Crystalline Lenses of the Cichlid Fish *Aequidens pulcher*. *Current Biology* **19**, 122-126.

Sivak, J. G. and Luer, C. A. (1991). Optical development of the ocular lens of an elasmobranch *Raja eglanteria*. *Vision Research* **31**, 373-382.

Somerfield, P. J. and Clarke, K. R. (1995). Taxonomic levels, in marine community studies, revisited. *Marine Ecology Progress Series* **127**, 113-119.

Sroczyński, S. (1977). Spherical aberration of crystalline lens in the roach *Rutilus rutilus*. *Journal of Comparative Physiology A Sensory Neural and Behavioral Physiology* **121**, 135-144.

Streftaris, N., Zenetos, A. and Papathanassiou, E. (2005). Globalisation in marine ecosystems: the story of non-indigenous marine species across European sea. *Oceanography and Marine Biology* **43**, 419-453.

Walls, G. L. (1964). The vertebrate eye and its adaptive radiation. New York: The Cranbrook Press.

Witkovsky, P., Nicholson, C., Rice, M. E., Bohmaker, K. and Meller, E. (1993). Extracellular dopamine concentration in the retina of the clawed frog, *Xenopus laevis*. *Proceedings of the National Academy of Sciences of the United States of America* **90**, 5667-5671.

Paper III

Contents lists available at ScienceDirect

Vision Research

journal homepage: www.elsevier.com/locate/visres

Adjusting a light dispersion model to fit measurements from vertebrate ocular media as well as ray-tracing in fish lenses

Yakir L. Gagnon [a,*], Ronald H.H. Kröger [a], Bo Söderberg [b]

[a] Department of Cell and Organism Biology, Lund University, Helgonavägen 3, 22 362 Lund, Sweden
[b] Department of Theoretical Physics, Lund University, Sölvegatan 14, 22 362 Lund, Sweden

ARTICLE INFO

Article history:
Received 22 July 2009
Received in revised form 2 February 2010

Keywords:
Dispersion
Spherical lens
Model
Fish
Ray-trace

ABSTRACT

Color dispersion, i.e., the dependency of refractive index of any transparent material on the wavelength of light, has important consequences for the function of optical instruments and animal eyes. Using a multi-objective goal attainment optimization algorithm, a dispersion model was successfully fitted to measured refractive indices of various ocular media and the longitudinal chromatic aberration determined by laser-scanning in the crystalline lens of the African cichlid fish, *Astatotilapia burtoni*. The model describes the effects of color dispersion in fish lenses and may be applicable to the eyes of other vertebrates as well.

1. Introduction

Dispersion is the dependency of a medium's refractive index (RI) on light frequency or wavelength in vacuum. This phenomenon has influenced the design of imaging devices and the evolution of eyes. Since the refractive power of a lens is dependent on wavelength, there is chromatic defocus in polychromatic light. In manufactured optical devices, the problem of chromatic defocus is minimized by using combinations of lenses made of different materials (Hecht, 2002). The biological solution is however different; well-focused color images are created by a single multifocal lens. The optical function of such lenses is studied mainly in fishes because they have good color vision and simple optical systems. Under water, the cornea has negligible refractive power such that the crystalline lens alone creates the images. Typical fish lenses are furthermore spherical, which considerably simplifies optical analyses.

A multifocal lens has distinct zones of different focal lengths for monochromatic light. If polychromatic light is incident on the lens, each zone creates a well-focused image for a different spectral range (Kröger, Campbell, Fernald, & Wagner, 1999). Multifocal lenses are present in a large variety of vertebrates (animals with a backbone) (Gustafsson, Collin, & Kröger, 2008; Hanke, Kröger, Siebert, & Dehnhardt, 2008; Karpestam, Gustafsson, Shashar, Katzir, & Kröger, 2007; Kröger et al., 1999; Lind, Kelber, & Kröger, 2008; Malkki & Kröger, 2005; Malmström & Kröger, 2006) and are thus a very successful solution.

The mode of operation of a multifocal lens is, however, counter-intuitive; a sharp color image is overlaid by defocused light that has passed through zones of the lens of unsuitable refractive power. One may therefore wonder what information transfer capacity such lenses can have.

Multifocal crystalline lenses are gradient index lenses (GRIN lenses), with the highest RI in the center and lowest RI at the surface of the lens. This gradient greatly reduces longitudinal spherical aberration (LSA). The residual LSA of the lens is carefully tuned and leads to its multifocality (Kröger et al., 1999). The performance of the lens is critically dependent on the shape of the refractive index gradient (RIG) and small differences in the RIG can lead to relevant and significant differences in the optical properties of the lens (Kröger, Campbell, & Fernald, 2001). So far, determination of the correct RIGs (i.e. not estimated RIG) of fish lenses has been difficult because of the necessary high accuracy. A combined approach of measurements and computational modeling seems to be the only viable approach. For this, knowledge on the dispersive properties of ocular media across the visible spectrum is necessary.

While theoretical dispersion equations rely on physical constants and hold true for relatively homogeneous materials, the complexity of the material found in living vertebrate lenses (e.g. water, different proteins and lipids, ions, ion complexes, etc.) discourages their use. The multitude of different dispersive factors (electrons at various energetic levels and electric dipole molecules) results in the same number of parameters to be included in the

* Corresponding author. Fax: +46 46 222 44 25.
E-mail addresses: 12.yakir@gmail.com (Y.L. Gagnon), ronald.kroger@cob.lu.se (R.H.H. Kröger), bo.soderberg@thep.lu.se (B. Söderberg).
URL: http://www.lu.se/o.o.i.s/7758 (Y.L. Gagnon).

0042-6989/$ - see front matter © 2010 Elsevier Ltd. All rights reserved.
doi:10.1016/j.visres.2010.02.020

dispersion equation. Alternatively, the lens material's RI, n, can be described as a function of the wavelength it was measured at, λ, and a reference RI, n_0, the same material has at a reference wavelength, λ_0, with the following dispersion formula suggested by Kröger (1992):

$$n(\lambda_0, \lambda, n_{\lambda_0}) = 2\frac{n_{\lambda_0} + m_b(\lambda_0^2 - \lambda^2) - b_b(\lambda_0 - \lambda)}{1 + m_m(\lambda_0^2 - \lambda^2) - b_m(\lambda_0 - \lambda)} - n_{\lambda_0}, \quad (1)$$

where m_b, b_b, m_m, and b_m are parameters lacking any physical relevance but have units μm^{-2}, μm^{-1}, μm^{-2}, and μm^{-1} respectively. This formula is based on measurements of RI at four wavelengths in a large variety of ocular media performed by Sivak and Mandelman (1982).

While Sivak and Mandelman measured dispersion directly in freshly dissected eye material, Kröger and Campbell determined longitudinal chromatic aberration (LCA) in lenses of the African cichlid fish, *Astatotilapia* (formerly *Haplochromis*) *burtoni*. Laser beams were scanned through freshly dissected lenses and LSAs were measured for four wavelengths of laser light. In the current study, we combine the refractive indices measured in dissected eye material with the LCA measured by laser-scanning of *A. burtoni* lenses to find a set of dispersion model parameters that fits both datasets.

2. Fitting directly measured dispersion

In Sivak and Mandelman's study, the ocular media were grouped into four different types: vitreous, aqueous, cornea, and lens. Each group encompassed a different range of refractive indices, with low values for vitreous and aqueous, and high ones for lens material. All of these values and ocular media groups were used in fitting the dispersion model because the entire RI range is required for modeling the lenses of fishes and other animals. While the cornea is excluded in ray-tracing the fish lens (it has negligible refractive power), it resembles the lens capsule in both RI range and collagen content, making it a good proxy for the capsule that is incorporated in ray-tracing the lens.

A nonlinear multiple regression analysis (Seber & Wild, 1989) was initially used to fit Eq. (1) to the Sivak and Mandelman dataset. A constraint function was used in order to limit the problem by allowing only realistic and relevant solutions. The derivative of the dispersion model across the measurement wavelength (λ) had to be negative (i.e. lower refractive indices for longer wavelengths). This had to be true for a wavelength span between 400 nm and 700 nm, and for refractive indices between 1.36 and 1.54. Finally, no refractive indices below 1.2 or above 1.7 were allowed. The results of the initial fit were used as a starting guess in an optimization that found parameter values that satisfied the required constraints. Parameters resulting in the best possible fit (with the highest r^2 value) were found using a third optimization constrained by the requirements mentioned above. This optimization used the same independent variables determined by Kröger (1992) from the dataset measured by Sivak and Mandelman (i.e. λ, λ_0, and n_0) to calculate the dispersed refractive index (n) using Eq. (1) and compared them to the measured values. This resulted in an r^2 of 0.9991 (Table 1).

3. Fitting the longitudinal chromatic aberration

The modeled lens used in this study was based on both the morphological results by Gagnon, Söderberg, and Kröger (2008) and the optical properties determined by Kröger, Campbell, Munger, and Fernald (1994) for *A. burtoni*. The lens was surrounded by a capsule of 0.9% lens radius (R) in thickness and with a RI of 1.394. The lens had a constant index zone of 1.362, extending from 94% R to the capsule (Gagnon et al., 2008). The RIG ranged from the lens center to 94% R. The RI of the surrounding medium was set to 1.334. The lens was modeled so that its longitudinal spherical aberration (LSA) curve fitted the LSA curve found by Kröger et al. (1994). All of the above values are valid for a wavelength of 633 nm.

Table 1
The dispersion model's parameters (i.e. a, b, c, and d) for all three fits, and their corresponding coefficients of determination (r^2) to both datasets. The three fits were to the Sivak and Mandelman dataset separately, to the Kröger and Campbell dataset separately, and to both combined. The two datasets the fits were compared to were the Sivak and Mandelman dataset and the Kröger and Campbell dataset. Values of r^2 are provided for both datasets.

Dataset	a (μm^{-2})	b (μm^{-1})	c (μm^{-2})	d (μm^{-1})	r^2_{Sivak}	$r^2_{Kröger}$
Sivak	0.6394	0.9094	0.5201	0.7400	0.9991	0.8496
Kröger	0.7437	0.9686	0.5503	0.7236	0.9932	0.9994
Combined	0.7247	0.9489	0.5717	0.7581	0.9990	0.9993

Ray-tracing and inferring the lenses' RIG was done with the Abel transform and its inverse form, as in earlier studies (Barrell & Pask, 1978; Campbell, 1984; Campbell & Sands, 1984; Chu, 1977; Fletcher, Murphy, & Young, 1954; Gagnon et al., 2008; Kröger et al., 1994; Kröger & Campbell, 1996; Pierscionek, 1988, 1994, 1995; Pierscionek & Augusteyn, 1995). The reader is advised to consult the mentioned reports (e.g., Chu, 1977; Campbell, 1984; Gagnon et al., 2008) for more detailed descriptions of the mathematical procedures involved in calculating ray trajectories. Generally, these procedures require the lens to have a RI distribution that is radially symmetric. The correctness of this assumption has been bolstered specifically for the lenses of *A. burtoni* by the results of Fernald and Wright (1983).

Laser-scanning results in an LSA curve showing the laser beam's back center distance (BCD, the axial distance from the center of the spherical lens to the point where the refracted laser beam intercepts the optical axis) as a function of beam entrance position (BEP, the lateral distance between the optical axis of the lens and the beam entering the lens; see LSA curves in Fig. 3B for examples). For a more detailed description of the methods involved in these measurements the reader is advised to consult the suggested literature (e.g. Fig. 4 in Malkki & Kröger (2005)). The measured LSA curves were used to calculate the deflection angles of the laser beam for each given BEP at all four laser wavelengths (457, 488, 515, and 636 nm). The deflection angle curves obtained were approximated with a Chebfun function (Trefethen, Hale, Platte, Driscoll, & Pachón, 2009) (numerical estimations partly based on Chebyshev expansions). This function was used to ray-trace the modeled lens (see Chu, 1977; Campbell, 1984; Gagnon et al., 2008, for the mathematical procedure). Since most of the incident energy is lost by reflection for BEPs larger than 0.95R (Sroczyński, 1977) and the laser-scanning method produces unreliable results for small BEP values (Malkki & Kröger, 2005), no BCD values for BEP larger than 0.95R or smaller than 0.05R were calculated in the ray-tracing process.

An optimization was used to find a set of parameters for Eq. (1) (i.e. a, b, c, and d) that fitted the LCAs (Kröger & Campbell, 1996) had obtained. The parameters obtained from the directly measured dispersion fit (see Section 2), were used as an initial guess of the dispersion parameters for the optimization process. This optimization resulted in a set of model parameters producing LSA curves that corresponded to the measured ones with an r^2 of 0.9982 (Table 1).

4. Fitting both datasets

A multi-objective goal attainment optimization algorithm was used to fit the dispersion model to both datasets simultaneously

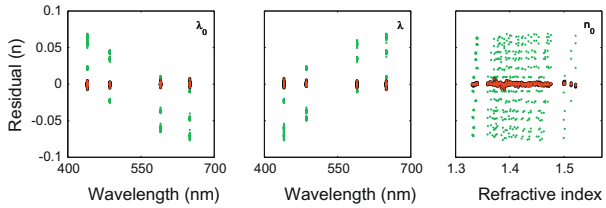

Fig. 1. Differences in refractive index from the dispersion model. The differences between the dataset measured by Sivak and Mandelman and the refractive indices calculated were obtained by using the parameters from the Kröger and Campbell fit (green), the Sivak and Mandelman fit (red), and the combined fit to both datasets (black). Note that the differences from the combined fit are almost as low as from the Sivak and Mandelman fit.

in order to find a set of parameters that would fit both datasets nearly as well as each separate fit did. A multi-objective algorithm is concerned with the simultaneous optimization of a set of functions. The algorithm is given a set of functions, all dependent on one set of parameters, a set of goals the functions need to attain, a set of weights that controls the deviation of the functions' output from the goals, and an initial guess for the parameters' values. Starting at the initial guess, the algorithm adjusts the values of the parameters so that the functions' outputs approach the weighted goals via iterative optimization. The algorithm attempts to either over-attain or under-attain the goals, depending on the sign of the weights (see MATLAB R2009b documentation for further details and Fleming & Pashkevich (1985)).

The r^2 value calculated for fitting the Sivak and Mandelman dataset separately, and the one obtained for when fitting the Kröger and Campbell dataset separately (both were 0.99) were used as the goals for the multi-objective goal attainment optimization. This algorithm used two separate functions to assess whether a set of new parameters was successful or not. The first function calculated the r^2 between the Sivak and Mandelman dataset and a calculated one based on the new parameters. The second function returned the r^2 between the LCA measured in *A. burtoni* by Kröger and Campbell and the LSA curves that were ray-traced through the modeled lens using three different wavelengths (457, 488, and 515 nm). The effect of the parameters in Eq. (1) is canceled out when $\lambda = \lambda_0$. For this reason, no ray-tracing was needed for the wavelength of 633 nm. The outcomes of these two functions were made to equal as much as possible the previously mentioned r^2 values via the multi-objective goal attainment optimization algorithm. The weights assigned to the functions were equal, meaning that both functions' outputs were regarded as equally important, and any deviation from the goals was leveled between the two.

This procedure resulted in a new set of parameters with an r^2 value of 0.9990 and 0.9982 for the Sivak and Mandelman dataset and the Kröger and Campbell dataset, respectively, both being equal up to the third decimal to the coefficients of determination acquired by fitting the datasets separately (Table 1).

5. Analysis of fits

The parameters obtained by the separate fits to each measured dataset were different. We investigated how well both sets of parameters fitted to the alternative dataset. The parameters from the Kröger and Campbell fit resulted in an r^2 value of 0.2987 for the Sivak and Mandelman dataset (Table 1). The residuals were ~ 0.1 at the ends of the wavelength interval (both for measurement and reference wavelength, see green dots in Fig. 1), which is more than twice the residuals obtained when fitting the Sivak and Mandelman dataset (red dots in Fig. 1).

The parameters from the Sivak and Mandelman fit resulted in LSA curves that differed from those measured by Kröger and Campbell with an r^2 of 0.8612 (see Table 1 and Fig. 2). The difference between the LCA obtained with the parameters from the Sivak and Mandelman fit and the original LCA measured by Kröger and Campbell was about as large as the difference in BCD between the different laser wavelengths ($\sim 0.03R$, see Fig. 3A for comparison of wavelength induced BCD shift).

Using the parameters obtained from the combined fit to both datasets produced the RIG curves in Fig. 3A. The LSA curves corresponding to these RIGs are shown in Fig. 3B (dashed lines). They closely followed the measured LSA curves (solid lines).

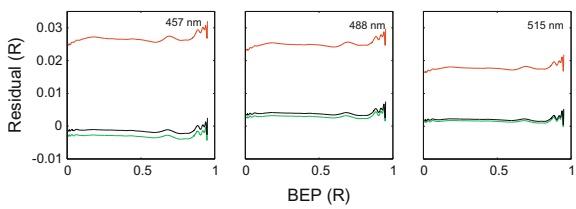

Fig. 2. Differences in BCD (ΔBCD) from the dispersion model. The ΔBCDs between the dataset measured by Kröger and Campbell and the LSAs calculated were obtained by using the parameters from the Kröger and Campbell fit (green), the Sivak and Mandelman fit (red), and the combined fit to both datasets (black). Note that the ΔBCDs from the combined fit are almost indistinguishable from the Kröger and Campbell fit. BCD is the axial distance from the center of the spherical lens to the point where the refracted laser beam intercepts the optical axis and BEP is the distance between the entering beam and the optical axis (both in lens radius units). The ΔBCDs are given for only three of the four wavelengths used by Kröger and Campbell since the fourth wavelength (633 nm) is the reference wavelength (λ_0).

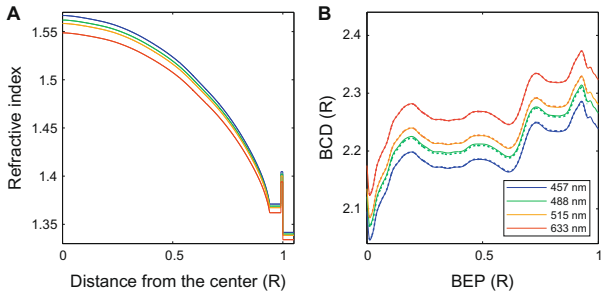

Fig. 3. (A) The refractive index gradients of the *A. burtoni* lens at different wavelengths. The *x*-axis denotes the distance from the lens's center in units of lens radius (*R*) while the *y*-axis is the refractive index at the wavelengths 457 (blue), 488 (green), 515 (orange), and 633 nm (red). These were calculated from the combined fit of the parameters to the Kröger and Campbell and Sivak and Mandelman datasets. (B) The LSA curves of the *A. burtoni* lens at four wavelengths of light (457, 488, 515, and 633 nm, color coded as in A). The *X*-axis denotes the distance between the entering ray of light and the lens' optical axis (BEP). The *Y*-axis is the distance between the center of the lens and the point where the exiting ray of light intercepts the optical axis (BCD). Both are in units of the lens' radius (*R*). The solid lines are the measured LSA curves (Kröger & Campbell, 1996), while the dashed lines are the calculated LSA curves based on the combined fit of the parameters to the Kröger and Campbell and Sivak and Mandelman datasets.

6. Conclusions

The model suggested by Kröger (1992) describes the directly measured refractive indices of vertebrate eye media (Sivak & Mandelman, 1982) equally well as the observed laser scans through fish lenses (Kröger & Campbell, 1996). The parameters' robustness has been increased by optimizing the model to fit another, independent dataset obtained with a different method (namely the Kröger and Campbell dataset).

The model's parameters are intrinsically dependent on the two datasets. The diversity of the different vertebrate eye media used in the Sivak and Mandelman dataset guarantees that new dispersion measurements cannot differ much from the existing dataset and therefore would not affect the end result of this study in a significant manner.

The dispersion model in this study is not based on any theoretical understanding of the dispersion phenomenon. The obtained parameters should therefore be used with caution at wavelengths shorter than 400 nm or longer than 700 nm and/or at refractive indices lower than 1.3 or higher than 1.6. The model however fulfills its function by approximating the observed data well. This makes the complex matter of describing dispersion in living eye media with four parameters possible and accessible for other studies.

References

Barrell, K. F., & Pask, C. (1978). Nondestructive index profile measurement of noncircular optical fibre preforms. *Optics Communications, 27*(2), 230–234.

Campbell, M. C. W. (1984). Measurement of refractive index in an intact crystalline lens. *Vision Research, 24*(5), 409–416.

Campbell, M. C. W., & Sands, P. J. (1984). Optical quality during crystalline lens growth. *Nature, 312*(5991), 291–292.

Chu, P. L. (1977). Nondestructive measurement of index profile of an optical-fibre preform. *Electronics Letters, 13*(24), 736–738.

Fernald, R. D., & Wright, S. E. (1983). Maintenance of optical quality during crystalline lens growth. *Nature, 301*(5901), 618–620.

Fleming, P., & Pashkevich, A. (1985). Computer aided control system design using a multi-objective optimisation approach. In *Control conference* (Vol. 1, pp. 174–179). Cambridge, UK.

Fletcher, A., Murphy, T., & Young, A. (1954). Solutions of two optical problems. *Proceedings of the Royal Society of London A, 223*, 216–225.

Gagnon, Y. L., Söderberg, B., & Kröger, R. H. H. (2008). Effects of the peripheral layers on the optical properties of spherical fish lenses. *Journal of the Optical Society of America A, 25*, 2468–2475.

Gustafsson, O. S. E., Collin, S. P., & Kröger, R. H. H. (2008). Early evolution of multifocal optics for well-focused colour vision in vertebrates. *Journal of Experimental Biology, 211*, 1559–1564.

Hanke, F. D., Kröger, R. H. H., Siebert, U., & Dehnhardt, G. (2008). Multifocal lenses in a monochromat: The harbour seal. *Journal of Experimental Biology, 211*, 3315–3322.

Hecht, E. (2002). *Optics*. San Francisco: Addison Wesley.

Karpestam, B., Gustafsson, J., Shashar, N., Katzir, G., & Kröger, R. H. H. (2007). Multifocal lenses in coral reef fishes. *Journal of Experimental Biology, 210*, 2923–2931.

Kröger, R. H. H. (1992). Methods to estimate dispersion in vertebrate ocular media. *Journal of the Optical Society of America A, 9*(9), 1486–1490.

Kröger, R. H. H., & Campbell, M. C. W. (1996). Dispersion and longitudinal chromatic aberration of the crystalline lens of the african cichlid fish *Haplochromis burtoni*. *Journal of the Optical Society of America A, 13*(12), 2341–2347.

Kröger, R. H. H., Campbell, M. C. W., & Fernald, R. D. (2001). The development of the crystalline lens is sensitive to visual input in the African cichlid fish, *Haplochromis burtoni*. *Vision Research, 41*, 549–559.

Kröger, R. H. H., Campbell, M. C. W., Fernald, R. D., & Wagner, H. J. (1999). Multifocal lenses compensate for chromatic defocus in vertebrate eyes. *Journal of Comparative Physiology A: Sensory Neural and Behavioral Physiology, 184*(4), 361–369.

Kröger, R. H. H., Campbell, M. C. W., Munger, R., & Fernald, R. D. (1994). Refractive index distribution and spherical aberration in the crystalline lens of the african cichlid fish *Haplochromis burtoni*. *Vision Research, 34*, 1815–1822.

Lind, O. E., Kelber, A., & Kröger, R. H. H. (2008). Multifocal optical systems and pupil dynamics in birds. *Journal of Experimental Biology, 211*, 2752–2758.

Malkki, P. E., & Kröger, R. H. H. (2005). Visualization of chromatic correction of fish lenses by multiple focal lengths. *Journal of Optics A: Pure and Applied Optics, 7*, 691–700.

Malmström, T., & Kröger, R. H. H. (2006). Pupil shapes and lens optics in the eyes of terrestrial vertebrates. *Journal of Experimental Biology, 209*(1), 18–25.

Pierscionek, B. K. (1988). Nondestructive method of constructing 3-dimensional gradient index models for crystalline lenses. 1. Theory and experiment. *American Journal of Optometry and Physiological Optics, 65*(6), 481–491.

Pierscionek, B. K. (1994). Refractive index of the human lens surface measured with an optic fibre sensor. *Ophthalmic Research, 26*(1), 32–35.

Pierscionek, B. K. (1995). The refractive index along the optic axis of the bovine lens. *Eye (London, England), 9*, 776–782.

Pierscionek, B. K., & Augusteyn, R. C. (1995). The refractive index and protein distribution in the blue eye trevally lens. *Journal of the American Optometric Association, 66*(12), 739–743.

Seber, G. A. F., & Wild, C. J. (1989). *Nonlinear regression*. Auckland: John Wiley & Sons Inc..

Sivak, J. G., & Mandelman, T. (1982). Chromatic dispersion of the ocular media. *Vision Research, 22*(8), 997–1004.

Sroczyński, S. (1977). Spherical aberration of crystalline lens in the roach *Rutilus rutilus*. *Journal of Comparative Physiology A: Sensory Neural and Behavioral Physiology, 121*(1), 135–144.

Trefethen, L. N., Hale, N., Platte, R. B., Driscoll, T. A., & Pachón, R. (2009). Chebfun version 3, Oxford University. <http://www.maths.ox.ac.uk/chebfun/>.

Paper IV

Optical advantages and function of multifocal spherical fish lenses

Yakir Gagnon[1,*], Bo Söderberg[2], Ronald Kröger[1]
1 Department of Biology, Lund University, Lund, Sweden
2 Department of Theoretical Physics, Lund University, Lund, Sweden
∗ **E-mail: 12.yakir@gmail.com**

Abstract

Many fish lenses exhibit multiple focal lengths when laterally scanned with a laser beam. Although this multifocality has been discovered in a majority of vertebrate eyes, its visual benefit has not yet been demonstrated nor fully understood. Optical properties were therefore modeled and compared between four lens types, the lens of *Astatotilapia burtoni*, an African cichlid fish species with distinct multifocal lenses, an equivalent monofocal lens, and two artificial multifocal lenses. The optical properties used to compare between these lenses were longitudinal spherical aberration curves, point spread functions, modulation transfer functions, and imaging characteristics. The multifocal lenses performed better than the monofocal lens by displaying a better balance between spatial and spectral information. The factors affecting the quality and function of multifocal lenses are discussed as well.

Introduction

Vision is an important source of information for many animals and a variety of different eye types has evolved [1]. Vertebrate eyes are camera-type eyes and are generally similar in design to a photographic camera. However, the optical systems of these eyes are apparently much simpler than a good camera objective that requires a number of lenses to correct for various kinds of optical aberrations. There are at maximum only two lenses in a vertebrate eye: the cornea and the crystalline lens.

In aquatic vertebrates, the cornea is surrounded by water on the outside and the watery aqueous humor on the inside. Both media have similar and relatively high refractive indices and if the cornea is thin, which is the case in most species, its refractive power is negligible [2,3]. The task of focusing light on the retina is thus left to the lens alone. Among the aquatic vertebrates, the lenses of bony fishes (teleosts) have received the most attention, mainly because of easy access to fresh material and the simple geometry of the lenses, which are typically spherical [4–6]. Vertebrate lenses are made of fiber cells; thin cells that stretch from pole to pole in concentrically arranged layers.

Spherical lenses made of homogenous materials (e.g. glass) suffer from longitudinal spherical aberration (LSA). Maxwell was the first to note that fish lenses are almost free of LSA. He suggested that LSA is greatly reduced in fish lenses by a refractive index gradient (RIG) with the highest refractive index (RI) in the center and lowest RI at the surface of the lens [7].

Another optical problem arises from dispersion: the RI of any transparent medium, except for vacuum, is a function of the wavelength of light. In consequence, optical systems focusing a wide range of wavelengths (polychromatic light) suffer from longitudinal chromatic aberration (LCA): light of different wavelengths is focused at different distances from the optical system. This leads to chromatic blur on the retina. The blurring effect is most pronounced in optical systems of high refractive powers (i.e. a system with a short focal length relative to its aperture diameter). Fish lenses are powerful with normalized focal lengths of 2.2–3.3 lens radii [8,9].

As a mechanism that compensates for LCA, many fish lenses have several focal lengths when examined with monochromatic light, i.e. they are multifocal. The lens is made of shell-like zones, each with a different focal length. The distances between the focal points along the optical axis are equal to the focal length differences due to LCA between the wavelengths that are of highest importance to the animals. This means that these wavelengths are correctly focused on the retina. A sharp color image is created on the background of defocused light that has passed through "wrong" zones in the lens [10]. The multifocal principle compensating for the defocusing effect of LCA is present in a variety of fishes [8,10–13] and tetrapods [14–16].

Although the multifocal principle is present in many vertebrate eyes, its actual visual benefit and function has not yet been demonstrated. In this study we used computer modeling to compare a variety of optical properties between four lens types, representing the lens of *Astatotilapia burtoni* (the African cichlid fish species in which the multifocal principle was discovered), an equivalent monofocal lens, and two other hypothetical lenses. For each lens, we determined the LSA, RIG, point spread function (PSF), modulation transfer function (MTF), and imaging characteristics. The aim of this study was to test the multifocal principle.

Results

PSF and MTF

The Burtoni lens created a complex pattern of retinal illumination with peaks in the PSF, i.e. high values for $I(\theta_0)$, at or close to the λ_{max} of the cones of *A. burtoni* (Figure 1). This mirrors results obtained by using measured LSAs [10], indicating that the Burtoni lens recreated the optical properties of real *A. burtoni* lenses. The Monofocal lens created a sharp peak at 523 nm and the PSF broadened rapidly towards shorter and longer wavelengths. The PSFs of the Step-function lens had three distinct peaks at the λ_{max} values the lenses were optimized for. The peak in the blue range, created by the outmost zone in the lens, was considerably sharper than the peaks at longer wavelengths (Figure 1). The $I(\theta_0)$ of the Mismatch lens peaked at 445, 508, and 587 nm. The peak in the long wavelength range was broader than the equivalent peak in the Step function lens (i.e. more wavelengths in the vicinity of 587 nm had high $I(\theta_0)$ indicating sharp focus).

The MTFs showed high contrast (e.g. the Step-function had about 0.96 contrast at 562 nm) for spatial frequencies as high as 27 cycles per degree, i.e. the maximum sampling frequency. This was true, however, only at the wavelengths where the PSFs had high $I(\theta_0)$ values (Figure 1). The Burtoni lens had relatively low contrast (about 0.78 at 562 nm) at the cut-off frequency for those wavelengths.

Images

The filtered hyperspectral images resulted in an RGB image for each lens-retina combination (Figures 2). All lens-retina combinations resulted in equally bright images (this depended on the fact that the sums of the PSFs and absorption curves were equal to one). The Camera and Mismatch retinas produced more saturated colors than the Natural retina. The patches in the images under the Mismatch retina were red tinted. The Monofocal lens produced green tinted images. The Step function image was clearer under the Camera retina than it was under the Mismatch retina. The opposite was true for the Mismatch lens. There was little variation between the different lenses' images under the Natural retina.

A closer look at the three color channels of the images under the Camera retina showed that while the green channel of the Monofocal lens' image was well focused, both the red and especially the blue channels were severely defocused. All three channels of the Mismatch lens' image were defocused. All lenses' blue channel was the most defocused one of the three.

The image histograms showed that the Burtoni lens had highest contrast under the Camera retina. The Monofocal lens had broad pixel intensity distribution in the green channel indicating high contrast under the Camera retina and slightly lower focus under the Mismatch retina. Under the Natural retina this channel was relatively defocused. The red and blue channels had however very low contrast with narrow and pointy histograms of which the Mismatch retina had the worst. As expected from the images in Figure 2, the Step-function lens had narrower histograms under the Mismatch Retina while the opposite was true for the Mismatch lens. The red channel histograms of the Mismatch retina were all shifted to the right, indicating higher pixel intensities than found in the red channel of the other two retinas.

Discussion

Shortcomings in the experimental measurements this study relays on affect the results of this study. The LSA curves the lenses are based on are an average of many lenses which might smooth and flatten certain characteristics in the individual LSAs. This smoothing is enhanced by the laser beam diameter used to scan the lenses. The performance of the multifocal lenses we present is therefore a conservative estimate. It is however safe to constitute a number of new insights regarding the factors affecting these multifocal lenses.

Dispersion and depth of focus

The $I(\theta_0)$ peaked at the intended wavelengths in the designed lenses (Figure 5 and Figure 1). The parts of the PSF that were not correlated with the intended function of the lenses were a result of mainly two factors and their interaction: dispersion and depth of focus.

Dispersion's dependency on wavelength is not linear; dispersion is stronger for shorter wavelengths than it is for longer ones. That is the reason defocusing in the Monofocal lens at short wavelengths is not equal to

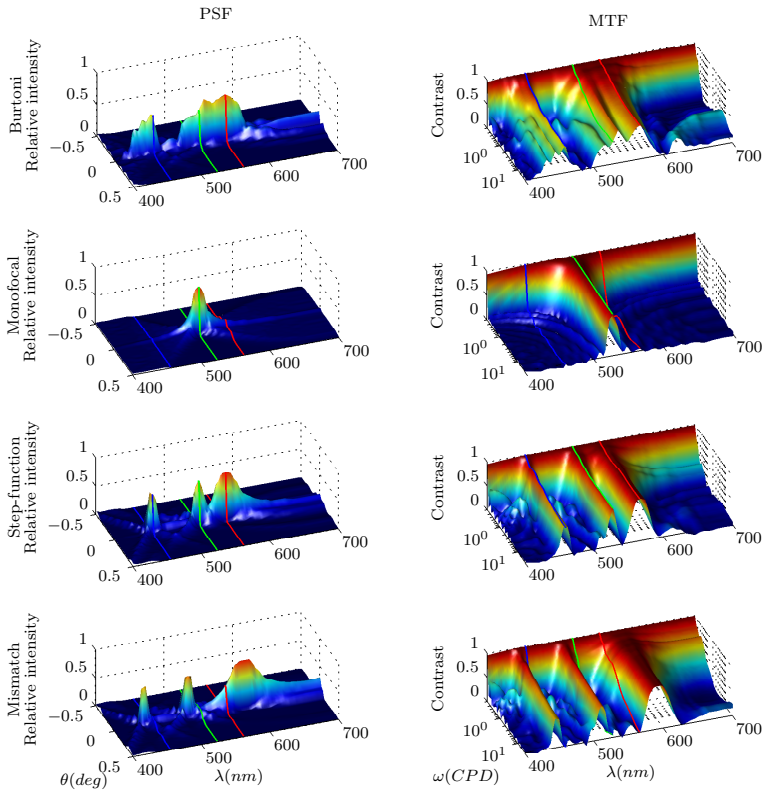

Figure 1. The left column shows the point spread functions (PSF) of all four lenses and the modulation transfer functions (MTF) are on the right. Each row depicts one lens, from top to bottom: Burtoni, Monofocal, Step-function, and Mismatch. The x-axis in the PSF panels is the wavelength in nm of the focused light. The y-axis is the spread angle in degrees; the angle between the intersection of the optical axis with the retina, the nodal point of the lens, and the intersection of the exiting ray of light with the retina. This angle depicts the light's deviation from a perfect focus. The z-axis is the intensity of absorbed light in the photoreceptors. The x-axis in the MTF panels is the wavelength in nm of the focused light. The y-axis is the spatial frequency in units of cycles per degree (logarithmic scale) of the signal being focused. Due to the photoreceptor size this frequency has a cut-off at 27 cycles per degree. The z-axis represents the contrast the spatial frequency is perceived at when viewed at each wavelength. The surface color denotes the height along the z-axis in all panels. The three λ_{max} values found in the trichromatic retinas are represented as color-coded lines superimposed on the surfaces.

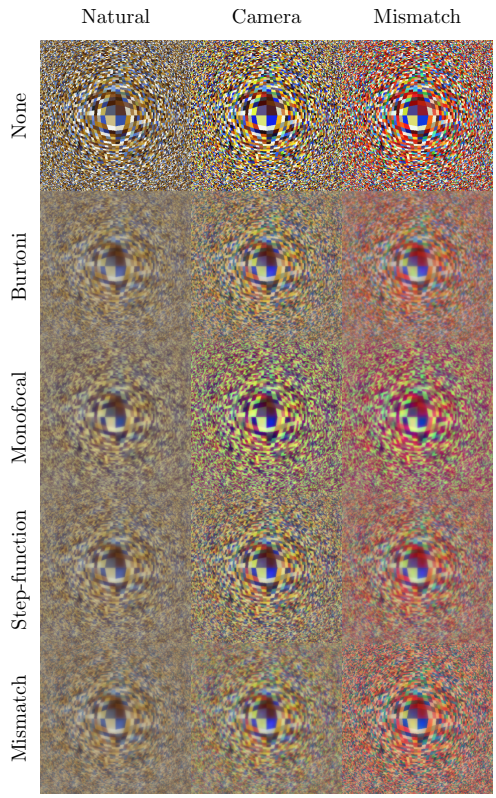

Figure 2. The hyperspectral images as seen through the four lenses and sampled under the three retinas. The lenses are displayed per row (from top to bottom: None, Burtoni, Monofocal, Step-function, and Mismatch) and the retinas are per column (from left to right: Natural, Camera, and Mismatch). The first row, "None", includes the hyperspectral images sampled under the retinas without any filtering (i.e. these did not go through a lens before being sampled). The yellow slice highlights the part that was used in the comparison shown in Figure 3. This figure displays the estimated signals received at the first layer of the retina. Post processing (e.g. white-balancing, histogram equalization, opponent processing, etc.) that occurs in subsequent layers (both morphological and physiological) will considerably change the perceived image. It is therefore important to remember that certain image aspects that are presented here in their "raw" form, such as haziness, are corrected for higher up in the visual pathway. Due to the raw nature of this representation, certain aspects of these images can be misleading. The false contrast perceived in the Monofocal lens sampled under the Camera retina does not represent a real increase in the information content of that image (see Figure 3 for a better understanding of the comparison between the images).

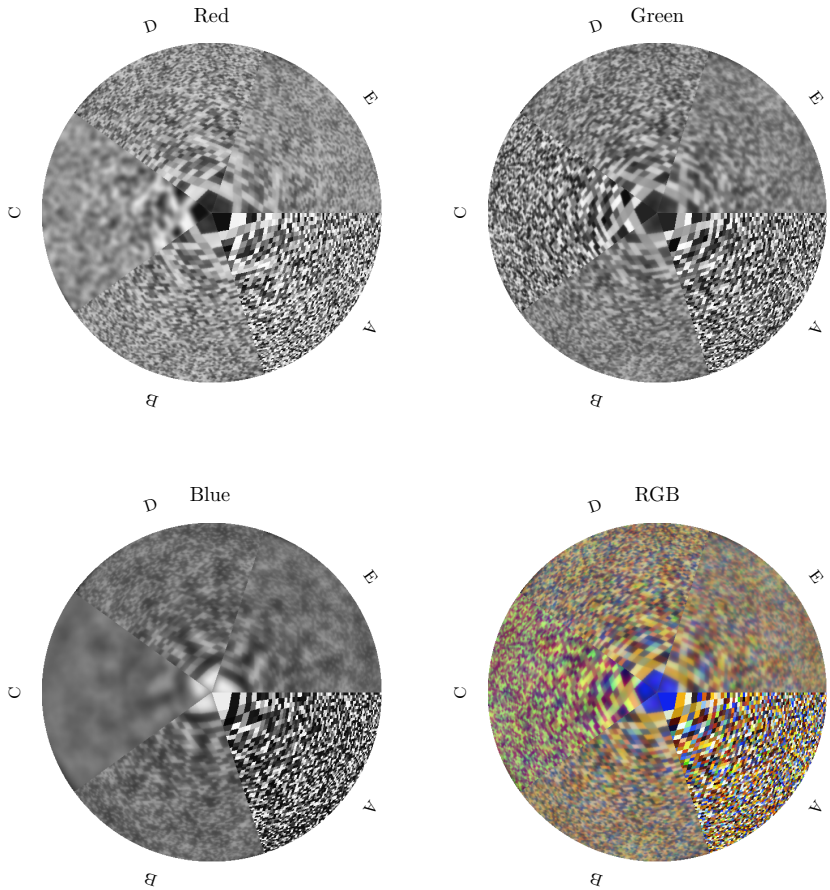

Figure 3. A comparison of the (enlarged) slice taken from each row in the Camera retina column in Figure 2 (second column). The same slice was taken from the resulting four filtered + not filtered hyperspectral image under the Camera retina. This slice was rotated and fit into the resulting wheel for better comparison. The slices are from the None, Burtoni, Monofocal, Step-funtion, and Mismatch images and labeled A, B, C, D, and E respectively. The Red, Green, and Blue wheels display the three color channels present in the RGB wheel. Notice the poor color content in the Monofocal slice, where all the smaller patches have darker/brighter shades of green. This is visible in the blue and red channels where the Monofocal slice has the worst contrast. The Mismatch slices have bad contrast in all three channels. No obvious differences are present between the Burtoni and Step-function slices.

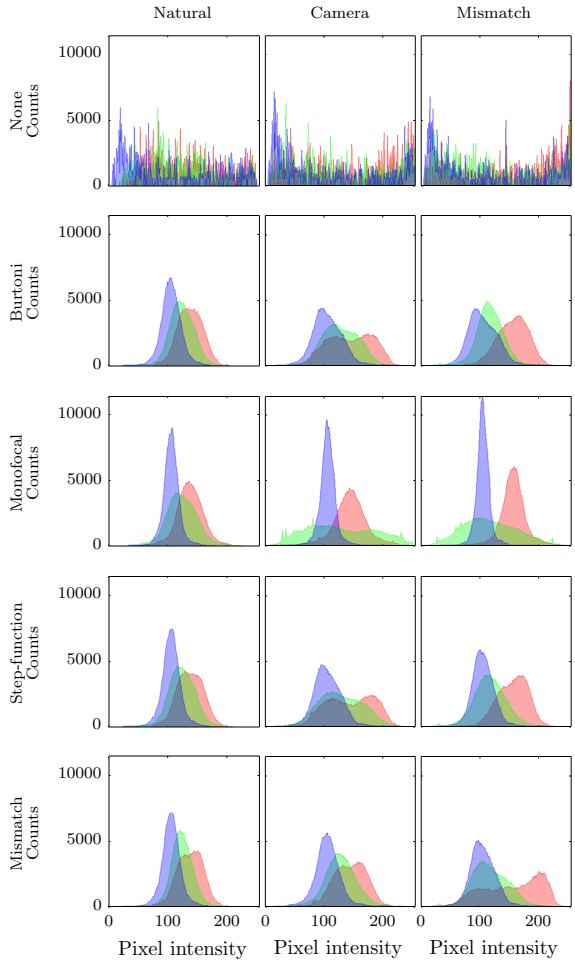

Figure 4. The image histograms for the filtered and sampled hyperspectral images presented in Figure 2. The lenses are displayed per row (from top to bottom: None, Burtoni, Monofocal, Step-function, and Mismatch) and the retinas are per column (from left to right: Natural, Camera, and Mismatch). The first row includes the histogram of the hyperspectral images sampled under the retinas without any filtering (i.e. these did not go through a lens before being sampled). The x-axis is the pixel intensity ranging from 0 to 255 (2^8 intensity steps). The y-axis is the frequency of pixels with the corresponding intensity. The trichromatic retinas have three histograms for each of their color channels, red, green, and blue (color-coded). The histograms describe the distribution of pixel intensities in the images. This can be used to compare contrast between similar images. A broad distribution of pixel intensities, such as in the histogram of the None filtered images, results in a higher contrast. A pointy narrow histogram indicates that the image has a very limited range of pixel intensities resulting in a bland image poor in contrast. Notice that while the green channel of the Monofocal image sampled under the Camera retina has a broad histogram indicating high contrast, its red and blue channels are pointy and narrow resulting in low contrast.

defocusing at long wavelengths, with the former being starker than the latter. It also explains the difference in $I(\theta_0)$ red peak thickness between the Step-function and Mismatch lenses. Defocusing was stronger for neighboring wavelengths around the shorter wavelength of the red peak in the Step-function lens than it was in the Mismatch lens. Furthermore it reflects the fact that the blue channel in the RGB images was always the most defocused one. This kind of wavelength dependent defocusing can be seen in all lenses (Figure 1).

Depth of focus plays a major role in shaping the distribution of relative intensities at the central θ. Depth of focus is inversely correlated to the distance between the incoming beam of light and the optical axis of the system, i.e. BEP. Smaller BEP values allow for a larger depth of focus and less aberrations. Thus, discrepancies between the wavelength of the incoming light and the intended wavelength are less detrimental for smaller BEPs than they are for larger BEPs. Therefore the specific BCDs in combination with their BEP values affect which wavelengths are to be focused by the lens. Both the Step function and Mismatch lenses had shorter BCDs for smaller BEPs, allowing the focusing of longer wavelength closer to the optical axis (Figure 5 and Figure 1). Similarly to the effects of dispersion, focusing deteriorated faster for short wavelengths than for long wavelengths, explaining the wider range of focused long wavelengths and the narrower short wavelength band.

The amount of light that is focused at a certain wavelength is determined by the area of the lens-zone that is devoted to focusing that specific wavelength and affects the contrast of an image in that wavelength. Since each zone or radial distance can only be used for one wavelength the delegation of zones to specific wavelengths limits the focusing of other wavelengths. With depth of focus, dispersion, and photoreceptor size all affecting the PSF and contrast, the allocation of focused wavelengths is not trivial. It is however clear that naively dividing the lens LSA into three equal zones, each responsible for focusing one different wavelength (e.g. the Step-function lens), the functionality of the lens improves. The resulting multifocal lens is superior to a monofocal lens since one very sharp channel together with very two blurry channels function worse than three equally blurred channels (Figure 3).

Peripheral visual filtering

The Monofocal lens's MTF quickly lost contrast for all wavelengths but the green λ_{max} while the other lenses retained relatively high contrast at other wavelength intervals (Figure 1). This main difference is evident in the modulated images, with lack of distinctly colored patches in the Monofocal lens's image (slice C in Figure 3). This caused the localized high pixel intensities of the green channel to dominate amongst the smeared average pixel intensity of the other two channels (resulting in green hues in the images of the Monofocal lens). The loss of some spatial information in the multifocal lenses allows the gain of spectral information while the opposite is true for the Monofocal lens. This tradeoff between spatial and spectral information seems to be more beneficial in the multifocal lenses.

All MTFs except Burtoni's showed that contrast was high at the retina's cut off frequency for wavelengths where $I(\theta_0)$ was also high. This indicated that the spatial frequency at which the lens' contrast would significantly deteriorate (e.g. 0.3) is considerably higher than that of the cut-off frequency of the retina. The Burtoni lens seemed to be more adapted to the retina's limited spatial frequency capacity than the other model lenses are. This follows from the smaller area of the zones responsible for focusing λ_{max} in the Burtoni LSA compared to the Step-function lens (compare the amount of overlap between Burtoni LSA curve's plateaus and those of the Step-function LSA in Figure 5). The relatively high spatial frequencies the other lenses conveyed could lead to aliasing problems. Special pixel patterns reduce this problem, but cannot eliminate it [17]. Overlap in spectral sensitivities and cross-talk between spectral channels can also reduce aliasing [17], but lead to problems with image quality. While images under the Natural retina were relatively similar (equal image quality regardless of the lens), it produced more blurry images than the Camera and/or Mismatch retinas. Less overlap in the spectral sensitivity can also lead to artifacts (albeit easily corrected for in later processing). The red hues in the images of the Mismatch retina were caused by the larger separation of the red sensitive photoreceptors from the green ones causing red colors to be more saturated (column Mismatch in Figure 4).

Multifocal lenses fit Wehner's matched filter idea [18]. The lens-retina combinations' performance was closely correlated to how well the lenses' $I(\theta_0)$ distribution resembled the retinae' absorption curves. Only the matching combinations of retina - lens resulted in good performance. The question whether these three specific λ_{max} values are quintessential for the survival of the (in this case cichlid) fish or if another set of λ_{max} would have functioned just as well is not relevant unless the lens matches the λ_{max} of the photoreceptors.

The idea of matched filters additionally included the notion of 'peripheralisation' of these filters; filter out unnecessary information as soon as possible in the sensory pathway. The multifocal lens exhibits such 'peripher-

alisation' since it filters out non essential information before it reaches the retina. It does not focus wavelengths that are not absorbed by the retina nor does it focus spatial frequencies much higher than the cut-off frequency of the retina. This study has shown that such economical behavior is very profitable when assigning the lens zones different wavelength-responsibility. By focusing only the relevant wavelengths and to the required amount the optical system maximizes the spatial-spectral information the animal receives.

Adaptation and regulation

Considering the wide spread adaptive variation of visual pigments in fish retina [19,20], an equal adaptive variation of the optical properties of fish lenses should follow, accompanied by mechanisms that regulate the lens properties to match those of the retina. The adaptation occurring in fish retina is through a genetic process involving amino acid substitution in the opsin molecule. While this adjustment depends on a mutation between generations the lens adaptation can take place within few hours to 10 months [13,21]. This implies that any adaptive variation in the visual system of these fish must be a bottom-up process with changes mediating from the retina to the lens.

It is interesting to see that lenses that differ in LSA, PSF, MTF, and modulated images have relatively small differences in their RIGs. These minute differences are caused by small fluctuations in the crystalline protein concentration found in different parts of the lens. This indicates that a very well tuned RIG regulatory mechanism is required in order to maintain and adjust the functionality of the lens. This is further bolstered by studies by Schartau et al. [13, 22, 23].

Materials and Methods

Model lenses

The basic properties of the model lenses were chosen according to results on the morphology and optical properties of fish lenses [24,25]. The RI of the surrounding medium was set to 1.334 (equal to that of the aqueous and vitreous humour). The lens had a capsule 0.009 lens radius (R) in thickness with an RI of 1.394. A zone of constant index (1.362) extended from the capsule inwards to 0.94 R. The RIG ranged from 0.94 R to the lens center [24]. The RIs mentioned above were valid for 633 nm. Longitudinal chromatic aberration was accounted for by using the dispersion function by Gagnon et al. [26] that is suitable for vertebrate ocular media in general and *A. burtoni* lenses in particular. The spherically curved retina was concentric to the lens and positioned at 2.233 R from the lens center [25].

We created four different model lenses, named the Burtoni lens, the Monofocal lens, the Step-function lens, and the Mismatch lens (Figure 5). The lenses' optical properties were defined by their LSA curves. A measured LSA curve describes the deflection of a laser beam as a function of where the beam entered the lens. The independent variable of this function is the lateral distance between the optical axis of the lens and the entering beam (beam entrance position, BEP). The dependent variable is the distance between the center of the lens and the point where the exiting beam - deflected by the lens - intercepted the optical axis (back center distance, BCD). Due to the inverse relationship of wavelength and RI, this property affects the wavelength being focused, where longer BCDs focus shorter wavelengths and vice versa. The RIG of a spherical lens can be inferred from its LSA curve using the inverse Abel transform [24,25,27–36]. The reader is advised to consult the mentioned reports [24,28,35] for detailed descriptions of the mathematical procedures. All calculations were preformed in Matlab (2010a) using the chebfun package [37] which allows high accuracy and analytical-like solutions.

The Burtoni lens was an example of a natural multifocal lens [10] and had an LSA curve as measured in *A. burtoni* lenses [25]. The Monofocal lens focused the wavelength of maximum absorbance (λ_{max}) of *A. burtoni* middle wavelength sensitive cones (523 nm; [38]). The Step-function lens had three zones, each focusing one of the three λ_{max} of the cones of *A. burtoni*. The inner zone focused 455 nm, the middle zone 523 nm, and the outer zone 562 nm [38]. The Mismatch lens focused slightly different wavelengths, but with an equal mean λ_{max}. These were equal to 445 nm for the inner zone, 508 nm for the middle zone, and 587 nm for the outer zone. The area of each zone that is devoted to focusing a certain wavelength controls the amount of focused light in that wavelength, where larger zones result in more light and vice versa. More focused light leads to sharper images at that wavelength. The zone areas accepting light were therefore equal, i.e. zone width decreased with increasing zone radius (a square root function).

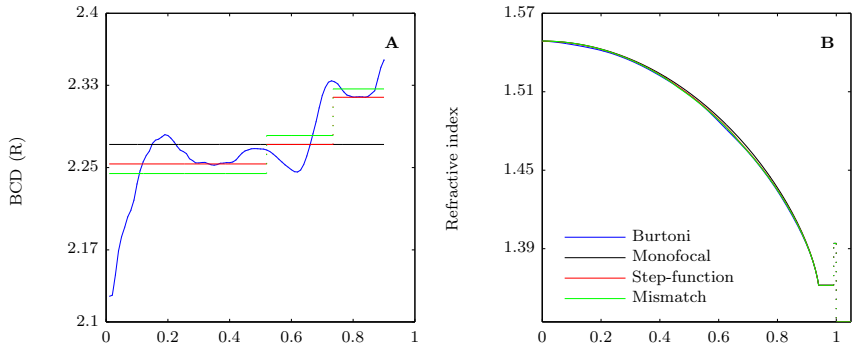

Figure 5. A) The longitudinal spherical aberration curves of the four lenses. The different lenses are color-coded (legend in panel B): Burtoni (blue), Monofocal (black), Step-function (red), Mismatch (green). The x-axis denotes the beam entrance position (BEP) while the y-axis is the back center distance (BCD) of the laser beam, both are in lens radius (R) units (i.e. 1 represents the lens' surface). **B) The refractive index gradients of the four lenses.** The lenses are color coded as in A. The x-axis is the distance from the lens center in units of R. The y-axis is the refractive index at wavelength 633 nm.

Ray-tracing and sampling

Ray-tracings were performed for polychromatic light (50 wavelengths between 400 and 700 nm) using each lens's RIG at 633 nm, the dispersion function by Gagnon et al. [26], and the Abel transform. In order to account for the larger contributions of more peripheral rays to retinal illumination in a real, three-dimensional imaging situation, the ray entrance positions in the two-dimensional model were distributed according to a square root transformation. PSFs calculated from 10^6 rays (i.e. 10^6 BEP values) showed to be sufficiently stable when compared to analytical approximations of the PSFs. The deflection angle of a refracted ray was used to determine the angular deviation between the optical axis and the point where the incoming ray intercepted the retina.

With a focal length of 2.233 R, a lens radius of 1.5 mm, and an estimated photoreceptor cell density of 52500 cells per mm^2 [38] the inter-receptor angle, $\Delta\theta$, in the *A. burtoni* retina was approximately 0.037°. This value was used as the bin width for ray sampling in the retinal plane, with the central bin centered on the optical axis (0°). Since increasing deviation angles correspond to a larger number of photoreceptors/pixels sharing the incoming light, each ray's contribution to a bin's illumination was weighted accordingly. The weighting factor was $\frac{1}{4\pi \sin^2 \frac{\Delta\theta}{4}}$ for the central bin and $\frac{1}{4\pi \sin\theta \sin \frac{\Delta\theta}{2}}$ for all other bins, where $\Delta\theta$ was the inter-receptor angle and θ was the angle between the OA and each consecutive receptor. This procedure resulted in a discrete PSF at each wavelength describing how light from a point in object space illuminates the photoreceptors after being focused by the lens. Since light intensity was equal among wavelengths (white light) and to maintain the brightness of the convolved image, the PSFs were divided by their sum, namely 10^6. The illumination of the central pixel (i.e. $-\frac{\Delta\theta}{2} \leq \theta \leq \frac{\Delta\theta}{2}$), $I(\theta_0)$, was used as a focus indicator. $I(\theta_0)$ is high if the image of a point object is well-focused. The distribution of the central pixel intensities as a function of wavelength describes LCA's effects on image quality.

The MTF of a lens was determined by fast Fourier transformation (magnitude) of the PSF. MTFs were calculated for spatial frequencies from 0 to 27 cycles per degree, which was the highest possible frequency (cut-off frequency) set by the sampling interval of 0.037°. An MTF describes how quickly image contrast deteriorates with increasing spatial frequency.

The hyperspectral image

A hyperspectral image is a stack of image tiers where each tier shows the same scene in a different wavelength interval. Typically, the wavelength interval is narrow (10 nm), allowing for high spectral resolution with stacks containing up to 30 tiers or even more. We created an artificial hyperspectral image to illustrate the performances of the different model lenses. In a checkerboard pattern (201 × 201 squares), each square patch was assigned

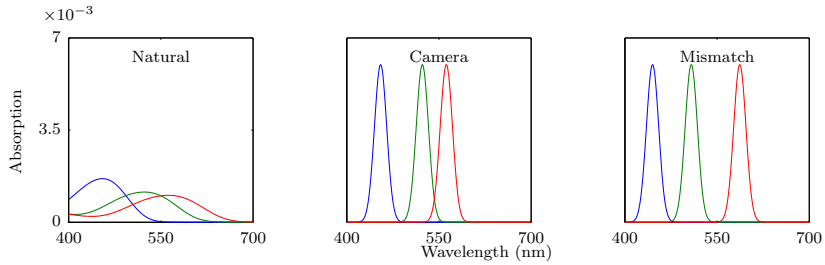

Figure 6. The absorption curves of the three retinas: Natural, Camera, and Mismatch. The x-axis denotes the wavelength in nm. The y-axis is the absorption. The red, green, and blue photoreceptors are color-coded. Note that the curves are normalized so that their sum equals one.

a relative reflectance spectrum in a pseudo-random manner such that no adjacent (vertically, horizontally, and diagonally) squares had the same spectrum. The spectra were taken from more than 200 species of Hawaiian, Australian, and Caribbean reef fish [39]. The colored checkerboard pattern was spatially transformed by squaring the polar radial component of the location of each vertex. The resulting mesh was not square and therefore cropped to fit an image of 600×600 pixels. Only a centered 500×500 pixels region of interest was used in the final RGB images to avoid zero-padding artifacts around the edges of the image (a dark frame surrounding the image). Since each image pixel represented one photoreceptor, this hyperspectral image occupied 18.5° on the retina, resulting in spatial frequencies ranging from approximately 1 to 10 cycles per degree (note that the model retina had a sampling density of 27 photoreceptors per degree). The final hyperspectral image was 600×600 pixels large with 50 wavelengths from 400 to 700 nm.

Spatial and spectral filtering

Imaging of a scene by a lens leads to spatial filtering and the loss of detail depends on the quality (PSF) of the lens. We convolved each wavelength-tier of the hyperspectral image with the PSF of the model lens at the same wavelength. The next step was spectral filtering according to the sensitivities of the photoreceptors/pixels in the retina. We used four different retinas. These were named the Natural retina, the Camera retina, and the Mismatch retina.

In the Natural retina, there were three spectral photoreceptor/pixel types with the λ_{max} of the cones of *A. burtoni* (455, 523, and 562 nm; [38]). Absorption spectra were estimated using the Govardovskii templates for visual pigments (Figure 6; [40]) with published histological data and photonic properties of the cones [38, 41]. All absorption curves were divided by their sum in order to avoid unequal brightness between the image channels (requiring white-balancing). Corrections for adaptive processes and retinal processing were not applied. The pixels in the Camera retina had the same λ_{max} values as the Natural retina, but with bell-shaped (Gaussian) absorption spectra. The Gaussian functions had variances of about 14 nm^2, resulting in relatively little overlap between spectral channels (Figure 6). The Mismatch retina had the same bell-shaped absorption spectra but with different λ_{max} values than that of the other two retinas, namely 445, 508, and 587 nm (Figure 6).

After multiplying each pixel in each tier with the pixel's absorption spectrum, the stimulations of corresponding pixels were summed across the entire stack. This was done separately for each of the three pixel types, resulting in an RGB image. The same procedure of spectral filtering and stimulation summing was also applied on the original hyperspectral image (i.e. the hyperspectral image prior to the lens modulation). These represented the best possible scenarios with regard to lens quality and were used as references for comparisons. All final images were multiplied by 255 and converted to UINT8 images (max spectral reflectance was equal to or smaller than

one).

Comparing the filtered images

In each image, pixels of the same stimulation level (0-255) were counted separately for each channel. A broad and flat distribution of pixel counts indicated a sharp and patchy image, i.e. a good representation of the original unfiltered image. If spatial and spectral filtering evened out the differences between the pixels in the original image, the distribution of pixel counts was narrow and pointed [42]. This method is reliable when comparing intrinsically similar images with sharp borders between differently colored areas.

Corresponding slices from the Camera retina images were juxtaposed to a close-up wheel pattern to facilitate comparisons by visual inspection.

References

1. Land MF, Nilsson DE (2002) Animal eyes. Oxford: Animal Biology Series.
2. Mandelman T, Sivak JG (1983) Longitudinal chromatic aberration of the vertebrate eye. Vision Research 23: 1555–1560.
3. Matthiessen L (1893) Beiträge zur dioptrik der kristalllinse. X Zeitschrift fr vergleichende Augenheilkunde 7: 102–146.
4. Pumphrey RJ (1961) Concerning vision. London: Cambridge University Press, 193–208 pp.
5. Sivak JG, Luer CA (1991) Optical development of the ocular lens of an elasmobranch *Raja eglanteria*. Vision Research 31: 373–382.
6. Walls GL (1964) The vertebrate eye and its adaptive radiation. New York: The Cranbrook Press.
7. Maxwell J (1854) Some solutions of problems 2. Cambridge and Dublin Mathematical Journal 8: 188–195.
8. Kröger RHH, Fritsches KA, Warrant EJ (2009) Lens optical properties in the eyes of large marine predatory teleosts. Journal of comparative physiology a-neuroethology sensory neural and behavioral physiology 195: 175–182.
9. Matthiessen L (1882) Ueber die beziehungen, welche zwischen dem brechungsindex des kerncentrums der krystalllinse und den dimensionen des auges bestehen. Pflger's Archiv 27: 510–523.
10. Kröger RHH, Campbell MCW, Fernald RD, Wagner HJ (1999) Multifocal lenses compensate for chromatic defocus in vertebrate eyes. Journal of Comparative Physiology A Sensory Neural and Behavioral Physiology 184: 361–9.
11. Karpestam B, Gustafsson J, Shashar N, Katzir G, Kröger RHH (2007) Multifocal lenses in coral reef fishes. Journal of experimental biology 210: 2923–2931.
12. Malkki PE, Löfblad E, Kröger RHH (2003) Species - specific differences in the optical properties of crystalline lenses of fishes. ARVO Annual Meeting Abstract Search and Program Planner 2003: 3483.
13. Schartau JM, Sjögreen B, Gagnon YL, Kröger RHH (2009) Optical plasticity in the crystalline lenses of the cichlid fish *Aequidens pulcher*. Current Biology 19: 122–126.
14. Hanke FD, Kröger RHH, Siebert U, Dehnhardt G (2008) Multifocal lenses in a monochromat: the harbour seal. Journal of Experimental Biology 211: 3315–3322.
15. Lind OE, Kelber A, Kröger RHH (2008) Multifocal optical systems and pupil dynamics in birds. Journal of Experimental Biology 211: 2752–2758.
16. Malmström T, Kröger RHH (2006) Pupil shapes and lens optics in the eyes of terrestrial vertebrates. Journal of Experimental Biology 209: 18–25.

17. Kröger R (2004) Anti-aliasing features in fish retina. Investigative Ophthalmology and Visual Science 45: 2785.

18. Wehner R (1987) 'matched filters' - neural models of the external world. Journal of Comparative Physiology A: Neuroethology, Sensory, Neural, and Behavioral Physiology 161: 511–531.

19. Lythgoe JN, Muntz WRA, Partridge JC, Shand J, Williams DMB (1994) The ecology of the visual pigments of snappers (lutjanidae) on the great barrier reef. Journal of Comparative Physiology A: Neuroethology, Sensory, Neural, and Behavioral Physiology 174: 461–467.

20. Bowmaker J, Govardovskii V, Shukolyukov S, Zueva JL, Hunt D, et al. (1994) Visual pigments and the photic environment: The cottoid fish of lake baikal. Vision Research 34: 591–605.

21. Kröger RHH, Campbell MCW, Fernald RD (2001) The development of the crystalline lens is sensitive to visual input in the african cichlid fish, *Haplochromis burtoni*. Vision Research 41: 549–559.

22. Schartau JM, Kröger RHH, Sjögreen B (2010) Short-term culturing of teleost crystalline lenses combined with high-resultotion optical measurements. Cytotechnology 62: 167–1743.

23. Schartau JM, Kröger RHH, Sjögreen B (2010) Dopamine induces optical changes in the cichlid fish lens. PLoS ONE 5: e10402.

24. Gagnon YL, Söderberg B, Kröger RHH (2008) Effects of the peripheral layers on the optical properties of spherical fish lenses. Journal of the Optical Society of America A 25: 2468–2475.

25. Kröger RHH, Campbell MCW, Munger R, Fernald RD (1994) Refractive index distribution and spherical aberration in the crystalline lens of the african cichlid fish *Haplochromis burtoni*. Vision Research 34: 1815–1822.

26. Gagnon YL, Kröger RHH, Söderberg B (2010) Adjusting a light dispersion model to fit measurements from vertebrate ocular media as well as ray-tracing in fish lenses. Vision Research 50: 850–853.

27. Kröger RHH, Campbell MCW (1996) Dispersion and longitudinal chromatic aberration of the crystalline lens of the african cichlid fish *Haplochromis burtoni*. Journal of the Optical Society of America A 13: 2341 – 2347.

28. Campbell MCW (1984) Measurement of refractive index in an intact crystalline lens. Vision Research 24: 409–416.

29. Campbell MCW, Sands PJ (1984) Optical quality during crystalline lens growth. Nature 312: 291–292.

30. Pierscionek BK (1988) Nondestructive method of constructing 3-dimensional gradient index models for crystalline lenses .1. theory and experiment. American Journal of Optometry and Physiological Optics 65: 481–491.

31. Pierscionek BK (1994) Refractive index of the human lens surface measured with an optic fibre sensor. Ophthalmic Research 26: 32–35.

32. Pierscionek BK (1995) The refractive index along the optic axis of the bovine lens. Eye (London, England) 9: 776–782.

33. Pierscionek BK, Augusteyn RC (1995) The refractive index and protein distribution in the blue eye trevally lens. Journal of the American Optometric Association 66: 739–43.

34. Fletcher A, Murphy T, Young A (1954) Solutions of two optical problems. Proceedings of the Royal Society of London A 223: 216–225.

35. Chu PL (1977) Nondestructive measurement of index profile of an optical-fibre preform. Electronics Letters 13: 736–738.

36. Barrell KF, Pask C (1978) Nondestructive index profile measurement of noncircular optical fibre preforms. Optics Communications 27: 230–234

37. Trefethen LN, Hale N, Platte RB, Driscoll TA, Pachón R (2009). Chebfun version 3. Oxford University. http://www.maths.ox.ac.uk/chebfun/.

38. Fernald RD, Liebman PA (1980) Visual receptor pigments in the african cichlid fish haplochromis burtoni. Vision Research 20: 857–864.

39. Marshall NJ, Jennings K, McFarland WN, Loew ER, Losey GS, et al. (2003) Visual biology of hawaiian coral reef fishes. slowromancapii@. colors of hawaiian coral reef fish. The American Society of Ichthyologists and Herpetologists 3: 455–466.

40. Govardovskii VI, Fyhrquist N, Reuter TOM, Kuzmin DG, Donner K (2000) In search of the visual pigment template. Visual neuroscience 17: 509–528.

41. Warrant E, Nilsson D (1998) Absorption of white light in photoreceptors. Vision Research 38: 195–207.

42. Stark J, Fitzgerald W (1996) An alternative algorithm for adaptive histogram equalization. Graphical Models and Image Processing 58: 180–185.